Diversity and spatial patterns of foraminiferal assemblages in the eastern Clarion–Clipperton Zone (abyssal eastern equatorial Pacific)

Aurélie Goineau[a], Andrew J Gooday[*]

National Oceanography Centre, Southampton, University of Southampton Waterfront Campus, European Way, Southampton SO14 3ZH, UK

[a] Present address: 1, Rue du Champ de Foire, 44530 Guenrouët, France

[*]Corresponding author. E-mail address: ang@noc.ac.uk (A.J. Gooday)

Abstract

Foraminifera are a major component of the abyssal meiofauna in parts of the eastern Pacific Clarion-Clipperton Zone (CCZ) licensed by the International Seabed Authority for polymetallic nodule exploration. We analysed the diversity and distribution of stained ('live') and unstained (dead) assemblages (0-1 cm layer, >150-μm sieve fraction) in megacorer samples from 11 sites (water depths 4051 - 4235 m) within three 30 x 30 km 'strata' in the United Kingdom 1 (UK1 Strata A and B; 5 and 3 samples, respectively) and Ocean Minerals Singapore (3 samples) license areas and separated by distances of up to 28 km within a stratum and 224 km between strata. Foraminiferal assemblage density, diversity and composition at the higher taxon/morphogroup level were largely consistent between samples. Stained assemblages were dominated (>86%) by single-chambered monothalamids, mainly spheres, tubes, komokiaceans and forms that are difficult to categorise morphologically. Hormosinaceans were the most common multichambered group (~10%), while calcareous taxa (mainly rotaliids) represented only ~3.5% of stained tests. Dead foraminifera were more evenly distributed between monothalamids (56%) and multichambered taxa (44%). Almost all test fragments were monothalamids, mainly tubes. Morphospecies were added regularly with each new sample and totalled 580 (stained + dead, complete + fragments), of which 159 occurred in all three strata, 222 were shared between UK1 Strata A and B, 209 between UK1A and the OMS Stratum, and 193 between UK1B and the OMS Stratum. Individual strata yielded 310 – 411 and individual samples 132 – 228 putative morphospecies. The majority (550) of the 580 species were represented by intact tests of which 462 included at least some that were stained. Most of the stained (~80%) and stained + dead (~75%) species were monothalamids, almost all of them undescribed. Many species were rare; 146 of the 550 species with complete tests (stained + dead) were singletons and 53 doubletons. MDS plots suggest that assemblage composition falls within 95% confidence limits across the 11 samples, although with a weak grouping of UK1A samples. A distance-decay plot revealed only a small degree of species turnover between the 3 strata. However, Morisita's index suggested that most individual species represented by ≥10 complete tests had aggregated distributions. We conclude that the foraminiferal assemblages at our eastern CCZ sites are highly diverse, dominated by monothalamids, and display a fairly high degree of uniformity across our study site, but a patchy distribution at the level of individual morphospecies.

Keywords: Benthic foraminifera; monothalamids; seabed mining; polymetallic nodules; abyssal biodiversity; biogeography

1. Introduction

Foraminifera are a major component of benthic communities in many marine habitats, from intertidal to hadal settings. Their rich fossil record, and importance as indicators of past ocean environments, has led to a very extensive body of literature on these testate (shell-bearing) protists, much of it directed towards practical applications in palaeoceanography, palaeoecology, and biostratigraphy (Murray, 2006; Jorissen et al., 2007; Jones, 2014). As a result, many of the formally described species have fairly robust, multichambered tests, usually composed of secreted calcium carbonate and with a good fossilization potential (Jones, 1994; Murray, 2007; Holbourn et al. 2013). At the same time, there has been an increasing awareness among biologists that foraminifera play an important ecological role in marine ecosystems, including deep-sea settings where they sometimes represent a large proportion of the meiofauna, macrofauna and megafauna (Tendal and Hessler, 1977; Bernstein et al., 1978; Snider et al., 1984; Gooday et al., 1992; Gooday, 2019; Alt et al., 2019). As the organic-matter supply to the seafloor declines with increasing water depth, the proportion of calcareous foraminifera decreases and forms with agglutinated tests become more important (e.g., Kurbjeweit et al., 2000; Gooday, 2003; Cornelius and Gooday, 2004; Phipps et al., 2012). In abyssal settings, agglutinated species predominate and below the carbonate compensation depth (CCD), calcareous foraminifera largely (although not entirely) disappear (Saidova, 1966, 1981). In these regions, the foraminiferal assemblages are often dominated by single-chambered taxa (monothalamids). Many of these 'primitive' foraminifera have delicate agglutinated tests with very little fossilization potential and, as a result, they are poorly known and largely undescribed (e.g., Nozawa et al., 2006; Kamenskaya et al., 2012; Goineau and Gooday, 2017).

Monothalamids, or putative monothalamids, are a dominant component of the meiofauna (Nozawa et al., 2006; Gooday and Goineau, 2019), macrofauna (Tendal and Hessler, 1977;Bernstein et al., 1978) and megafauna (Amon et al., 2016; Gooday et al., 2017). in the Clarion Clipperton Zone (CCZ) and other areas of the abyssal Pacific. The CCZ, which occupies much of the equatorial Pacific, hosts extensive sea-floor deposits of polymetallic ('manganese') nodules that have considerable potential commercial value (Hein et al., 2013), although their exploitation would involve risks to seabed-dwelling fauna, including foraminifera, requiring detailed monitoring and protection strategies (Wedding et al., 2013, 2015; Levin et al., 2016; Jones et al., 2017; Miller et al., 2018). This vast region lies outside national jurisdictions, and the exploitation of resources within it are controlled by the International Seabed Authority (ISA), a UN body that enters into contracts for exploration and prospecting in areas of ~75,000 sq km with companies and other entities that are interested in the seabed mining of nodules and are sponsored by states that are party to the Law of the Sea Convention (Lodge et al., 2014; Lodge and Verlaan, 2018). We studied modern foraminifera in two such areas located in the eastern part of the CCZ: the United Kingdom 1 area (contractor UK Seabed Resources Ltd; UKSRL), and the Ocean Minerals Singapore area (OMS, contractor of the same name). This work formed part of the ABYSSal baseLINE (ABYSSLINE) project, funded by UKSRL, the purpose of which was to conduct a baseline survey of benthic faunas in these two areas, as required by the ISA under the terms of the exploration contracts.

In an earlier paper (Goineau and Gooday 2017), we presented an overview of benthic foraminiferal assemblages based on a morphological analysis of specimens picked from the 0-1 cm layer (>150 µm fraction) of five megacorer samples collected during the AB01 cruise in the UK1 area. These samples were dominated by monothalamids, many of them with tubular or spherical tests. A total of 416 morphospecies was recognized during this earlier study, the vast majority of them undescribed. Here, we build on this previous work by analyzing 6 additional samples, 3 from another part of the UK1 area and 3 from the OMS area. As in our earlier study, we distinguish between complete and fragmented tests as well as between dead specimens and

those that were considered to have been alive at the time of collection. Our goals are to 1) evaluate foraminiferal diversity across the three studied strata, and 2) determine the coherence of assemblages within a single stratum and within a license area.

2. Material and methods

2.1. Study area and environmental data

Two cruises conducted within the ABYSSLINE framework, AB01 (2013) and AB02 (2015), sampled within 30 x 30 km areas (so-called'strata', a term that refers here to areas of seafloor and should not be confused with geological strata) in the UK1 (Stratum A and Stratum B) and OMS areas (Fig. 1). A total of 11 sites was sampled, 5 in UK1 Stratum A (UK1A), 3 in UK1 Stratum B (UK1B), and 3 in the Ocean Minerals Singapore (OMS) Stratum (Fig. 1, Table 1; Supplementary Fig. 1). Distances between pairs of sites within a particular stratum were as follows: UK1A, 7.2 – 28.3 km (mean 15.8 km); UK1B, 7.9 – 19.9 km (mean 14.6 km); OMS, 9.8 – 19.9 km (mean 15.9 km). Distances between sites in different strata were as follows: UK1A to UK1B, 131.2 – 199.7 km (mean 148.2 km); UK1A to OMS, 197.6 –223.8 km (mean 207.6 km); UK1B to OMS, 72.5 – 89.6 km (mean 82.4 km).

Glover et al. (2016) provide a general account of the ABYSSLINE project and study area, while Amon et al. (2016) and Goineau and Gooday (2017) summarise available environmental information obtained for UK1A during the AB01 cruise. Polymetallic nodules were common at all sites. For additional data on sediment granulometry, porosity and sorting, total organic carbon and total nitrogen content from the Global Sea mineral Resources (GSR) contract area, located to the west of the UK1 and OMS areas and in somewhat deeper water (~4500 m), see Pape et al. (2017) and De Smet (2017).

2.2. Sample collection and processing

Our shipboard and laboratory methods closely followed those described by Goineau and Gooday (2017). Samples were obtained using an OSNIL-type megacorer, equipped with 12 coring tubes of 10 cm internal diameter. As soon as possible after collection cores were extruded and sliced into 0.5-cm-thick layers down to 2 cm depth, and thereafter into 1-cm-thick layers down to 10 cm depth. Only the upper two layers (i.e., 0-1 cm) were analysed for the present study.

In the laboratory, each complete sediment slice (0-0.5 cm and 0.5-1.0 cm) was allowed to settle for 2 days in a graduated cylinder in order to measure the volume of sediment (very little further volume reduction occurred after this period) before being split into $1/8^{th}$ fractions using a wet splitter (Jensen 1982). After splitting, the volume of the splits to be sorted (either 3 or 4 of the 8 splits) was measured in the same way. This procedure was introduced because the volume of the intact slices varied between cores and between the upper and lower sediment layers, while determining the volume of the splits allowed the accuracy of the splitting to be checked. Sample splits were sieved on 300 and 150 μm screens and the sieves with their sediment residues immersed in Rose Bengal solution overnight before being hand-sorted for foraminifera under a stereo-microscope.

All stained ('live') as well as dead specimens, both complete and fragmentary, were removed from the sample residues, usually with a pipette. Distinguishing between foraminifera that were alive at the time of collection and dead (empty) shells is an essential requirement in ecological studies of foraminiferal assemblages (Murray, 2000). Since the 1950s, the standard method has been to stain samples with a solution of Rose Bengal (Walton 1955). This protein stain colours cytoplasm red, making foraminiferal shells that contain a cell body stand out from

those that do not. When used with care, it yields accurate results (Murray and Bowser, 2000). We therefore stained the sieve residues by immersing them overnight in Rose Bengal solution, followed by gentle washing to remove excess stain. To avoid false positives, we also routinely placed stained specimens in glycerol (which renders the test more transparent) in a cavity slide and examined them at a high magnification under a compound microscope to confirm that the stained material was cytoplasm. In order to keep track of the multitude of species, all specimens were photographed and selected images of each species copied onto PowerPoint slides. These constituted a working catalogue that we constantly referred to and updated as an aid to organising specimens into putative morphospecies.

2.3. Statistical analyses and diversity estimation

Statistical analyses and diversity estimations were calculated using Excel and the open source software EstimateS (Version 9). Using complete specimens (either live or live plus dead combined), we calculated the Fisher alpha (α), Shannon ($H^{'}$, using natural logarithm) and Evenness (E) indices, and generated *individual-based* rarefaction curves for each sample (Colwell et al., 2012). The curves did not reach an asymptote and therefore we extrapolated them up to 1,500 individuals (Colwell et al., 2012), and calculated the Chao1 to estimate the expected total number of species for each sample.

We produced *sample-based* rarefaction curves based on complete stained and dead specimens combined. This method estimates the expected number of species in t pooled samples (Colwell et al., 2012). Since the curve derived from the 11 samples had not reached an asymptote, we extrapolated it to 30 samples (Colwell et al., 2012). Diversity estimators based on the pooled data were then calculated in order to assess the expected total number of species. Because our 11 samples were of different sizes (3 complete samples, 8 split samples), we followed the recommendations of Hortal et al. (2006) and calculated the Chao1, Abundance Coverage-based Estimator (ACE), Jacknife 1 and Jacknife 2. The abundance-based estimators Chao1 and ACE were calculated using the number of complete specimens (stained and dead combined), while Jacknife 1 and 2, which are incidence-based estimators, were calculated based on complete specimens and fragments (stained and dead combined).

3. Results

The raw data (species-level counts of stained and dead tests and test fragments) for this study are summarised in Supplementary Table S1 and the most abundant species in different categories in Supplementary Table S2). The more common morphospecies in our samples are briefly described and illustrated by Goineau and Gooday (2017; Figures 4, 5 and supplementary material therein) and in Fig. 2 and the supplementary material of the present paper (Taxonomic Appendix and Figs S9-S12).

3.1. Abundance

The total numbers of complete stained foraminiferal tests picked from the 0–1 cm layer of 5 samples from UK1A ranged from 514 to 966 (mean 676), compared with 302 to 588 (mean 467) in 3 samples from UK1B, and 222 to 877 (mean 516) in 3 samples from the Ocean Minerals Singapore (OMS) Stratum (Table 2). These numbers corresponded to densities of 71–146 indiv.10 cm^{-2} (UK1A), 68–165 indiv.10 cm^{-2} (UK1B) and 30–171 indiv.10 cm^{-2} (OMS Stratum). The numbers of stained fragments were variable but consistently lower than those of

complete stained individuals, ranging from 143 to 763 per sample in UK1A, compared with 103 to 334 in UK1B, and 83 to 485 in the OMS Stratum (Table 2). The corresponding densities were 22–97 frag.10 cm^{-2} (UK1A), 29–76 frag.10 cm^{-2} (UK1B) and 11–94 frag.10 cm^{-2} (OMS Stratum).

The numbers and corresponding densities of complete dead tests were consistently lower, by a factor of 1.1 to 4.7 (usually between 2 and 4), compared to the stained tests (Table 2). With two exceptions (MC20, MC25), numbers and densities of dead fragments were also lower, in some cases much lower (MC02), than for the stained assemblage. However, the numbers varied considerably, particularly in the case of the OMS Stratum, where densities were 7, 46 and 69 dead fragments per 10 cm^2 in the three samples.

3.2. Main taxa and morphological groups

The overall composition of the stained assemblage (complete tests) was similar at the higher taxon/group level in all eleven samples and across all 3 strata (Table 3). There are no statistically significant differences in their relative abundances in UK1A (5 samples) compared to UK1B plus OMS Strata combined (6 samples), except in the case of the *Nodellum*-like group and the saccamminids, both of which are significantly more abundant in UK1A in terms of absolute and percentage abundance ($p < 0.01$, t test). Monothalamids (89.1% of complete stained tests overall) were the main component with the most abundant groups in all samples being spheres (19.3%), tubular/spindle-like forms (19.1%), and monothalamids that are difficult to classify morphologically (‘unclassified monothalamids’ 22.7%) . Komokiaceans (particularly baculellids, 6.8%) and komoki-like forms (4.5%) were also fairly common. Among the multichambered forms the agglutinated hormosinaceans (6.8%) were consistently ranked top with rotaliids (2.0%) being the most common calcareous taxon.

The dead assemblage (complete tests) showed no statistically significant differences in the relative abundances of the main groups between the UK1A and the UK1B plus OMS Strata combined. The distribution of complete dead tests was more even between the monothalamid (55.8%) and multichambered taxa (44.2%) than it was in the case of stained individuals (Table 4). Also, in contrast to the stained assemblage, the multichambered hormosinaceans (19.9%) were the most abundant constituent in all strata, with ‘other textulariids’ (10.5%), rotaliids (5.54%) and trochamminids (4.49%) being more abundant, both absolutely and relatively, than in the stained assemblage.

Monothalamids represented almost all (96% in 3 strata combined) of the stained and dead fragments combined (Supplementary Tables S3, S4). The only exception was OMS sample MC20, where they accounted for less than three-quarters (73.8%) of fragments. Tubular foraminifera were particularly prone to fragmentation, making up almost half (47.8 %) of stained + dead fragments in the combined dataset. The other groups common as fragments were the komokiacean families Baculellidae (14.3% overall) and Komokiidae (12.1%) and unclassified monothalamids (11.3%).

3.3 Species richness, alpha species diversity and estimated species diversity

Putative morphospecies were added regularly with each new sample. The rate at which they were added declined progressively, although the upward trend in the cumulative number of species was maintained (Fig. 3). The grand total number of species was 580, of which 546 were represented by complete tests (stained, dead or both), including 10 gromiids (Table 5). Plots of species ranked by abundance reveal a relatively small number of abundant species and a long tail of rare species, a pattern evident in the case of stained, dead, and stained + dead specimens (Supplementary Figs S2A, S3A, S4A, respectively). More than a quarter (146 = 26.7%) of

species with complete tests (either stained or dead) were singletons and 53 (9.71%) doubletons (Table 6).

The total number of species present in particular strata was 411 in UK1A (5 samples), 324 in UK1B (3 samples) and 310 in the OMS Stratum (3 samples) (Table 5), while the total number in individual samples ranged from 132 to 228 (Supplementary Figs S5). The majority of species (462 = 79.7%) included at least some complete stained individuals, although less than half (224 = 45.5%) of that number were confined to the stained assemblages. Fewer species (264 = 45.5%) were represented by some dead tests and fewer still by stained (130 = 22.4%) and dead (113 = 19.5%) fragments, with the number confined to one of these categories being correspondingly lower (74, 12, 14, respectively). Individual samples yielded 76 - 186 stained species and 106 - 224 stained + dead species. The majority (79.4% overall) of the stained species and a somewhat lower proportion (74. 6% overall) of the stained + dead species were monothalamids (Table 5). The most specious multichambered taxon was the hormosinaceans (overall, 27.4% of multichambered species and 6.4% of all species); the most specious monothalamids were the spheres, tubes and unclassified taxa (together, 58% of all monothalamid species and 43% of all species).

Values of rarefied species richness [$E(S_{100})$] and diversity metrics were generally similar across the three strata (Table 6). The UK1A samples tended to have slightly higher $E(S_{100})$ values than samples from UK1B and the OMS Stratum. Similarly, diversity indices ($H^{'}$ and Fisher α) were somewhat higher overall in UK1A than the other two areas. None of the individual-based rarefaction curves based on stained and stained + dead tests reached an asymptote for any of our 11 samples (Supplementary Fig. S6). The extrapolated curves of species numbers were tending to level off for samples MC04, MC09, MC13 and MC20 at 750–1,500 individuals, but still increasing at >1,500 individuals for the 7 remaining samples. The sample-based rarefaction curve for all 11 samples extrapolated to 30 samples and based on the entire assemblage (i.e. complete live and dead specimens combined) showed signs of levelling off after about 20 samples (Supplementary Fig. S7), suggesting that 20 samples might have yielded ~90% of species. Estimates for the actual diversities, based on Chao 1, ranged from 111 ± 16 (MC13, UK1B) to 257 ± 26 (MC07, UK1A) for the stained assemblage, and 68 ± 15 to 183 ± 51 for the dead assemblage (Table 6). They followed the same patterns as $E(S_{100})$, $H^{'}$ and Fisher α, being generally highest in UK1A and lowest in the OMS Stratum. Abundance-based estimators ACE and Chao1 based on all samples from a single stratum combined (i.e. combined numbers of complete stained and dead specimens) estimated totals of, respectively, 483 and 501 ± 28 species in UK1A, 489 and 516 ± 51 in UK1B, and 358 and 356 ± 21 in OMS (Fig. 4). The incidence-based estimators Jacknife 1 and 2, which are based on the occurrence of complete specimens and fragments (live and dead combined), estimated totals of, respectively, 638 and 565 ± 20 species in UK1A, 521 and 463 ± 33 in UK1B, and 471 and 427 ± 17 species in OMS. Combined data from all 11 samples yielded estimates ranging from 680 (ACE) to 877 species (Jacknife 2) (Fig. 4).

3.4. Turnover and distribution of species

MDS plots based on the ‘entire’ assemblage (i.e., all species including monothalamids) represented by a) complete stained specimens, b) complete stained plus dead specimens, and c) all specimens (stained plus dead, complete plus fragments) reveal some tendency for the samples to be grouped according to strata (Fig. 5, left-hand column). In particular, the 5 samples from UK1A form a loose grouping, whereas those from UK1B and the OMS Stratum tend to be more or less intermingled. On the other hand, this pattern is not evident when only multichambered taxa are considered (Fig. 5, right-hand column). Nevertheless, irrespective of the category (stained, dead etc), all 11 samples fall within a space defined by the 95% confidence level,

indicating that the species composition is statistically identical. Similarly, a 'decay-distance' plot of Bray-Curtis Similarity against distance between samples reveals minimal differences between the species composition of samples separated by increasing distances (Fig. 6). There are no significant differences between the Bray-Curtis Similarity of samples within strata (distances = 7.2- 28.3 km; unfilled symbols in Fig. 6) and values based on the UK1B vs OMS and UK1A vs UK1B comparisons (filled triangles and circles). The only significant difference ($p < 0.05$) is between samples within strata and the UK1A vs OMS comparison (distances = 198 – 224 km; filled squares), and this becomes non-significant if the two highest Bray-Curtis values are removed. This suggests that the foraminiferal fauna in the upper 1-cm layer of the sediment (>150-µm fraction) is fairly uniform across the three sampled strata.

Of the 580 morphospecies identified in the 11 samples, 159 occurred in all three strata, 222 were shared between UK1A and B, 209 between UK1A and the OMS Stratum, and 193 between UK1B and the OMS Stratum (Fig. 7). The numbers of species confined to particular strata were 139 (UK1A), 68 (UK1B) and 67 (OMS). Within individual strata, the numbers of species shared between pairs of samples was 65–117 out of a total of 411 (UK1A, 5 samples), 65–80 out of a total of 324 (UK1B, 3 samples) and 66–92 out of a total of 310 (OMS, 3 samples).

Disregarding singletons (Table 6), which by definition are confined to one sample, the majority (303 = ~78%) of the 388 species represented by complete specimens (stained + dead) were found in 5 or fewer samples, while only 11 (3.35%) occurred in all 11 samples and 10 (2.58%) in 10 samples (Fig. 8). The stained and dead assemblages followed a similar pattern, although the proportion of more widely distributed species was somewhat lower, particularly for dead species confined to a few samples (Supplementary Fig. S8). The maximum number of specimens assigned to species confined to only 1-2 samples was also much lower (n = 17) in the dead assemblage (Supplementary Figs. S3B) than in the stained and stained + dead assemblages (n = 282 and 296, respectively; Supplementary Figs. S2B, S4B).

In general, the abundant species were fairly widely distributed. Of the 20 species in the stained assemblage found across 9-11 sites (Supplementary Fig.S2C), 14 were ranked among the top 20 species in terms of abundance. However, species restricted to 1 or 2 samples also included a few that were abundant (Supplementary Fig. S2B). Notable among these was a distinctive radiolarian inhabitant (Fig. 2C,D) that was represented by 281 specimens in the MC25 sample and 1 specimen in the MC13 sample (both located in UK1B). Despite its restricted distribution, this was the second-ranked species overall. The pattern was similar for the dead (Supplementary Fig. S3C) and stained + dead (Supplementary Fig. S4C) assemblages, although the numbers of species found across 9-11 sites was lower (14) in the former and higher (34) in the latter compared to the 20 above-mentioned species in the stained assemblage.

At the species level, the Morisita index revealed that spatial patchiness was common among species represented by ≥10 complete tests (Table 7). With one exception, values of this metric for the 111 species represented by stained tests were between 1.2 and 11, corresponding to varying degrees of aggregation; the exceptional value was 0.9, indicating a regular distribution (McClain et al., 2011). In the stained + dead assemblage, 137 species yielded Morisita Index values ≥1.1 (aggregated), one had a value of 0.8 (regular) and four a value of 1.0, indicating a random distribution. In both cases, the majority of the species included in the analysis (70% of stained and 77% of stained + dead) fell within the range 1.1-3.9. The highest values were associated with species that were more or less confined to one sample.

4. Discussion

4.1. Limitations of study

The analysis of deep-sea foraminiferal assemblages, particularly the monothalamid component, poses problems that are less evident when analysing metazoan meiofauna and macrofauna. Notable among these are the criteria for regarding specimens as having been alive when collected and the fragmentation of delicate tests (Fig. 2E-G). We discuss these issues elsewhere (Goineau and Gooday, 2017; Supplementary Material in Gooday and Goineau, 2019). Further challenges are created by the high levels of diversity. During the present study we recognised well over 500 putative morphospecies, the majority of them undescribed monothalamids. Keeping track of this collection of largely unknown species, discriminating between them, and ensuring that they were identified as consistently as possible between samples proved a major task. Some species were easy to recognise but certain groups, notably the tubular and spindle-shaped stercomata-bearing forms, exhibited considerable morphological variability. Every specimen picked from the samples was photographed and photographs of all morphotypes were assembled on PowerPoint slides for easy comparison. In all cases of doubt, specimens were compared directly by placing them side by side in glycerol in open cavity slides and examining them under both a stereo- and a compound microscope. Where a specimen or fragment was too indistinct to be placed in a species or to be recognised as a previously unseen ('new') species, it was classified as indeterminate. The morphological variability displayed by some of the monothalamids is another likely source of error. Notable examples of morphologically variable morphospecies include Tube sp. 48 and Tube sp. 54, illustrated in Figures 4a-c a d 4g-i, respectively, of Goineau and Gooday (2017). This problem meant that particular caution was used when recognising single specimens (singletons) as distinct species. Despite these precautions, the above-mentioned issues mean that it was impossible to exclude all errors. Nevertheless, we are confident that the large size of our dataset (Supplementary Table S1) ensures that the overall taxonomic composition of the assemblage, and the patterns of diversity and distribution revealed by this study, are robust.

There are some discrepancies between data presented for UK1A samples in Goineau and Gooday (2017, Tables 2-4) and those included in the present paper. These arose for several reasons. 1) The UK1A dataset used in the present study includes specimens >150 µm picked from an additional split of the MC11 sample as part of a study of finer sediment fractions (Gooday and Goineau, 2019). 2) The original UK1A dataset has been carefully revised in the light of new material obtained from the UK1B and OMS samples. For example, some forms that were originally regarded as separate species have been combined. 3) Some monothalamid species have been moved between major groupings. Overall, our new dataset is more conservative, as well as more extensive, than that of Goineau and Gooday (2017).

4.2. Comparison with previous foraminiferal studies in the eastern Pacific

Enge et al. (2011, Table 1 therein) reported 'live' foraminiferal densities ranging from 194 to 364 (mean 279 ±72) individuals 10 cm^{-2} in the 0-1 cm layer of 4 core samples from abyssal Station M on the Californian margin. These densities are substantially higher than those obtained from our samples (Table 2), a disparity partly attributable to the finer size fraction (>63-µm) analysed by Enge et al. (2011). The proportion of 'soft-shelled' monothalamids ('saccamminids') in this upper layer ranged from 39.6% to 53.0%, and reached higher values (up to 71%) in deeper sediment layers (2-3 cm). In a later study, Enge et al. (2012) analysed 6 core samples (including the 4 from their 2011 paper) collected at two sites in the region of Station M. They recorded a mean density of 365 stained individuals 10 cm^{-2} for the 0-1 cm layer at the new site (StnM09), where 29% and 30% pf specimens (0-5 cm layer) were 'soft-shelled' monothalamids.

There are many similarities between the foraminiferal species in our samples and those

reported in several studies from nearby parts of the Clarion Clipperton Zone (CCZ). Kamenskaya et al. (2012) record a variety of macrofaunal-sized monothalamids from three samples (>500 and 250-500 μm fractions) collected at sites (~11° 00´N, 119° 40´W; 4,380-4,410 m depth) in the Interoceanmetal Joint Organisation (IOM) license area in the eastern CCZ (Fig. 1). Some of those illustrated in this paper (e.g., *Staphylion* sp,; some of the chain-like forms, and many of the tubes; Kamenskaya et al., 2012, Figures 2-4, therein) are present in our samples. In a preliminary survey of meiofaunal (>32 μm) foraminifera obtained at two other sites in the IOM area, Radziejewska et al. (2006) illustrated some common non-calcareous species, most of which are represented in the UK1 and Ocean Minerals Singapore (OMS) areas. A more extensive study of meiofaunal foraminifera was conducted by Nozawa et al. (2006) at the Kaplan East site (~15°N, 119°W, ~4100 m depth). Despite the different size fractions (>32 μm compared with >150 μm fraction in the present study), the general composition of the assemblages in the Kaplan East and ABYSSLINE samples was quite similar, with groups such as *Lagenammina*, *Nodellum*-like forms, saccamminids and psammosphaerids ('spheres') being common. Many of the individual species illustrated by Nozawa et al. (2006) are recognisable in our samples. These previous studies therefore suggest that there is a general uniformity of foraminiferal assemblages at similar water depths across the eastern CCZ.....

4.3. High foraminiferal diversity in the eastern Clarion Clipperton Zone

Individual samples from the UK1 and OMS areas yielded 132 to 228 putative morphospecies (Fig. 7; Supplementary Fig. S5), leading to a total number of 580 in all samples combined (Table 5). Even allowing for, say, a 10% overestimate due to the likely sources of error mentioned above, these are very diverse assemblages, and the total does not include species confined to finer size fractions (Gooday and Goineau, 2019) or deeper sediment layers (Goineau and Gooday unpublished). Previous analyses of trends in foraminiferal species richness with water depth, based on stained + dead assemblages of hard-shelled species, have yielded inconsistent patterns; in some areas (e.g., NW Atlantic) diversity increases with depth onto abyssal plains, while in other areas (e.g., Gulf of Mexico, High Arctic) diversity decreases with depth (reviewed in Rex and Etter, 2010). Nevertheless, high levels of local foraminiferal species richness at abyssal depths are not unprecedented when monothalamids are included. The numbers of morphospecies in the top 1 cm layer of individual multicorer samples (>63 μm fraction) at sites on the Porcupine, Madeira and Cape Verde Abyssal Plains ranged from 135 to146 (including phytodetrital layer), 100 to 149 and 117, respectively, while 217 species were recognised in a similar sample from the Arabian Sea. (Gooday et al., 1998). Other deep-sea meiofaunal taxa may also be highly specious. The huge number (682) of harpacticoid copepod species recorded by George et al. (2013) at two sites in the Angola Basin (SW Atlantic; 5389 m and 5448 m depth) is particularly notable. These sites yielded 172 and 600 species from 35 and 40 multicores, respectively; all but 5 were undescribed. Miljutina et al. (2010) recognised 325 nematode species from 2 box cores and 21 multicores in the central CCZ. Nematode generic richness in the CCZ may also be very high (reviewed in Radziejewska 2014).

In the present study, 42.2% of species represented by complete stained individuals and 51.9% of those represented by complete dead individuals were singletons or doubletons (Table 6). A predominance of rare species is a ubiquitous feature of diverse biological communities (Magurran 2004), including those from marine settings (Connolly et al., 2014). There is evidence from the NW Atlantic that deep-sea benthic communities have a more even distribution of individuals among species, and more rare species, than those in shelf environments (Rex and Etter, 2010). More than half (384) of the 682 harpacticoid species in the above-mentioned study of George et al. (2013) were singletons, and a further 111 doubletons. This is a common pattern among different taxa in the equatorial Pacific, including macrofaunal isopods and polychaetes

458 (Glover et al., 2002; Janssen et al., 2015; Wilson 2017) and meiofaunal nematode genera (Pape
459 et al., 2017), as well as foraminifera from this and other oceans (Gooday 1986, 1996; Gooday et
460 al., 2006; Buzas et al., 2013; Goineau and Gooday, 2017). As Paterson et al. (1998) remarks,
461 where species richness is very high and rare species are common, it may never be possible to
462 collect all species present in a particular area without analysing unrealistic numbers of samples.
463 The sample-based rarefaction curve shown in Supplementary Fig. S7 suggests that it would be
464 necessary to analysed at least 20 samples to find around 90% of the smaller foraminiferal species
465 in our three study areas. Thus, chronic undersampling makes establishing whether or not species
466 are endemic almost impossible, a conclusion reinforced by the modelling study of Tittensor et al.
467 (2010).
468 What are the mechanisms that allow so many foraminiferal species to co-exist in
469 relatively small volumes of sediment? Rex and Etter (2010, pp. 123-125) suggest that
470 foraminiferal diversity may be particularly high in the abyssal NW Atlantic (as reported by
471 Buzas and Gibson, 1969) because 1) the food supply is sufficient to maintain populations at a
472 level that does not depress diversity, 2) low macrofaunal and megafaunal densities lead to less
473 depletion of limited food supplies as well as reduced predation by animals on foraminifera, and
474 3) the ability to reproduce asexually avoids the need that animals have to find mates. They
475 further suggest that 'dormancy', asexual reproduction and efficient dispersal mechanisms may
476 help immigrant foraminiferal species originating from distant sources to persist in abyssal
477 settings ('source-sink dynamics'). These arguments could apply equally in the eastern CCZ.
478 Another factor may be that many monothalamids in our samples probably have a largely static
479 life style that likely limits competition between species. This is suggested by test morphologies
480 (e.g., tubular, branching or highly irregular) that would make movement on or through the
481 sediment difficult, and by the frequent occupancy by foraminifera of cryptic microhabitats,
482 particularly radiolarian tests in the case of the CCZ, from which they cannot excape (Goineau
483 and Gooday, 2015). Attachment to small hard particles (e.g. micronodules) is also common.
484 Jumars (1975a, 1975b) invoked 'environmental grain structure' to explain why largely sedentary
485 ('small ambit') polychaete species were more diverse than more mobile species in the much
486 shallower setting of the San Diego Trough (1230 m depth). In the CCZ, the scale of the
487 'environmental grain structure', created in particular by radiolarian tests as well as by the
488 nodules themselves, may be highly relevant to at least some individual foraminifera and
489 therefore well suited to enhancing foraminiferal diversity.
490
491 *4.4. Spatial patterns across the sampled area*
492
493 Our study revealed an overall uniformity in the relative abundance of the main foraminiferal
494 taxa/groups, which showed no significant variations across the three strata (Table 3). In MDS
495 plots based on 'entire' assemblages (i.e., including monothalamids), as well as those based on
496 multichambered taxa alone, all samples lie within the 95% confidence envelope, indicating a
497 large degree of uniformity (Fig. 5). However, particularly in the case of the complete stained
498 tests, the five UK1A samples form a weak group that is somewhat separated from a second
499 group comprising three of the UK1B and two of the OMS samples, with the third OMS sample
500 (MC21) as an outlier. A loose clustering of the UK1A samples is also evident in plots based on
501 the stained + dead tests and on presence/absence data for all specimens (stained and dead,
502 complete and fragmentary) combined. This indication of a weak spatial structure within our
503 species-level dataset is consistent the greater average distance between UK1A sampling sites and
504 those in the other two strata (148 km for UK1B and 208 km for OMS) than between sites in the
505 UK1B and OMS strata (82 km) (Supplementary Fig. S1). The distance-decay relationship
506 (Fig.6) reveals a significant difference in assemblage composition only when the two most
507 distant strata (UK1 Stratum A and OMS; mean sample spacing 208 km) are compared. At

similar spatial scales (60-270 km) within the Global Sea mineral Resources (GSR) contract area in the eastern CCZ, Pape et al. (2017) reported that metazoan meiofaunal assemblages were 'largely comparable' in terms of abundance, composition and diversity at the higher taxon level and when considering nematode families and genera. Among higher taxa only minor groups that represented <1% of the assemblage showed any real spatial variation. Nematode families and genera fluctuated in abundance between samples and sites but in both cases the same taxa were dominant. De Smet et al. (2017) reported a similar degree of homogeneity in the abundance, diversity and assemblage composition of macrofauna at the same GSR sites.

Since the UK1A samples were taken in October 2013 and the UK1B and OMS samples in February and March 2015 (Table 1), it is possible that temporal variations could influence the weak spatial patterns observed in the MDS plot. Deep-sea foraminiferal populations can vary on both seasonal and inter-annual time scales (Gooday and Rathburn, 1999; Gooday et al., 2010; Glover et al., 2010), normally in response to fluctuating inputs to the seafloor of organic matter ('phytodetritus') derived from surface production (Gooday, 2002). Utilisation of this labile material leads to the development of enhanced populations of opportunistic species, typically rotaliids (Gooday, 2003). However, the lack of any clear difference in the relative abundance of stained rotaliids, or any other group, between the 2013 and 2015 samples (Table 3) suggests that temporal variation was not important. Surficial phytodetritus deposits were also never observed in any of our core samples.

Our samples revealed a greater degree of spatial structure in the dispersion patterns of individual species. Including singletons, almost half (252 = 43.4%) of all species were recorded from only one stratum with 211 (36.4%) restricted to a single core. This could indicate the existence of many species with narrow distributions. On the other hand, 238 (~95%) of the 251 species confined to one stratum were represented by less than 10 specimens, and 187 (74.5%) were either singletons or doubletons (complete or fragmentary, stained or dead). Moreover, 181 (85.8%) of the 211 species confined to a single core were represented by 1 or 2 specimens. Given the evidence for small-scale faunal patchiness in the deep sea (Grassle and Morse-Porteous, 1987; Snelgrove and Smith 2002; McClain et al., 2011; McClain and Schlacher, 2015), including among abyssal Pacific foraminifera (Bernstein et al., 1978; Bernstein and Meador, 1979), and the small sediment area sampled by each of our cores (~78 cm^2), these rare species are more likely to be undersampled, in which case little can be concluded regarding their distributions (Glover et al., 2002; McClain and Hardy, 2010). This point is underlined by the fact that some well-known, globally-distributed multichambered species (Gooday and Jorissen 2012) are rare in our samples; for example, *Cyclammina cancellata, Hoeglundina elegans* and *Laticarinata pauperata* are each represented by single specimens.

The Morisita index suggests that the majority of species represented by 10 or more complete tests had aggregated distributions (Table 7), with the highest values of this index being associated with species that were more or less confined to one sample. A particularly good example of the latter is a monothalamid, the second-ranked species in the stained assemblage with 282 specimens, that inhabits radiolarian tests and builds a short wide tube on the exterior (Fig. 2C, D). With the exception of a single example from sample MC13, all specimens (complete and stained) were found in sample MC25, yielding a Morisita index of 10.9. Bernstein et al. (1978) detected aggregation among foraminifera at scales from cms to kms in the abyssal North Pacific. This contrasts with the predominantly random dispersion patterns of macrofaunal (mainly polychaetes) and meiofaunal (harpacticoid copepods) taxa at scales from a few cms to 100 km in studies at bathyal and abyssal sites in the Pacific and NE Atlantic Oceans (reviewed in Rex and Etter, 2010). However, these earlier results were based on variance-to-mean ratios, rather than the Morisita index recommended by McClain et al. (2011). Using this latter approach, McClain et al. (2011) detected aggregated distributions among polychaete species in samples collected across scales of between 1 and 350 m at a lower bathyal (3203 m depth) site in

the NE Pacific to the north of the CCZ. They concluded that some metazoan macrofaunal species (>300 μm) had aggregated distributions at small spatial scales in their nested samples, but that, despite a huge amount of species-level variation between samples, there was only weak spatial structure in assemblage composition across the entire sampling area. Although the spatial scale of their study is smaller, and the experimental design more rigorous, the results of McClain et al. (2011) are comparable to ours. In the aforementioned GSR area of the eastern CCZ, Pape et al. (2017) report that the abundance of 14 species of the nematode genus *Halalaimus* was highly variable between sites (and between the two sampling periods at B6SO2), with only 2 species common to the three sites and half restricted to one site (Pape et al., 2017). However, *Halalaimus* abundance in individual samples was low (Table 3 in Pape et al., 2017), suggesting that undersampling may have been responsible for some of this variability.

4.5. Distributions at larger scales

Species turnover is generally higher with increasing water depth than it is in a horizontal sense, reflecting the greater degree of environmental change along bathymetric transects (Rex and Etter, 2010; McClain and Hardy, 2010; McClain and Rex 2015). There is also evidence for a greater degree of genetic differentiation along depth gradients on environmentally complex continental margins than horizontally across the more uniform abyssal plains (Taylor and Rotterman, 2017). At the same time, rates of β-diversity measured along bathymetric contours (i.e. horizontally) tend to decrease with depth among both macrofaunal metazoans (bivalves; McClain and Rex, 2015) and foraminifera (Buzas et al., 2013). These trends in β-diversity are consistent with the wide species ranges that appear to be common among some macrofaunal taxa, notably polychaetes, on Pacific and other abyssal plains (Glover et al., 2002; McClain and Hardy, 2010; Janssen et al., 2015; Wilson, 2017).

Our sample sites are situated at similar latitudes (116° 27.601' to 117° 22.284'W), and occupy a modest depth range (4051 – 4224 m) in an approximately N-S direction. They are therefore not exposed to any great extent to the east - west gradients of increasing depth and decreasing sea-surface productivity along the CCZ (Hannides and Smith, 2003; Smith and Demopoulos, 2003; Morgan, 2012). Organic-matter flux to the seafloor, which is directly related to surface productivity and water depth, is believed to strongly influence rates of β-diversity in the deep sea (reviewed in McClain and Rex, 2015), although the mechanisms involved are not well understood (McClain and Schlacher, 2015). Another factor may be sediment properties, which according to Leduc et al. (2012), explain about 25% of nematode species β-diversity on the continental slope west of New Zealand (350-3100 m depth). Nematode assemblages from nodule-free and nodule-bearing parts of the CCZ are significantly different in terms of diversity (higher where nodules are present) and the relative abundances of genera (Miljutina et al., 2010. Singh et al., 2016). Nodules are present at all our sites and the sediments are radiolarian oozes that appear to be uniform, although we lack detailed granulometric data. Given the relative consistency in environmental conditions (depth, surface productivity, sediment type) across our abyssal study areas, the overall faunal similarity is unsurprising. Nevertheless, the distance-decay relationship (Fig. 5) suggests that the spatial separation of samples across a maximum distance of 224 km (the maximum sample separation between UK1A and OMS Strata) could have some influence on the composition of species assemblages.

More widely, many of the foraminifera that can be identified belong to well-known multichambered deep-sea morphospecies that have been reported from different oceans (Table 4) and are often regarded as having 'cosmopolitan' distributions (e.g. Gooday and Jorissen, 2012; Holbourn et al. 2013). A number of monothalamids (e.g. *Lagenammina difflugiformis*) or presumed monothalamids (e.g. *Edgertonia floccula, Resigella moniliforme*) have similar

distributions. For a few calcareous species, notably *Epistominella exigua* (Pawlowski et al., 2007; Lecroq et al., 2009) but also the top-ranked rotaliid in our samples *Nuttallides umbonatus* (Pawlowski and Holtzmann unpublished), wide ranges in different ocean basins at lower bathyal and abyssal depths are supported by genetic data. This is consistent with previous evidence for wide ranges among many foraminiferal species across abyssal plains, perhaps reflecting the apparent ease with which foraminiferal propagules can be transported over large distances (Alve and Goldstein, 2003, 2010), combined with slower evolutionary rates in the deep sea (Buzas and Culver, 1984). Wide morphospecies distributions are reported for other meiofaunal taxa at abyssal depths across different ocean basins and oceans, for example, species of the harpacticoid copepod genus *Mesocletodes* (Menzel et al., 2011). As mentioned above, foraminifera have the added advantage of being able to reproduce asexually, which may allow rare species to maintain low-density populations.

Concluding remarks

Foraminifera, and particularly monothalamids, are a major and ubiquitous component of deep-sea benthic communities across all size classes. In the abyssal Pacific they dominate the sediment-dwelling meiofauna (Snider et al., 1984; Nozawa et al., 2006), macrofauna (Tendal and Hessler, 1977) and megafauna (Amon et al., 2016; Gooday et al., 2017; Simon-Lledo et al., 2019), as well as the biota encrusting polymetallic nodules and other hard substrates (Mullineaux, 1987; Veillette et al., 2007; Gooday et al., 2015). The present study underlines the enormous diversity of these foraminiferal populations in the nodule-rich ecosystems of the Clarion-Clipperton Zone. The analysis of further samples from other parts of the CCZ will undoubtedly reveal more hitherto unknown species. Our results also suggest that, although many species are found only in one stratum or one sample, rarity combined with undersampling makes it is impossible to establish whether any are endemic to these particular areas without analyzing unrealistic numbers of samples.

In addition to their biodiversity, much remains to be learnt about the ecology of abyssal foraminifera. For example, little is known about life spans, rates of growth, or the prevalence of sexual vs asexual reproduction, while diets remain largely a matter of speculation (Gooday et al., 2008). Nevertheless, field observations combined with experimental studies, together with their shear abundance, suggest that foraminifera must play an important ecological role in the deep sea (Gooday, 2003). It is clear that some calcareous species are important processers of pulsed inputs of labile organic-matter, while foraminifera of all types are consumed, in turn, by specialist predators and incidentally by deposit feeders, creating a link between lower and higher levels of deep-sea food webs (Lipps and Valentine, 1970; Gooday et al., 1992). Evidence from volcanic ash and turbidite deposits that foraminifera, including the megafaunal xenophyophores, are among the early recolonisers of new sedimentary substrates led Gooday and Goineau (2019) to speculate that opportunistic species may be quick to occupy areas that have been seriously disturbed, directly or indirectly, by mining. Finally, large xenophyophore tests, which occur everywhere across the CCZ, often in considerable numbers, are an important source of habitat structure for metazoans and other foraminifera (Levin and Thomas, 1988; Hughes et al., 2004).

Biologists working in the deep sea are now more aware of foraminifera than they were in the past. However, there is still a tendency to overlook them. Although they are not always an easy group to study, we would argue that their abundance, diversity and potential ecological significance make it important to include these ubiquitous and extremely successful protists in studies of the seafloor communities in areas likely to be mined in the future.

Acknowledgements

We are grateful to Craig Smith for his leadership of the overall ABYSSLINE project and particularly the two cruises (AB01 and AB02), as well as Ivan Voltski and Alexandra Weber for their help with core collection and processing at sea. We thank Kate Davis for preparing the figures in the main text, Brian Bett and Noelie Benoist for advice on statistics, and Brian Bett for generating Supplementary Figure S1 and distances between samples.

Compliance with ethical standards

Funding. This study, and the wider ABYSSLINE project, was funded through a commercial arrangement with UK Seabed Resources Ltd. The funder played no role in the study design, the collection, the analysis and interpretation of the data, or the writing of the manuscript, although the company read and approved the final version for publication.

Competing interests. We declare that there are no competing interests

Author contributions

Both authors contributed equally to the paper. Six samples were analysed by AG, five by AJG and the authors together checked and collated the faunal data. AG analysed most of the data, prepared initial drafts of the figures (except Fig. 2) and the raw data spreadsheet (Table S1). AJG wrote most of the text, prepared the tables and much of the supplementary material.

Additional information

Supplementary material accompanies this paper.

References

Alt, C.H.S., Kremenetskaia (Rogacheva), A., Gebruk, A.V., Gooday, A.J., Jones, D.O.B., 2019. Bathyal benthic megafauna from the Mid-Atlantic Ridge in the region of the Charlie-Gibbs Fracture Zone fracture zone based on Remotely Operated Vehicle observations.Deep-Sea Res. I. https://doi.org/10.1016/j.dsr.2018.12.006.

Alve, E., Goldstein, S.T., 2002. Resting stage in benthic foraminiferal propagules: a key feature for dispersal? Evidence from two shallow water species. J Micropalaeontol 21, 95-96.

Alve, E., Goldstein, S.T., 2010. Dispersal, survival and delayed growth of benthic foraminiferal propagules. J. Sea Res. 63, 36-51.

Amon, D.J., Ziegler, A.F., Dahlgren, T.G., Glover, A.G., Goineau, A., Gooday, A.J., Wiklund, H., Smith, C.R., 2016. Insights into the abundance and diversity of abyssal megafauna in a polymetallic-nodule region in the eastern Clarion-Clipperton Zone. Sci. Rep. 6, http://doi.10.1038/srep30492.

Bernstein, B.B., Hessler, R.R., Smith, R., Jumars, P.A., 1978. Spatial dispersion of benthic foraminifera in the central North Pacific. Limnol. Oceanogr. 23, 401–416.Bernstein, B.B., Meador, J., 1979. Temporal persistence of biological patch structure in an abyssal benthic community. Mar. Biol. 51, 179-183.

Buzas, M.A., Culver, S.J., 1984. Species duration and evolution: benthic foraminifera on the Atlantic continental margin of North America. Science 225, 289-290.

Buzas, M.A., Gibson, T.G., 1969. Species diversity: benthonic foraminifera in western North Atlantic. Science 163, 72-75.

705 Buzas, M.A., Culver, S.J., 1984. Species duration and evolution: benthic foraminifera on the
706 Atlantic continental margin of North America. Science 225, 829-30.
707 Buzas, M.A., Hayek, L-A.C., Culver, S.J., Hayward, B.W., Osterman, L.E., 2013. Ecological
708 and evolutionary consequences of benthic community stasis in the very deep sea (>1500
709 m). Paleobiology 40,102-112.
710 Brault, S., Stuart, C.T., Wagstaff, M.C., Rex, M.A., 2013. Geographic evidence for source-sink
711 dynamics in deep-sea neogastropods of the eastern North Atlantic: an approach using nested
712 analysis. Glob. Ecol. Biogeogr. 22, 433–39.
713 Colwell, R.K., Chao, A., Gotelli, N.J., Lin, S.Y., Mao, C.X., Chazdon, R.L., Longino, J.T.,
714 2012. Models and estimators linking individual-based and sample-based rarefaction,
715 extrapolation and comparison of assemblages. J. Plant Ecol. 5, 3–21.
716 Connolly, S.R., MacNeil, M.A., Caley, M.J., Knowlton, N., Cripps, E., Hisano, M., Thibaut,
717 L.M., Bhattacharya, B.D., Benedetti-Cecchi, L., Brainard, R.E., Brandt, A., Bulleri, F.,
718 Ellingsen, K.E., Kaiser, S., Kröncke, I., Linse, K., Maggi, E., O'Hara, T.D., Plaisance, L.,
719 Poore, G.C.B., Sarkare, S.K., Satpathy, K.K., Schückel, U., Williams, A., Wilson, R.S.,
720 2014. Commonness and rarity in the marine biosphere. Proc. Natl. Acad. Sci. 111, 8524-
721 8539.
722 Cornelius , N., Gooday, A.J., 2004. 'Live' (stained) deep-sea benthic foraminifera in the western
723 Weddell Sea: Trends in abundance, diversity and taxonomic composition in relation to
724 water depth Deep-Sea Res. II 51, 1571-1602.
725 De Smet, B., Pape, E., Riehl, T., Bonifacio, P., Colson, L., Vanreusel, A., 2017. The community
726 structure of deep-sea macrofauna associated with polymetallic nodules in the eastern part of
727 the Clarion-Clipperton Fracture Zone. Front. Mar. Sci. 4, 103.
728 https://hdl.handle.net/10.3389/fmars.2017.00103.
729 Enge, A.J., Kucera, M., Heinz, P., 2012. Diversity and microhabitats of living benthic
730 foraminifera in the abyssal Northeast Pacific. Mar. Micropal. 96–97, 84–104.
731 George, K.H., Veit-Köhler, G., Martinez Arbizu, P., Sifried, S., Rose, A.,Willen, E.,Bröhldick,
732 K., Corgosinho, P.H., Drewes, J., Menzel, L., Moura, G., Schminke, H.K., 2013.
733 Community structure and species diversity of Harpacticoida (Crustacea:Copepoda) at two
734 sites in the deep sea of the Angola Basin (Southeast Atlantic). Org. Divers. Evol. http://doi.
735 10.1007/s13127-013-0154-2.
736 Glover, A.G., Smith, C.R., Paterson, G.L.J., Wilson, G.D.F., Hawkins, L., Sheader, M., 2002.
737 Polychaete species diversity in the central Pacific abysd: local and regional patterns, and
738 relationships with productivity. Mar. Ecol. Prog. Ser. 240, 157-170.
739 Glover, A.G., Gooday, A.J., Bailey, D.M., Billett, D.S.M., Chevaldonné, P., Colaço, A., Copley,
740 J., Cuvelier, D., Desbruyères, D., Kalogeropoulou, V., Klages, M., Lampadariou, N.,
741 Lejeusne, C., Mestre, N.C., Paterson, G.L.J., Perez, T., Ruhl, H., Sarrazin, J., Soltwedel, T.,
742 Soto, E.H., Thatje, S., Tselepides, A., Van Gaever, S., Vanreusel, A., 2010. Temporal
743 change in deep-sea benthic ecosystems: a review of the evidence from recent time-series
744 studies. Adv. Mar. Biol. 58, 1-95.
745 Glover, A.G., Dahlgren, T.G., Wiklund, H., Mohrbeck, I., Smith, C.R., 2016. An end-to-end
746 DNA taxonomy methodology for benthic biodiversity survey in the Clarion- Clipperton
747 Zone, central Pacific abyss. J. Mar. Sci. Eng. http://dx.doi.org/10.3390/jmse4010002.
748 Goineau, A., Gooday, A.J., 2017. Novel benthic foraminifera are abundant and diverse in an area
749 of the abyssal equatorial Pacific licensed for polymetallic nodule exploration. Sci. Rep. 7,
750 45288, http://doi.10.1038/srep45288.
751 Gooday, A.J., 1986. Meiofaunal foraminiferans from the bathyal Porcupine Seabight (northeast
752 Atlantic): size structure, standing stock, taxonomic composition, species diversity and
753 vertical distribution in the sediment. Deep-Sea Res. 33, 1345-1373.
754 Gooday, A.J., 1996. Epifaunal and shallow infaunal foraminiferal communities at three abyssal

NE Atlantic sites subject to differing phytodetritus input regimes. Deep-Sea Res. I 43, 1395-1421.

Gooday, A.J., 2002. Biological responses to seasonally varying fluxes of organic matter to the ocean floor: a review. J. Oceanogr. 58, 305-332.

Gooday, A.J., 2003. Benthic foraminifera (Protista) as tools in deep-water palaeoceanography: a review of environmental influences on faunal characteristics. Adv. Mar. Biol. 46**,** 1-90.

Gooday, A.J., 2019. Deep-sea benthic foraminifera, Chapter 09071 in: Cochran, J.K., Bokuniewicz, H., Yager, P. (Eds.), Encyclopedia of Ocean Sciences, 3rd Edition, Academic Press. https://doi.org/10.1016/B978-0-12-409548-9.09071-0.

Gooday, A.J., Goineau, A., 2019. The Contribution of Fine Sieve Fractions (63–150 mm) to Foraminiferal Abundance and Diversity in an Area of the Eastern Pacific Ocean Licensed for Polymetallic Nodule Exploration. Front. Mar. Sci. http://doi:10.3389/fmars.2019.00114

Gooday, A.J., Jorissen, F.J., 2012. Benthic foraminiferal biogeography: controls on global distribution patterns in deep-water settings. Ann. Rev. Mar. Sci. 4, 237–62.

Gooday, A.J., Rathburn, A.E., 1999.Temporal variability in living deep-sea benthic foraminifera: a review. Earth-Sci. Rev. 46, 187–212.

Gooday, A.J., Goineau, A., Voltski, I., 2015. Abyssal foraminifera attached to polymetallic nodules from the eastern Clarion Clipperton Fracture Zone: a preliminary description and comparison with North Atlantic dropstone assemblages. Mar. Biodiv. 45,. 391-412. http://doi.10.1007/s12526-014-0301-9

Gooday, A.J., Holzmann, M., Caulle, C., Goineau, A., Kamenskaya, O.E., Weber, A.A.T., Pawlowski, J., 2017. Giant foraminifera (xenophyophores) are exceptionally diverse in parts of the abyssal eastern Pacific where seabed mining is likely to occur. Biol. Conserv. 207, 106–116. https://doi.org/10.1016/j.biocon.2017.01.006.

Gooday, A.J., Levin, L.A., Linke, P., Heeger, T., 1992. The role of benthic foraminifera in deep-sea food webs and carbon cycling, in: Rowe, G.T. Pariente, V. (Eds), Deep-Sea Food Chains and the Global Carbon Cycle. Kluwer Academic Publishers, pp. 63-91.

Gooday, A.J., Nomaki, H., Kitazato, H., 2008. Modern deep-sea benthic foraminifera: a brief review of their biodiversity and trophic diversity, in: Austin, W. E. N., James, R. H. (Eds) Biogeochemical Controls on Palaeoceanographic Environmental Proxies. Geological Society, London, Special Publications 303, 97–119. http://doi:10.1144/SP303.8 0305-8719/08/

Gooday, A.J., Nozawa, F., Ohkawara, N., Kitazato, H., 2006. Foraminifera. ISA Technical Study No. 3, 10-14.

Gooday, A.J., Malzone, M.G., Bett, B.J., Lamont, P.A., 2010. Decadal-scale changes in shallow-infaunal foraminiferal assemblages at the Porcupine Abyssal Plain, NE Atlantic. Deep-Sea Res. II 57, 1362–1382.

Hannides, A., Smith, C.R., 2003. The northeast abyssal Pacific plain, in: Black, K.B., Shimmield, G.B. (Eds.), Biogeochemistry of Marine Systems. Boca Raton, FL: CRC Press, pp. 208-237.

Hein, J.R., Mizell, K., Koschinsky, A., Conrad, T.A., 2013. Deep-ocean mineral deposits as a source of critical metals for high- and green-technology applications: comparisons with land-based resources. Ore Geol. Rev. 51, 1-14.

Holbourn, A., Henderson, A., McLeod, N., 2013. Atlas of Benthic Foraminifera. Wiley-Blackwell.

Hortal, J., Borges, P.A.V., Gaspar, C., 2006. Evaluating the performance of species richness estimators: sensitivity to sample grain size. J. Anim. Ecol. 75, 274–287.

Hughes, J.A., Gooday, A.J., 2004. The influence of dead *Syringammina fragilissima* (Xenophyophorea) tests on the distribution of benthic foraminifera in the Darwin

Mounds region (NE Atlantic). Deep-Sea Res. I, 51**,** 1741-1758.
Janssen, A., Kaiser, S., Meissner, K., Brenke, N., Menot, L., Martinez Arbizu, P., 2015. A reverse taxonomic approach to assess macrofaunal distribution patterns in abyssal Pacific polymetallic nodule fields. PLoS One 10 (2): e0117790.
Jensen, P., 1982. A new meiofaunal splitter. Ann. Zool. Fennici 19, 233-236.
Jones, D.O.B., Amon, D.J., Chapman, A.S.A., 2017. Mining deep-ocean deposits: what are the ecological risks. Elements 14, 325-330.
Jones, R.W., 2014. Foraminifera and their Applications, Cambridge University Press, Cambridge.
Jones, R.W., 1994. The Challenger Foraminifera, Oxford University Press Oxford.
Jorissen, F., Fontanier, C., and Thomas, E. 2007. Paleoceanographical proxies based on deep-sea benthic foraminiferal assemblage characteristics, in: Hillaire-Marcel, C., de Vernal, A.: Proxies in Late Cenozoic Paleoceanography, Elsevier, Amsterdam, Boston, Heidelberg, London, New York, Oxford, Paris, San Diego, San Francisco, Singapore, Sydney, Tokyo, pp. 263-325.
Jumars, P.A., 1975a. Methods for measurement of community structure in deep-sea macrobenthos. Mar. Biol. 30, 245-252.
Jumars, P.A., 1975b. Environmental grain and polychaete species' diversity in a bathyal benthic community Mar. Biol. 30, 253-266.
Kamenskaya, O.E., Gooday, A.J., Radziejewska, T., Wawrzyniak-Wydrowska, B., 2012. Large, enigmatic foraminiferan-like protists in the eastern part of the Clarion-Clipperton Fracture Zone (abyssal eastern equatorial Pacific): biodiversity and vertical distribution in the sediment. Mar. Biodiv. 42, 311-327. DOI: 10.1007/s12526-012-0114-7.
Kurbjeweit, F., Schmiedl, G., Schiebel, R., Hemleben, Ch., Pfannkuche, O., Wallmann, K., Schäfer, P., 2000. Distribution, biomass and diversity of benthic foraminifera in relation to sediment geochemistry in the Arabian Sea. Deep-Sea Res. II 47, 2913-2955.
Lecroq, B., Gooday, A.J., Pawlowski, J., 2009. Global genetic homogeneity in the deep-sea foraminiferan *Epistominella exigua* (Rotaliida: Pseudoparrellidae). Zootaxa 2096, 23–32
Leduc, D., Rowden, A.A., Probert, P. K., Pilditch, C.A., Nodder, S.D., Vanreusel,A., Duineveld, G.C.A., Witbaard, R., 2012. Further evidence for the effect of particle-size diversity on deep-sea benthic biodiversity. Deep-Sea Res. I 13, 164-169.
Levin, L.A., C.L. Thomas, 1988. The ecology of xenophyophores (Protista) on eastern Pacific seamounts. Deep-Sea Res. 35, 2003-2027.
Levin, L.A., Mengerlink, K., Gjerde, K.M., Rowden, A.A., Van Dover, C.L., Clark, M.R., Ramirez-Llodra, Currie, B., B., Smith, C.R., Sato, K.N., Gallo, N., Sweetman, A.K., Lily, H., Armstrong, C.W., Brider, J., 2016. Defining ‘serious harm’ to the marine environment in the context of deep-seabed mining. Mar. Policy. 74, 245-259.
Lodge, M., Johnson, D., Le Gurun, G., Wengler, M., Weaver, P., Gunn, V., 2014. Seabed mining: International Seabed Authority environmental management plan for the Clarion-Clipperton Zone. Mar. Policy 49, 66-72.
Lodge, M., Verlaan, P.A., 2018. Deep-sea mining: international regulatory challenges and responses. Elements 14, 331-336.
Magurran, A.E, 2004. Measuring Biological Diversity. Blackwell Science, Maldon, Oxford, Carleton.
McClain, C.R, Nekola, J.C., Kuhnz, L., Barry, J.M., 2011. Local-scale faunal turnover on the deep Pacific seafloor. Mar. Ecol. Prog. Ser. 422, 193–200.
McClain, C.R., Hardy, S.M., 2010. The dynamics of biogeographic ranges in the deep sea. Proc. R. Soc. B 277, 3533–3546. doi:10.1098/rspb.2010.1057.
McClain, C.R., Rex, M.A., 2015. Toward a conceptual understanding of β-diversity in the deep-sea benthos. Annu. Rev. Ecol. Evol. Syst. 46, 623–642.

McClain, C.R., Schlacher, T.A. 2015. On some hypotheses of animal life at great depths on the sea floor. Mar. Ecol. 36, 849-872.

Menzel, L., George, K.H., Martinez Abizu, P., 2011. Submarine ridges do not prevent large-scale dispersal of abyssal fauna: A case study of *Mesocletodes* (Crustacea, Copepoda, Harpacticoida). Deep-Sea Res. I 58, 839–864.

Miljutina, M.A., Miljutin, D.M., Mahatma, R., Galéron, J., 2010. Deep-sea nematode assemblages of the Clarion-Clipperton Nodule Province (Tropical North-Eastern Pacific). Mar. Biodiv. 40, 1-15. Doi:10:1007/s12526-009-0029-0.

Miller, K.A., Thompson, K.F., Johnston, P., Santillo, D., 2018. An overview of seabed mining including the current state of development, environmental impacts, and knowledge gaps. Front. Mar. Sci. 4, 418. http://doi:10.3389/fmars.2017.00418.

Morgan, C., 2012. A geological model of polymetallic nodule deposits in the Clarion-Clipperton fracture Zone. ISA Briefing Paper 1/12, International Seabed Authority, Kingston Jamaica, 12p.

Mullineaux, L.S., 1987. Organisms living on manganese nodules and crusts: distribution and abundance at three North Pacific sites. Deep-Sea Res. 34. 165-184.

Murray, J. W. 2000. The enigma of the continued use of total assemblages in ecological studies of benthic foraminifera. J. Foram. Res. 30, 244–45.

Murray, J.W., 2006. Ecology and applications of benthic foraminifera, Cambridge University Press Cambridge, New York, Melbourne, Madrid, Cape Town, Singapore, São Paulo.

Murray, J.W., 2007. Biodiversity of living benthic foraminifera: How many species are there? Mar. Micro. 64, 163-176.

Murray, J.W., Bowser, S.S., 2000. Mortality, protoplasm decay rate, and reliability of staining techniques to recognize 'living' foraminifera: a review. Micropaleontology 30, 66–77.

Nozawa, F., Kitazato, H.,Tsuchiya, M., Gooday, A.J., 2006. 'Live' benthic foraminifera at an abyssal site in the equatorial Pacific nodule province: abundance, diversity and taxonomic composition. Deep-Sea Res. I 53, 1406–1422.

Pape, E., Bezerra, T.N., Hauquier, F., Vanreusel, A**.,** 2017. Limited spatial and temporal variability in meiofauna and nematode communities at distant but environmentally similar sites in an area of interest for deep-sea mining. Front. Mar. Sci. 4, 205, http://doi .org/10.3389/fmars.2017.00205.

Paterson, G.L.J., Wilson, G.D.F., Cosson, N., Lamont, P.A., 1998. Hessler and Jumars (1974) revisited: abyssal polychaete assemblages from the Atlantic and Pacific. Deep-Sea Res. II 45, 225-251.

Pawlowski, J., Fahrni J., Lecroq B., Longet, D., Cornelius, N., Excoffier, L., Cedhagen T., Gooday A. J., 2007. Bipolar gene flow in deep-sea benthic foraminifera. Mol. Ecol. 16, 4089–4096.

Phipps, M., Jorissen, F., Pusceddu, A., Bianchelli, S., De Stigter, H., 2012. Live benthic foraminiferal faunas along a bathymetrical transect (282–4987 m). on the Portuguese margin (NE Atlantic). J. Foramin. Res. 42, 66-81.

Radziejewska, T., 2014. Meiobenthos in the sub-equatorial Pacific Abyss: a proxy in anthropogenic impact evaluation. Springer, Heidelberg, New York, Dordrecht, London.

Radziejewska, T., Gooday, A.J., Koltan, M., Szyrwiel, E., 2006. Deep-sea non-calcareous foraminifera: some examples from the Pacific abyssal nodule field. Meiofauna Marina 15, 3–10.

Rex, M.A., Etter, R.J., 2010. Deep-Sea Biodiversity: Patterns and Scale. Harvard University Press, Cambrodge, Massachusetts, London, England.

Rex, M.A., McClain, C.R., Johnson, N.A., Etter, R.J., Allen, J.A., Bouchet, P., Warén, A.. 2005. A source–sink hypothesis for abyssal biodiversity. Am. Nat. 165,163–78.

Simon-Lledó, E., Bett, B.J., Huvenne, V.A.I., Schoening, T., Benoist, N.M.A., Jeffreys, R.M.,

Durden, J.M., Jones, D.O.B., 2019. Megafaunal variation in the abyssal landscape of the Clarion-Clipperton Zone. Prog. Oceanogr. 170, 119–133. https://doi.org/10.1016/j.pocean.2018.11.003

Singh, R., Mijulin, D.M., Vanreusel, A., Radziejewska, T., Miljutina, M.M., Tchesunov, A., Bussau, C., Galtsova, V., Martinez Arbizu, P., 2016. Nematode communities inhabiting the soft deep-sea sediment in polymetallic nodule fields: do they differ from those in the nodule-free abyssal areas? Mar. Biol. Res. 12, 345-359. http://doi:10.1080/17451000.2016.1148822.

Smith, C.R., Demopoulos, A.W.J., 2003. The deep Pacific Ocean floor, in: Tyler, P.A. (Ed.), Ecosystems of the Deep Oceans. Ecosystems of the World 28. Elsevier, Amsterdam, Boston, London, New York, Oxford, Paris, San Diego, San Francisco, Singapore, Sydney, Tokyo, pp. 179-218.

Snelgrove, P.V.R., Smith, C.R., 2002. A riot of species in an environmental calm: the paradox of the species-rich deep-sea floor. Oceanogr. Mar. Biol. 40, 311-342.

Snider, L.J., Burnett, B.R., Hessler, R.R., 1984. The composition and distribution of meiofauna and nanobiota in a central North Pacific deep-sea area. Deep-Sea Res. 31, 1225-1249.

Taylor, M.L., Roterman, C.N., 2017. Invertebrate population genetics across the Earth's largest habitat: the deep-sea floor. Mol. Ecol. http://doi:10.1111/mec.14237.

Tendal,O.S., Hessler, R.R., 1977. An introduction to the biology and systematic of Komokiacea. Galathea Rep. 14, 165–194.

Tittensor, D.P., Schlacher, T., Smith, C.R., Susko, E., 2010. Endemism at low sampling effort: real or artefact? In: Svavarsson, J., Halldórsson, H.P., □órðarson, S., dos Santos, E., 2010. 12th International Deep-Sea Biology Symposium, Reykjavik, Iceland, 7-11 June, 2010. Symposium Program and Book of Abstracts, pp. 84-85.

Saidova, Kh. M., 1966. Benthic foraminiferal faunas of the Pacific. Oceanology 6, 222-227.

Saidova, Kh. M., 1981. Recent benthic foraminiferal communities of the Pacific abyssal plains. Oceanology 21, 259-262.

Veillette, J., Sarrazin, J., Gooday, A.J., Galéron, J., Caprais, J.-C., Vangriesheim, A., Étoubleau, J., Christian, J.R., Juniper, S.K., 2007. Ferromanganese nodule fauna in the Tropical North Pacific Ocean: species richness, faunal cover and spatial distribution. Deep-Sea Res. I, 54, 1912-1935.

Walton W.R., 1955. Ecology of living benthonic foraminifera, Todos Santos Bay, Baja California. J. Paleontol. 29, 952-1018.

Wedding, L.M., Friedlander, A.M., Kittinger, J.N., Watling, L., Gaines, S.D., Bennett, M., Hardy, S.M., Smith, C.R., 2013. From principles to practice: a spatial approach to systematic planning in the deep sea. Proc. Roy. Soc. B 280, 20131684. http://dx.doi.org/10.1098/rspb.2013.1684.

Wedding, L.M., Reiter, S.M., Smith, C.R., Gerde, K.M., Kittinger, J.N. Friedlander, A.M., Gaines, S.D., Clark, M.R., Thurnherr, A.M., Hardy, S.M., Crowder, L.B., 2015. Managing mining of the deep seabed. Science 349, 144-145.

Wilson, G.D.F., 2017. Macrofauna abundance, species diversity and turnover at three sites in the Clipperton-Clarion Fracture Zone. Mar. Biodiv. 47, 323. http://doi.org/10.1007/s12526-016-0609-8.

949 **Figure 1**. Sampling localities in the eastern equatorial Pacific investigated in the present study
950 (UK1, OMS) and in earlier publications: Global Sea mineral Resources (GSR; Pape et al., 2017),
951 Interoceanmetal Joint Organisation (IOM: Radziejewska et al., 2006); Kaplan East (KE =
952 Kaplan East: Nozawa et al., 2006).
953
954 **Figure 2**: Representive morphospecies. *Reophax* sp. 5 incorporating red mineral grains;UK1A
955 Stratum, sample MC07 (A). *Deuterammina* aff. *grahami* Brönnimann and Whittaker 1988;
956 UK1A Stratum, sample MC07 (B). Monothalamid sp. 85, radiolarian inhabitant with a tube, the
957 second-ranked species overall but more or less confined to UK1B Stratum, sample MC25 (C,D).
958 Tube sp. 73; UK1B Stratum, sample MC13 (E). *Rhizammina* aff. *algaeformis*; OMS Stratum,
959 sample MC22 (F). *Rhizammina* sp. 5; UK1B Stratum, sample MC05 (G). *Baculella* aff. *hirsuta*;
960 OMS Stratum, stratum MC22 (H). Tube sp.8/49; UK1B Stratum, sample MC05 (I).
961
962 **Figure 3**: Number of 'new' species (i.e., those encountered for the first time) in each sample
963 (dotted line), and cumulative number of species added with the addition of new samples (full
964 line).
965
966 **Figure 4**: Total numbers of species recognised in the 3 strata (S) and estimated number of
967 species for the entire assemblage (ACE, Chao1, Jack 1, Jack 2). Abundance-based estimators
968 ACE and Chao1 were calculated based on complete specimens, live and dead combined;
969 incidence-based estimators Jacknife 1 and 2 ('Jack 1', 'Jack 2') were calculated based on
970 complete specimens and fragments, live and dead combined.
971
972 **Figure 5**: Multidimensional scaling (MDS) plots of the eleven samples based on Bray-Curtis
973 similarity indices computed with species presence-absence data and species relative abundances,
974 for the entire assemblage and for multichambered species only. Dotted ellipses are 95%
975 confidence regions of the samples. Samples MC02, MC05, MC07 and MC11 are from UK1
976 Stratum A, samples MC05, MC13 and MC25 are from UK1 Stratum B, and samples MC20,
977 MC21 and MC22 are from the OMS Stratum.
978
979 **Figure 6:** Similarity between samples with increasing distance, based on Bray-Curtis similarity
980 indices (Log_{10}) computed with species presence–absence data (live and dead complete
981 specimens, live and dead fragments). The open symbols refer to comparisons of samples within
982 a stratum, the filled symbols to comparisons of samples between strata. Within stratum and
983 between stratum values are significantly ($p < 0.05$) different only in the case of the UK1A vs
984 OMS comparison.
985
986 **Figure 7**: Species shared between samples or strata and confined to one single sample or
987 stratum. Five samples from UK1A Stratum (A). Three samples from UK1B Stratum (B). Three
988 samples from OMS Stratum (C). The three strata (D). The filled circles represent samples (A-C)
989 or strata (D). Bold values = total number of species recognised in the corresponding sample or
990 stratum; central underlined values = number of species occurring in all samples within a stratum
991 (A-C) or all strata (D); italicised values = number of species shared between samples or strata;
992 values in brackets = number of species confined to the corresponding sample or stratum.
993
994 **Figure 8.** Number of species (ignoring singletons) represented by stained + dead specimens,
995 arranged by the number of samples in which they occur (from 1 to11). A) Number of species. B)
996 Percentage of species. See Supplementary Fig. S8 for a version of this figure that includes data
997 for the stained and dead assemblages.
998

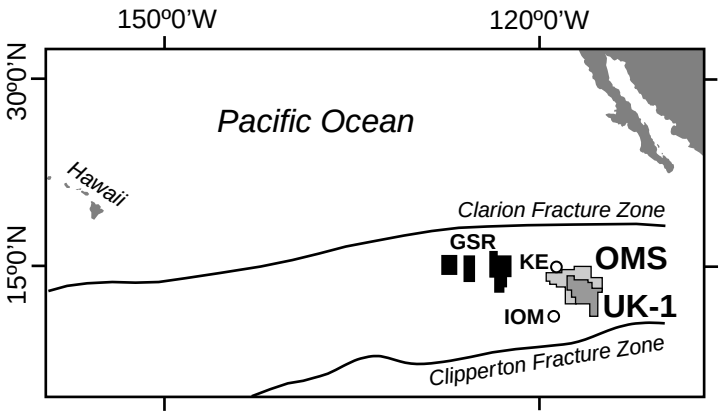
150º0'W
120º0'W
30º0'N
15º0'N
Pacific Ocean
Hawaii
Clarion Fracture Zone
GSR
KE
OMS
UK-1
IOM
Clipperton Fracture Zone

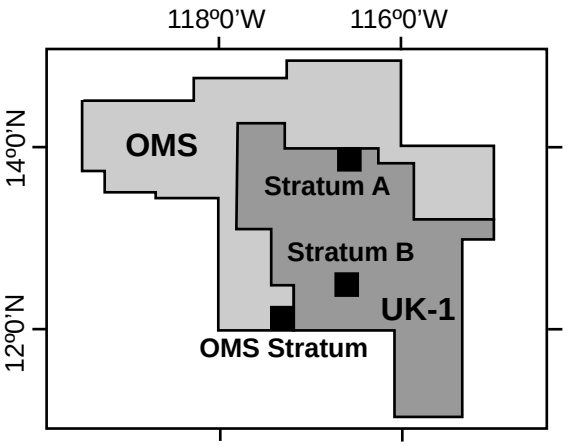
118º0'W
116º0'W
14º0'N
12º0'N
OMS
Stratum A
Stratum B
UK-1
OMS Stratum

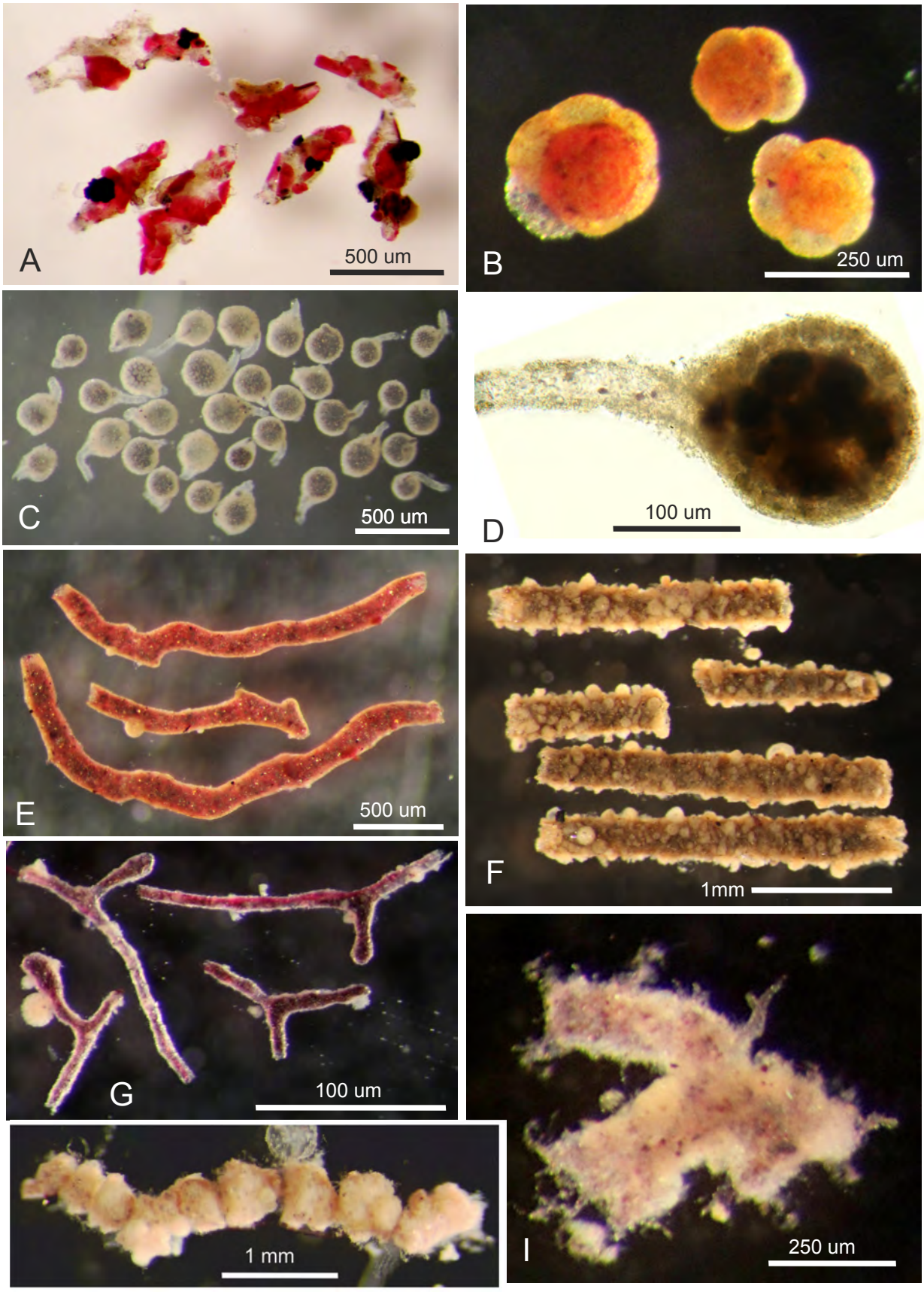
A
500 um
B
250 um
C
500 um
D
100 um
E
500 um
F
1mm
G
100 um
1 mm
I
250 um

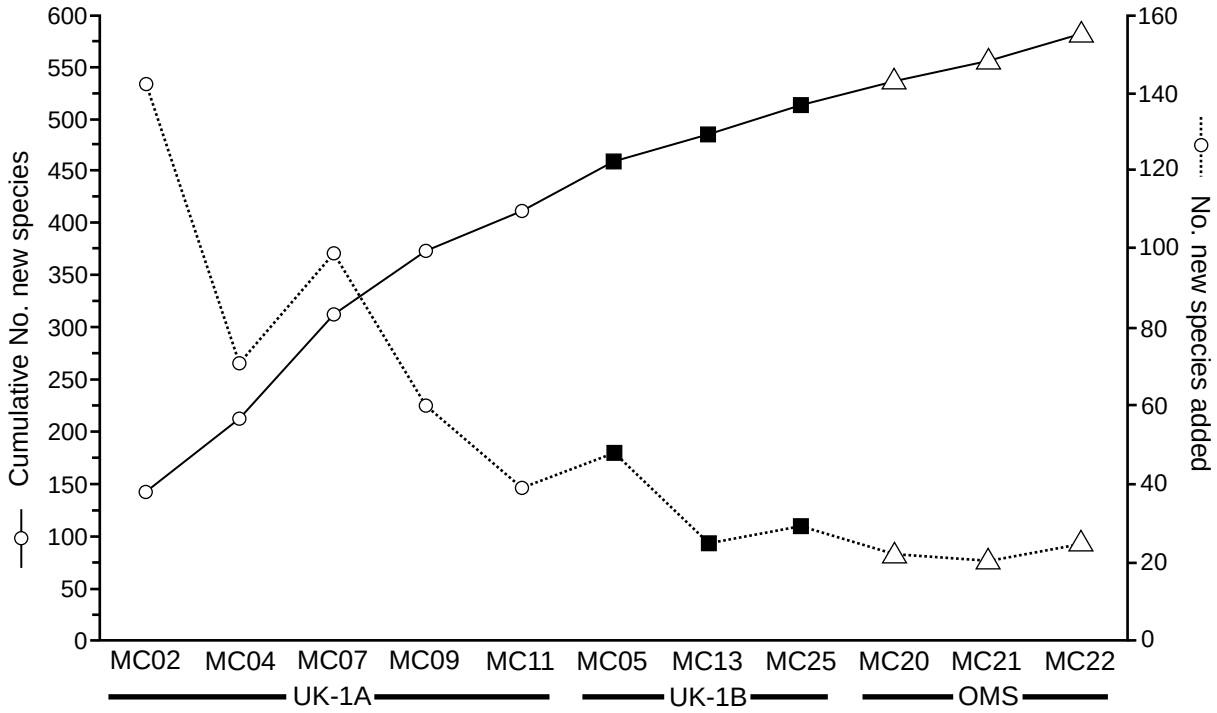
Cumulative No. new species
No. new species added
600
550
500
450
400
350
300
250
200
150
100
50
0
160
140
120
100
80
60
40
20
0
MC02
MC04
MC07
MC09
MC11
MC05
MC13
MC25
MC20
MC21
MC22
UK-1A
UK-1B
OMS

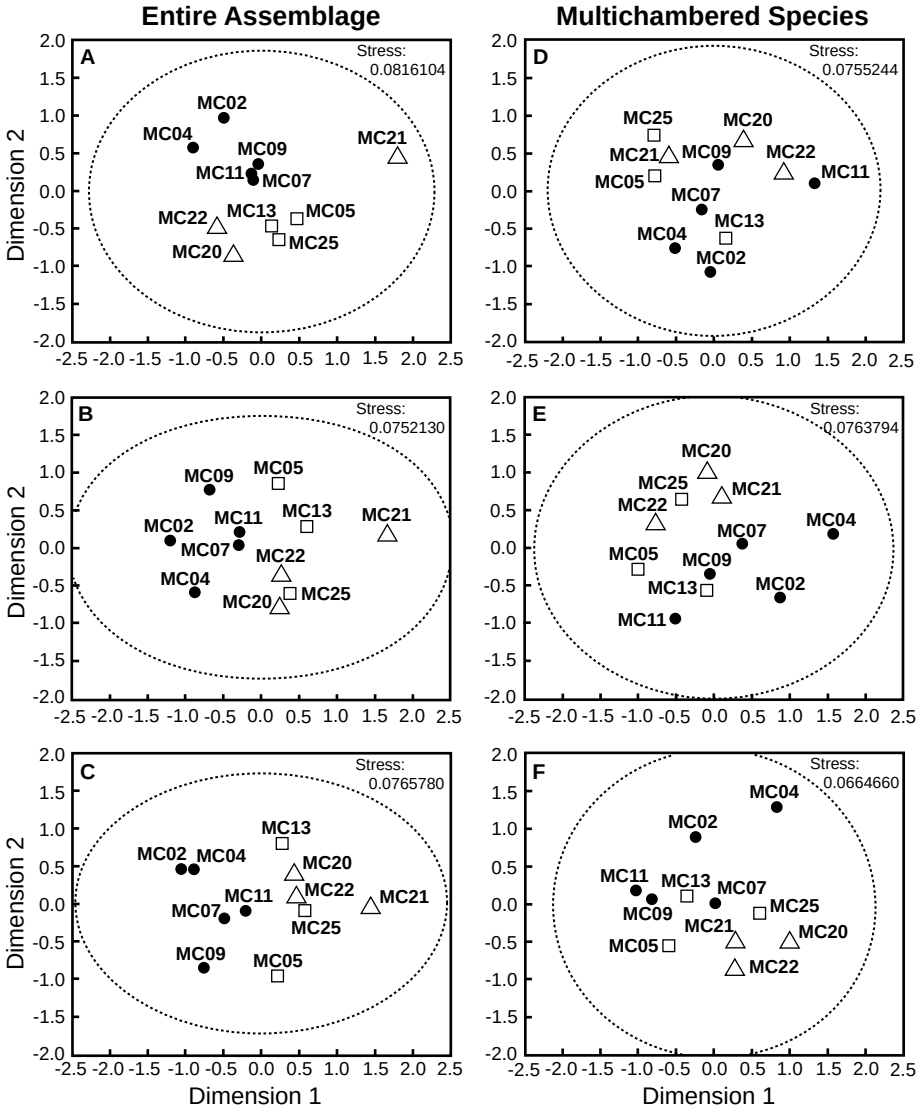
Entire Assemblage
Multichambered Species
A
Stress: 0.0816104
MC02
MC04
MC09
MC21
MC11
MC07
MC22
MC13
MC05
MC25
MC20
D
Stress: 0.0755244
MC25
MC20
MC21
MC09
MC22
MC11
MC05
MC07
MC13
MC04
MC02
B
Stress: 0.0752130
MC09
MC05
MC02
MC11
MC13
MC21
MC07
MC22
MC04
MC20
MC25
E
Stress: 0.0763794
MC20
MC25
MC21
MC22
MC04
MC07
MC05
MC09
MC13
MC02
MC11
C
Stress: 0.0765780
MC13
MC02
MC04
MC20
MC22
MC11
MC21
MC07
MC25
MC09
MC05
F
Stress: 0.0664660
MC04
MC02
MC11
MC13
MC07
MC09
MC25
MC21
MC20
MC05
MC22
Dimension 2
Dimension 1

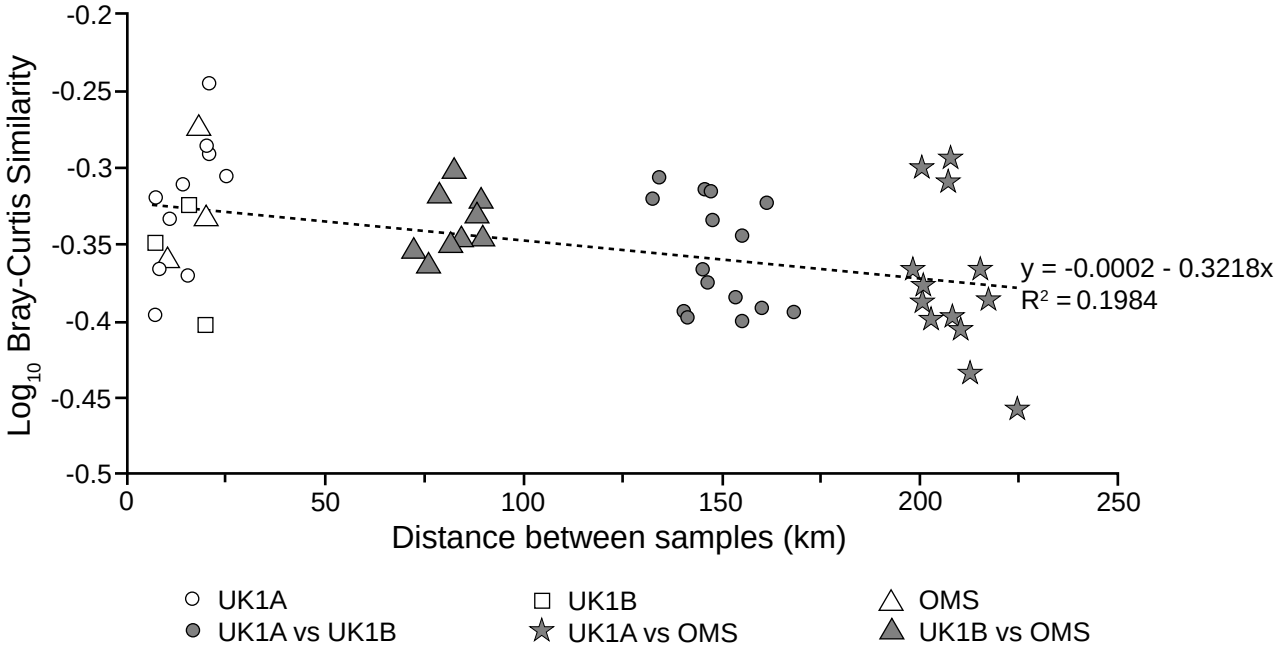
-0.2
-0.25
-0.3
-0.35
-0.4
-0.45
-0.5
Log10 Bray-Curtis Similarity
0
50
100
150
200
250
Distance between samples (km)
y = -0.0002 - 0.3218x
R2 = 0.1984
UK1A
UK1B
OMS
UK1A vs UK1B
UK1A vs OMS
UK1B vs OMS

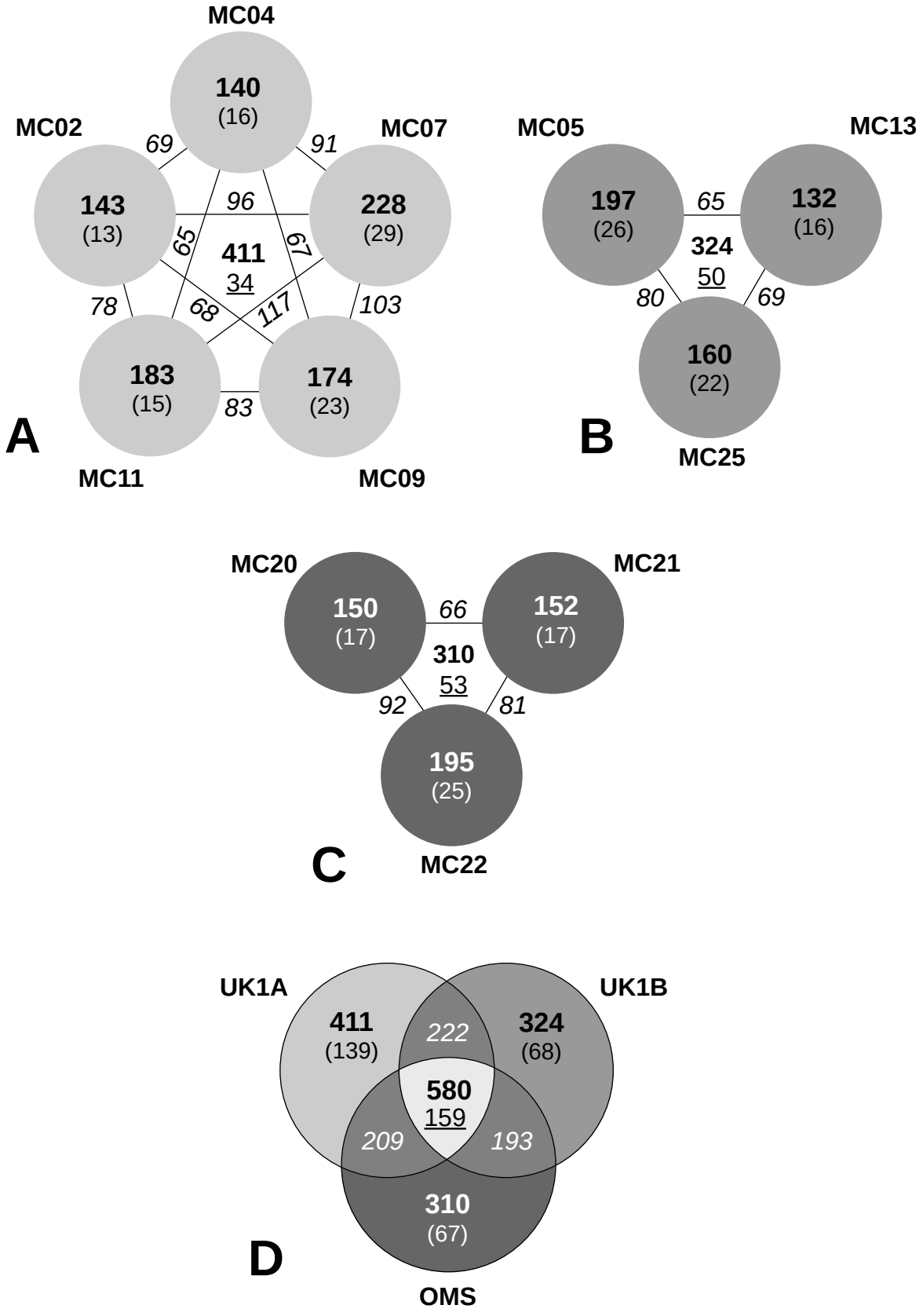
MC04
140
(16)
MC02
MC07
69
91
143
(13)
96
228
(29)
65
67
411
34
78
68
117
103
183
(15)
174
(23)
83
A
MC11
MC09
MC05
MC13
197
(26)
65
132
(16)
324
50
80
69
160
(22)
B
MC25
MC20
MC21
150
(17)
66
152
(17)
310
53
92
81
195
(25)
C
MC22
UK1A
UK1B
411
(139)
222
324
(68)
580
159
209
193
310
(67)
D
OMS

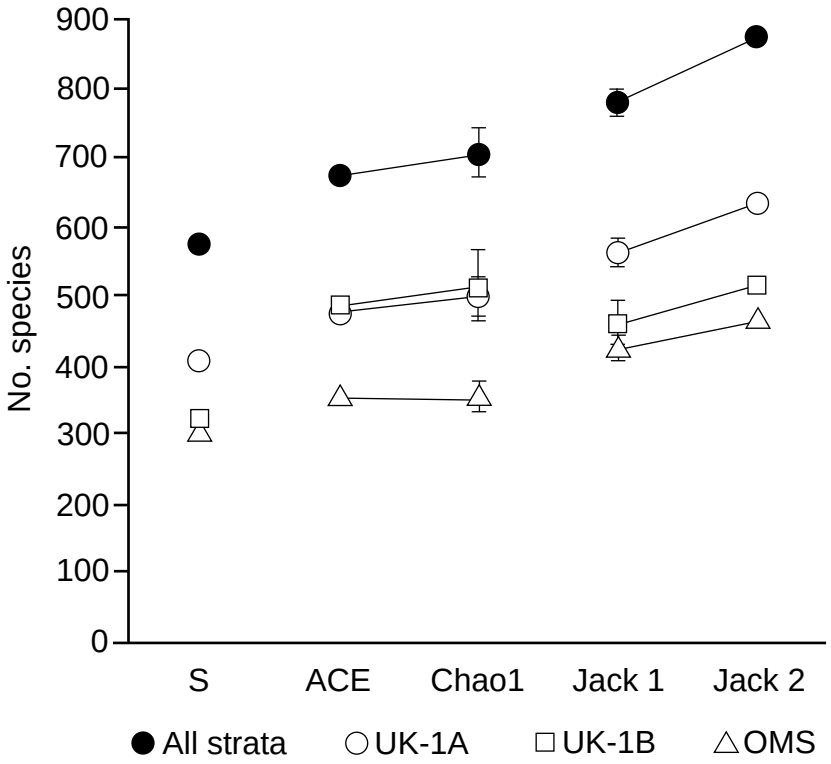
900
800
700
600
500
400
300
200
100
0
No. species
S
ACE
Chao1
Jack 1
Jack 2
All strata
UK-1A
UK-1B
OMS

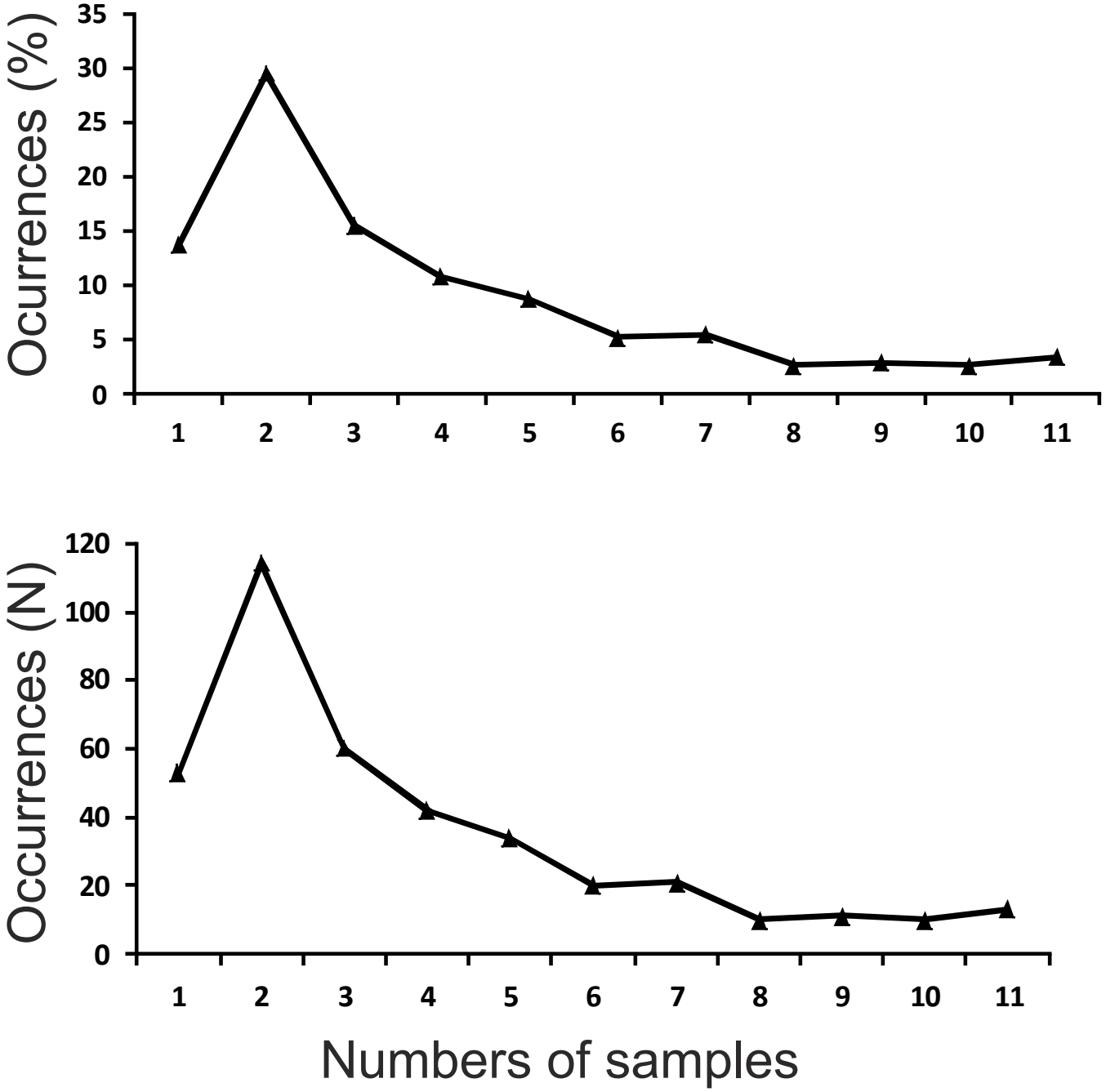
Ocurrences (%)
35
30
25
20
15
10
5
0
1
2
3
4
5
6
7
8
9
10
11
Occurrences (N)
120
100
80
60
40
20
0
1
2
3
4
5
6
7
8
9
10
11
Numbers of samples

Table 1. Station data for the eleven investigated sampling sites in the UK1A, UK1B and OMS strata. MC = megacorer.

Strata	Sampling sites	Samples	Latitude (°N)	Longitude (°W)	Water depth (m)
UK1A	B	MC02	13°50.792’	116°37.59’	4079
	D	MC04	13°57.796’	116°34.093’	4084
	G	MC07	13°45.706’	116°27.601’	4111
	H	MC09	13°53.299’	116°41.399’	4150
	J	MC11	13°54.104’	116°35.401’	4166
UK1B	U04	MC05	12°34.738’	116°43.425’	4235
	U07	MC13	12°27.056’	116°35.669’	4129
	U15	MC25	12°34.953’	116°39.060’	4224
OMS	S07	MC20	12°8.160’	117°12.897’	4110
	S10	MC21	12°3.273’	117°15.097’	4051
	S08	MC22	12°11.409’	117°22.284’	4179

Table 2. Abundance and density of 'live' (stained) complete and fragmented foraminiferal specimens (without xenophyophores and gromiids) in the 0–1 cm layer (>150-µm fraction) of individual samples and strata. Densities for individual strata and 'Total' are averaged values of samples within the corresponding stratum. 'No.' = actual number of individuals; 'Dens.' = number of individuals per 10 cm².

		'Live' complete		'Live' fragments		Dead complete		Dead fragments	
Sample	Splits	No.	Dens.	No.	Dens.	No.	Dens.	No.	Dens.
MC02	8/8	657	84	226	29	195	25	29	4
MC04	8/8	557	71	174	22	203	26	78	10
MC07	8/8	966	123	763	97	263	33	138	18
MC09	3/8	514	132	143	37	110	28	54	14
MC11	3/8	687	146	456	97	170	36	223	48
UK1-A mean		*676*	*111*	*352*	*56*	*188*	*30*	*104*	*19*
MC05	4/8	511	85	330	55	177	30	128	21
MC13	4/8	302	68	334	76	141	32	120	27
MC25	4/8	588	165	103	29	201	57	110	31
UK1-B mean		*467*	*106*	*256*	*53*	*173*	*40*	*119*	*26*
MC20	3/8	448	113	115	29	290	73	207	69
MC21	7/8	222	30	83	11	197	27	53	7
MC22	3/8	877	171	485	94	235	46	236	46
OMS mean		*516*	*105*	*228*	*45*	*241*	*49*	*165*	*41*
TOTAL mean		**575**	**103**	**272**	**51**	**198**	**39**	**125**	**29**

Table 3. Absolute and relative abundances of stained (L = 'live') and stained + dead complete specimens of the major taxa/groups in the three Strata. Xenophyophore fragments and gromiids are excluded.

Stratum	UK1A				UK1B				OMS				3 strata			
Morphological groupings	L	%	L+D	%	L	%	L+D	%	L	%	L+D	%	L	%	L+D	%
Multichambered																
Robertinids	2	*0.1*	2	*0.05*	1	*0.1*	1	*0.1*	1	*0.1*	1	*0.04*	4	*0.1*	4	*0.05*
Rotaliids	76	*2.2*	116	*2.7*	21	*1.5*	37	*1.9*	31	*2.0*	96	*4.2*	128	*2.0*	249	*2.9*
Lagenids	5	*0.1*	9	*0.2*	0	*0.0*	1	*0.1*	1	*0.1*	2	*0.1*	6	*0.1*	12	*0.1*
Miliolids	21	*0.6*	25	*0.6*	4	*0.3*	7	*0.4*	3	*0.2*	13	*0.6*	28	*0.4*	45	*0.5*
Ammodiscids	4	*0.1*	36	*0.8*	4	*0.3*	15	*0.8*	4	*0.3*	20	*0.9*	12	*0.2*	71	*0.8*
Hormosinids	201	*5.9*	402	*9.3*	101	*7.2*	203	*10.6*	128	*8.3*	259	*11.4*	430	*6.8*	864	*10.2*
Trochamminids	14	*0.4*	66	*1.5*	3	*0.2*	23	*1.2*	11	*0.7*	37	*1.6*	28	*0.4*	126	*1.5*
Other textulariids	32	*0.9*	148	*3.4*	11	*0.8*	63	*3.3*	12	*0.8*	73	*3.2*	55	*0.9*	284	*3.3*
Total identified	**339**	***10.0***	**761**	***17.6***	**143**	***10.2***	**334**	***17.2***	**181**	***11.7***	**473**	***20.8***	**663**	***10.5***	**1568**	***18.4***
Total indeterminate	**16**	***0.5***	**43**	***1.0***	**2**	***0.1***	**16**	***0.8***	**10**	***0.6***	**28**	***1.2***	**28**	***0.4***	**87**	***1.0***
Total multichambered	**355**	***10.5***	**804**	***18.6***	**145**	**10.3**	**350**	***18.0***	**191**	**12.3**	**501**	***22.0***	**691**	**10.9**	**1655**	***19.4***
Monothalamids																
Nodellum-like	87	*2.6*	114	*2.6*	22	*1.6*	29	*1.5*	10	*0.6*	18	*0.8*	119	*1.9*	161	*1. 9*
Lagenamminids	69	*2.0*	135	*3.1*	16	*1.1*	52	*2.7*	48	*3.1*	116	*5.1*	133	*2.1*	303	*3.6*
Flasks	158	*4.7*	248	*5.7*	84	*6.0*	158	*8.2*	81	*5.2*	168	*7.4*	323	*5.1*	574	*6.7*
Saccamminids	64	*1.9*	73	*1.7*	15	*1.1*	18	*0.9*	6	*0.4*	16	*0.7*	85	*1.3*	107	*1.3*
Droplet chambers	4	*0.1*	4	*0.1*	0	*0.0*	0	*0.0*	1	*0.1*	2	*0.1*	5	*0.1*	6	*0.1*
Spheres	696	*20.6*	732	*16.9*	204	*14.6*	231	*12.1*	322	*20.8*	366	*16.1*	1222	*19.3*	1329	*15.6*
Organic-walled	67	*2.0*	67	*1.6*	23	*1.6*	23	*1.2*	34	*2.2*	34	*1.5*	124	*2.0*	124	*1.5*
Hyperamminids	7	*0.2*	17	*0.4*	2	*0.1*	18	*0.9*	1	*0.1*	3	*0.1*	10	*0.2*	38	*0.4*
Tubes and spindles	690	*20.4*	822	*19.0*	200	*14.3*	252	*13.1*	320	*20.7*	391	*17.2*	1210	*19.1*	1465	*17.2*
Chain-like	59	*1.7*	70	*1.6*	51	*3.6*	70	*3.7*	54	*3.5*	70	*3.1*	164	*2.6*	210	*2.5*
Unclassified	697	*20.6*	761	*17.6*	474	*33.9*	519	*27.1*	263	*17.0*	314	*13.8*	1434	*22.7*	1594	*18.7*
Komokiacean-like	169	*5.0*	192	*4.4*	54	*3.9*	73	*3.8*	63	*4.07*	76	*3.3*	286	*4.5*	341	*4.0*
Komokiaceans																
Baculellidae	207	*6.1*	219	*5.1*	86	*6.2*	94	*4.9*	136	*8.8*	169	*7.4*	429	*6.8*	482	*5.7*
Komokiidae	52	*1.5*	64	*1.5*	22	*1.6*	30	*1.6*	17	*1.1*	25	*1.1*	91	*1.4*	119	*1.4*
Total identified	**2313**	***68.4***	**2751**	***63.7***	**1089**	***77.9***	**1363**	***71.1***	**1053**	***68.1***	**1401**	***61.7***	**4455**	***70.4***	**5515**	***64.8***
Total indeterminate	**713**	***21.1***	**767**	***17.7***	**164**	***11.7***	**204**	***10.6***	**303**	***19.6***	**367**	***16.2***	**1180**	***18.7***	**1338**	***15.7***
Total monothalamids	**3026**	**89.5**	**3518**	***81.4***	**253**	***89.6***	**1567**	***81.7***	**1356**	***87.7***	**1768**	***77.9***	**5635**	***89.1***	**6853**	***80.5***
													L		L+D	
Grand Total identified	**2652**	***78.4***	**3512**	***81.3***	**1232**	***88.1***	**1697**	***88.5***	**1234**	***79.8***	**1874**	***82.6***	**5118**	***80.9***	**7083**	***83.3***
Grand Total indeterminate	**729**	***21.6***	**810**	***18.7***	**166**	***11.9***	**220**	***11.5***	**313**	***20.2***	**395**	***17.4***	**1208**	***19.1***	**1425**	***16.7***
Grand Total	**3381**	-	**4322**	-	**1398**	-	**1917**	-	**1547**	-	**2269**	-	**6326**	-	**8508**	-

Table 4. Absolute and relative abundance of dead complete specimens of major taxa/groups in the three Strata. Xenophyophore fragments and gromiids are excluded.

	UK1A		UK1B		OMS		3 strata	
Morphological groupings	**N**	**%**	**N**	**%**	**N**	**%**	**N**	**%**
Multichambered								
Robertinids	0	0	0	0	0	0	0	0
Rotaliids	40	4.25	16	3.08	65	9.00	121	5,54
Lagenids	4	0.43	1	0.19	1	0.14	6	0.27
Miliolids	4	0.43	3	0.58	10	1.39	17	0.78
Ammodiscids	32	3.40	11	2.12	16	2.22	59	2.70
Hormosinids	201	21.4	102	19.7	131	18.1	434	19.9
Trochamminids	52	5.53	20	3.85	26	3.60	98	4.49
Other textulariids	116	12.3	52	10.0	61	8.45	229	10.5
Total identified	**422**	**44.8**	**191**	**36.8**	**292**	**40.4**	**905**	**41.5**
Total indeterminate	**27**	**2.87**	**14**	**2.68**	**18**	**2.49**	**59**	**2.70**
Total multichambered	**449**	**47.7**	**205**	**39.5**	**310**	**42.9**	**964**	**44.2**
Monothalamids								
Nodellum-like	27	2.87	7	1.35	8	1.11	42	1.92
Lagenamminids	66	7.01	36	6.94	68	9.42	170	7.79
Flasks	90	9.56	74	14.3	87	12.0	251	11.5
Saccamminids	9	0.96	3	0.58	10	1.39	22	1.01
Droplet chambers	0	0	0	0	1	0.14	1	0.05
Spheres	36	3.83	27	5.20	44	6.09	107	4.90
Organic-walled	0	0	0	0	0	0	0	0
Hyperamminids	10	1.06	16	3.08	2	0.28	28	1.28
Tubes	132	14.0	52	10.0	71	9.83	255	11.7
Chain-like	11	1.17	19	3.66	16	2.22	46	2.11
Unclassified	64	6.80	45	8.67	51	7.06	160	7.33
Komokiacean-like	23	2.44	19	3.66	13	1.80	55	2.52
Komokiaceans								
Baculellidae	12	1.28	8	1.54	33	4.57	53	2.43
Komokiidae	12	1.28	8	1.54	8	1.11	28	1.28
Total identified	**438**	**46.5**	**274**	**52.8**	**348**	**48.2**	**1060**	**48.6**
Total indeterminate	**54**	**5.73**	**40**	**7.71**	**64**	**8.86**	**158**	**7.24**
Total monothalamids	**492**	**52.3**	**314**	**60.5**	**412**	**57.1**	**1218**	**55.8**
Total identified	**860**	**91.4**	**465**	**89.6**	**640**	**88.6**	**1965**	**90.1**
Total indeterminate	**81**	**8.60**	**54**	**10.4**	**82**	**11.4**	**217**	**9.94**
Total	**941**		**519**		**722**		**2182**	

Stratum	**UK1-A**							**UK1-B**							**OMS**							**3 strata combined**						
Morphological groupings	L	L_{frag}	D	D_{frag}	L+D	**Tot**	*%*	L	L_{frag}	D	D_{frag}	L+D	**Tot.**	*%*	L	L_{frag}	D	D_{frag}	L+D	**Tot.**	*%*	L	L_{frag}	D	D_{frag}	L+D	**Tot.**	*%*
Multichambered																												
Robertinids	2	0	0	0	2	**2**	***0.5***	1	0	0	0	1	**1**	***0.3***	1	0	0	0	1	**1**	***0.3***	2	0	0	0	2	**2**	***0.3***
Rotaliids	14	0	11	0	18	**18**	***4.4***	9	0	4	0	10	**10**	***3.1***	10	0	12	0	17	**17**	***5.5***	21	0	17	0	27	**27**	***4.7***
Lagenids	1	0	4	0	5	**5**	***1.2***	0	0	1	0	1	**1**	***0.3***	1	0	1	0	2	**2**	***0.6***	2	0	6	0	8	**8**	***1.4***
Miliolids	5	0	1	0	5	**5**	***1.2***	2	0	2	0	3	**3**	***0.9***	2	0	3	0	3	**3**	***1.0***	5	0	3	0	6	**6**	***1.0***
Ammodiscids	2	0	3	0	3	**3**	***0.7***	2	0	3	0	3	**3**	***0.9***	3	0	3	0	3	**3**	***1.0***	3	0	3	0	3	**3**	***0.5***
Hormosinids	27	3	21	8	29	**29**	***7.1***	21	1	19	8	25	**27**	***8.3***	22	3	18	13	24	**26**	***8.4***	34	6	29	16	37	**37**	***6.4***
Trochamminids	10	0	10	0	14	**14**	***3.4***	2	0	8	1	9	**9**	***2.8***	5	0	7	1	10	**10**	***3.2***	12	0	15	1	18	**18**	***3.1***
Other textulariids	9	0	19	0	20	**20**	***4.9***	6	0	17	1	21	**21**	***6.5***	6	0	20	1	22	**22**	***7.1***	14	0	31	2	34	**34**	***5.9***
Total Multichambered	**70**	**3**	**69**	**8**	**96**	**96**	***23.4***	**43**	**1**	**54**	**10**	**73**	**75**	***23.1***	**50**	**3**	**64**	**15**	**82**	**84**	***27.1***	**93**	**6**	**104**	**19**	**135**	**135**	***23.3***
Monothalamids																												
Nodellum-like	11	1	4	2	11	**11**	***2.7***	5	0	5	1	6	**6**	***1.9***	5	1	4	2	5	**5**	***1.6***	11	2	7	2	12	**12**	***2.1***
Lagenamminids	8	0	7	0	9	**9**	***2.2***	5	0	8	1	11	**11**	***3.4***	5	0	6	0	7	**7**	***2.3***	9	0	11	1	13	**13**	***2.2***
Flasks	4	0	4	0	4	**4**	***1.0***	4	0	4	0	5	**5**	***1.5***	3	0	3	0	3	**3**	***1.0***	5	0	6	0	6	**6**	***1.0***
Saccamminids	17	0	5	0	19	**19**	***4.6***	11	0	2	0	12	**12**	***3.7***	5	0	4	0	8	**8**	***2.6***	24	0	8	0	27	**27**	***4.7***
Droplet chambers	2	0	0	0	2	**2**	***0.5***	0	0	0	0	0	**0**	***0.0***	1	0	1	0	1	**1**	***0.3***	2	0	1	0	2	**2**	***0.3***
Spheres	56	0	10	0	58	**58**	***14.1***	32	0	13	1	41	**41**	***12.7***	34	0	9	0	38	**38**	***12.3***	76	0	22	1	85	**85**	***14.7***
Organic-walled	15	1	0	0	15	**15**	***3.6***	10	2	0	0	10	**10**	***3.1***	11	1	0	0	11	**11**	***3.5***	22	2	0	0	22	**22**	***3.8***
Hyperamminids	3	0	2	1	4	**5**	***1.2***	1	1	4	2	5	**5**	***1.5***	1	1	2	3	3	**4**	***1.3***	3	2	6	4	6	**6**	***1.0***
Tubes	49	39	14	24	49	**66**	***16.1***	32	27	19	21	41	**56**	***17.3***	33	26	20	29	39	**53**	***17.1***	68	56	33	45	74	**96**	***16.6***
Chain-like	10	7	5	4	12	**15**	***3.6***	10	4	6	2	11	**12**	***3.7***	6	2	4	1	6	**7**	***2.3***	14	8	10	4	16	**20**	***3.4***
Unclassified	41	10	14	5	47	**47**	***11.4***	30	4	12	1	36	**37**	***11.4***	27	4	14	2	34	**36**	***11.6***	60	15	25	5	68	**68**	***11.7***
Komokiacean-like	18	6	4	3	18	**19**	***4.6***	10	3	5	1	14	**15**	***4.6***	8	4	8	3	10	**12**	***3.9***	20	10	11	6	21	**22**	***3.8***
Komokiaceans																												
Baculellidae	18	13	4	6	19	**22**	***5.4***	16	5	2	8	16	**19**	***5.9***	14	11	5	5	15	**17**	***5.5***	25	17	7	13	26	**28**	***4.8***
Komokiidae	16	7	5	5	18	**20**	***4.9***	11	8	4	3	13	**16**	***4.9***	7	5	4	5	9	**13**	***4.2***	20	11	10	8	23	**25**	***4.3***
Total Monothalamids	**268**	**84**	**78**	**50**	**285**	**312**	***75.9***	**177**	**54**	**84**	**41**	**221**	**245**	***75.6***	**160**	**55**	**84**	**50**	**189**	**215**	***69.4***	**359**	**123**	**157**	**89**	**401**	**432**	***74.5***
Xenophyophores	0	0	0	0	0	**0**	***0.0***	0	0	0	0	0	**0**	***0.0***	0	1	0	2	0	**3**	***1.0***	0	1	0	2	0	**3**	***0.5***
Gromiids	2	0	2	0	3	**3**	***0.7***	4	0	0	0	4	**4**	***1.2***	8	0	1	0	8	**8**	***2.6***	10	0	3	0	10	**10**	***1.7***
-																												
Total No. Species	**340**	**87**	**149**	**58**	**384**	**411**	**-**	**224**	**55**	**138**	**51**	**298**	**324**	**-**	**218**	**59**	**149**	**67**	**279**	**310**	**-**	**462**	**130**	**264**	**110**	**546**	**580**	**-**

Table 5. Number and proportion of species assigned to major foraminiferal groupings in the three Strata separately and combined. L = stained ('live') complete; L_{frag} = stained fragment; D = dead; D_{frag} = dead fragment; Tot = all four categories combined.

Table 6: Diversity indices based on stained ('live') complete specimens, and on dead complete specimens, computed for each sample based on the entire assemblage (including gromiids and xenophyophores). S = no. species; $\%S_{Tot}$ = proportion of species recognised in individual samples relatively to the total number of species in the 11 combined samples; Singl. = no. singletons; Doubl. = no. doubletons; $E(S_{100})$ = estimated number of species for 100 individuals; H = Shannon index; α = Fisher alpha; E = Evenness index; R1D = Rank 1 Dominance; Chao1 = estimated total number of species.

	Complete										Fragments	
'Live'	S	$\%S_{Tot}$	Singl.*	Doubl.*	$E(S_{100})$	H´	α	E	R1D	Chao 1	S	$\%S_{Tot}$
MC02	103	17.8	39	13	45.64	3.82	39.7	0.44	11.5	161 ± 24	13	2.2
MC04	103	17.8	35	14	53.07	4.09	49.1	0.58	6.1	155 ± 20	23	4.0
MC07	175	30.2	51	22	56.02	4.39	67.3	0.46	8.6	257 ± 26	47	8.1
MC09	135	23.3	59	19	57.78	4.33	70.9	0.56	5.6	230 ± 31	23	4.0
MC11	135	23.3	43	15	55.37	4.3	55.9	0.55	6.1	192 ± 20	37	6.4
UK1A total	*340*	*58.6*	*151*	*35*	–	*4.85*	*103.6*	–	*5.7*	*449 ± 27*	*87*	*15.0*
MC05	137	23.6	59	17	56.59	4.31	71.4	0.54	5.9	246 ± 34	23	4.0
MC13	74	12.8	30	11	42.11	3.52	34.6	0.46	11.3	111 ± 16	25	4.3
MC25	101	17.4	38	10	35.84	2.77	35.9	0.16	47.8	159 ± 22	24	4.1
UK1B total	*224*	*38.6*	*114*	*17*	–	*4.12*	*80.0*	–	*20.1*	*370 ± 39*	*55*	*9.5*
MC20	88	15.2	29	5	49	3.86	41.4	0.54	9.1	156 ± 30	22	3.8
MC21	78	13.4	29	9	52.68	3.92	48.7	0.65	9.3	145 ± 28	17	2.9
MC22	141	24.3	41	12	51.01	4.19	51.4	0.47	6.5	237 ± 33	39	6.7
OMS total	*218*	*37.6*	*85*	*19*	–	*4.61*	*76.5*	–	*4.6*	*339 ± 35*	*59*	*10.2*
TOTAL	**462**	**79.7**	**96**	**43**	**–**	**4.99**	**123.0**	**–**	***4.8***	**583 ± 27**	**130**	**22.4**

	Complete										Fragments	
Dead	S	$\%S_{Tot}$	Singl.	Doubl.	$E(S_{100})$	H□	α	E	R1-D	Chao 1	**S**	$\%S_{Tot}$
MC02	44	7.6	16	2	35	3.29	19.8	0.61	5.6	68 ± 15	7	1.2
MC04	49	8.4	15	4	35	3.13	21.0	0.47	9.2	74 ± 14	17	2.9
MC07	71	12.2	18	3	45	3.78	32.1	0.62	3.3	105 ± 17	17	2.9
MC09	49	8.4	16	7	48	3.56	36.6	0.72	4.1	86 ± 18	12	2.1
MC11	54	9.3	10	5	46	3.63	32.0	0.70	3.8	72 ± 10	38	6.6
UK1A total	*149*	*25.7*	*30*	*5*	–	*4.23*	*51.9*	–	*7.9*	*213 ± 23*	*58*	*10.0*
MC05	69	11.9	30	4	51	3.77	46.7	0.63	3.8	183 ± 51	30	5.2
MC13	62	10.7	26	6	54	3.87	46.9	0.78	2.7	105 ± 20	19	3.3
MC25	71	12.2	28	4	50	3.80	43.7	0.63	3.7	166 ± 43	18	3.1
UK1B total	*138*	*23.8*	*47*	*8*	–	*4.34*	*66.3*	–	*5.7*	*221 ± 27*	*51*	*8.8*
MC20	76	13.1	23	7	48	3.82	39.2	0.60	3.5	133 ± 25	30	5.2
MC21	71	12.2	25	7	50	3.75	40.9	0.60	4.3	108 ± 17	23	4.0
MC22	79	13.6	20	6	52	3.97	44.7	0.67	2.7	122 ± 19	37	6.4
OMS total	*149*	*25.7*	*25*	*12*	–	*4.34*	*61.0*	–	*5.8*	*224 ± 25*	*67*	*11.6*
TOTAL	**264**	**45.5**	**50**	**10**	**–**	***4.61***	**82.0**	**–**	*6.3*	**388 ± 34**	**110**	**19.0**

*The numbers of singletons and doubletons refer to numbers in individual samples, strata (italics) and the combined dataset (bold). These terms mean that there are only 1 or 2 specimens of any type (stained, dead or fragments) in a sample, stratum or combined dataset; i.e., a single stained specimen is not counted as a singleton if it is accompanied by one or more dead specimens or fragments.

1

Table 7. Morisita Index of spatial dispersion: distribution of species represented by ≥10 complete tests in different ranges. Values <1 = regular distribution; 1 = random distribution; >1 = clumped distribution. 'Live = stained.

	Number of species	
Morisita Index	**'Live'**	**'Live' + Dead**
<1	1	1
1	0	4
1.1-1.9	31	51
2-2.9	30	30
3-3.9	17	28
4-4.9	7	5
5-5.9	6	8
6-6.9	5	4
7-7.9	5	4
8-8.9	0	1
9-9.9	3	1
10-11	6	5
Total species	**111**	**142**

See Excel spreadsheet for Supplementary Tables S1, S2

Supplementary Table S3: Absolute abundance of stained ('L' = 'live'), dead (D) and stained +dead (L+D) fragments of major groupings in the 3 strata. For the 3 strata combined, percentage abundances are also given. Xenophyophores and gromiids omitted.

	UK1-A			UK1-B			OMS			3 Strata		
Main group	**L_{Frag}**	**D_{Frag}**	**$L+D_{frags}$**	**L_{Frag}**	**D_{Frag}**	**$L+D_{frags}$**	**L_{Frag}**	**D_{Frag}**	**$L+D_{frags}$**	**L_{Frag}**	**D_{Frag}**	**$L+D_{frags}$**
Multichambered												
Robertinids	0	0	0	0	0	0	0	0	0	0	0	0
Rotaliids	0	0	0	0	0	0	0	0	0	0	0	0
Lagenids	0	0	0	0	0	0	0	0	0	0	0	0
Miliolids	0	0	0	0	0	0	0	0	0	0	0	0
Ammodiscids	0	0	0	0	1	1	0	0	0	0	1	1
Hormosinids	15	35	50	3	32	35	16	62	78	34	129	163
Trochamminids	0	1	1	0	3	3	0	8	8	0	12	12
Other textulariids	0	3	3	0	1	1	0	5	5	0	9	9
Total identified	**12**	**26**	**38**	**1**	**16**	**17**	**15**	**45**	**60**	**28**	**87**	**115**
Total indeterminate	**3**	**13**	**16**	**2**	**21**	**23**	**1**	**30**	**31**	**6**	**64**	**70**
Total multichambered	**15**	**39**	**54**	**3**	**37**	**40**	**16**	**75**	**91**	**34**	**151**	**185**
Monothalamids												
Nodellum-like	2	9	11	0	1	1	1	3	4	3	13	16
Lagenamminids	0	0	0	0	2	2	0	0	0	0	2	2
Flasks	0	0	0	0	0	0	0	23	23	0	23	23
Saccamminids	0	0	0	0	0	0	0	0	0	0	0	0
Droplet chambers	0	0	0	0	0	0	0	0	0	0	0	0
Spheres	0	0	0	0	1	1	0	0	0	0	1	1
Organic-walled	2	0	0	6	0	6	4	0	4	12	0	12
Hyperamminids	0	1	1	4	5	9	1	13	14	5	19	24
Tubes	676	276	952	412	259	571	313	256	569	1401	791	2192
Chain-like	188	41	229	17	9	26	21	19	40	226	69	295
Unclassified	417	50	467	11	2	13	32	5	37	460	57	517
Komokiacean-like	39	12	51	18	3	21	24	13	37	81	28	109
Komokiaceans												
Baculellidae	253	37	290	68	16	84	224	59	283	545	112	657
Komokiidae	170	57	227	228	23	251	47	30	77	445	110	555
Total monothalamids identified	**1610**	**438**	**2048**	**743**	**264**	**1007**	**580**	**358**	**938**	**2933**	**1060**	**3993**
Total monothalamids indet.	**137**	**45**	**182**	**21**	**57**	**78**	**87**	**63**	**150**	**245**	**165**	**410**
Total monothalamids	**1747**	**483**	**2230**	**764**	**321**	**1085**	**667**	**421**	**1088**	**3178**	**1225**	**4403**
Grand Total identified	**1622**	**464**	**2087**	**744**	**280**	**1024**	**595**	**403**	**998**	**2961**	**1147**	**4108**
Grand Total indeterminate	**140**	**58**	**198**	**23**	**78**	**101**	**88**	**93**	**181**	**251**	**229**	**480**
Grand Total	**1762**	**522**	**2284**	**767**	**358**	**1125**	**683**	**496**	**1179**	**3212**	**1376**	**4588**

Supplementary Table S4: Relative abundance of stained ('L' = 'live') and dead (D) fragments of major groupings in the 3 strata. Xenophyophores and gromiids omitted

	UK1-A			UK1-B			OMS			3 Strata		
Main group	**%L_{Frag}**	**%D_{Frag}**	**%L+D_{frags}**	**%L_{Frag}**	**D_{Frag}**	**%L+D_{frags}**	**%L_{Frag}**	**%D_{Frag}**	**%L+D_{frags}**	**%L_{Frag}**	**%D_{Frag}**	**%L+D_{frags}**
Multichambered												
Robertinids	0	0	0	0	0	0	0	0	0	0	0	0
Rotaliids	0	0	0	0	0	0	0	0	0	0	0	0
Lagenids	0	0	0	0	0	0	0	0	0	0	0	0
Miliolids	0	0	0	0	0	0	0	0	0	0	0	0
Ammodiscids	0	0	0	0	0.28	0.09	0	0	0	0	0.07	0.02
Hormosinids	0.85	6.70	2.19	0.39	8.94	3.11	2.34	12.5	6.62	1.06	9.37	3.55
Trochamminids	0	0.19	0.04	0	0.84	0.27	0	1.61	0.67	0	0.87	0.26
Other textulariids	0	0.57	0.13	0	0.28	0.09	0	1.01	0.42	0	0.65	0.20
Total identified	**0.68**	**4.98**	**1.66**	**0.13**	**4.47**	**1.51**	**2.20**	**9.07**	**5.09**	**0.87**	**6.32**	**2.50**
Total indeterminate	**0.17**	**2.49**	**0.70**	**0.26**	**5.87**	**2.04**	**0.15**	**6.05**	**2.63**	**0.19**	**4.65**	**1.53**
Total multichambered	**0.85**	**7.47**	**2.36**	**0.39**	**10.3**	**3.55**	**2.34**	**15.1**	**7.72**	**1.06**	**11.0**	**4.03**
Monothalamids												
Nodellum-like	0.11	1.72	0.48	0	0.28	0.09	0.15	0.60	0.34	0.09	0.94	0.35
Lagenamminids	0	0	0	0	0.56	1.18	0	0	0	0	0.15	0.04
Flasks	0	0	0	0	0	0	0	4.64	1.95	0	1.67	0.50
Saccamminids	0	0	0	0	0	0	0	0	0	0	0	0
Droplet chambers	0	0	0	0	0	0	0	0	0	0	0	0
Spheres	0	0	0	0	0.28	0.09	0	0	0	0	0.07	0.02
Organic-walled	0.11	0	0	0.78	0	0.53	0.59	0	0.34	0.37	0	0.26
Hyperamminids	0	0.19	0.04	0.52	1.40	0.80	0.15	2.62	1.19	0.16	1.38	0.52
Tubes	38.4	52.9	41.68	53.7	72.3	50.7	45.8	51.6	48.3	43.6	57.5	47.8
Chain-like	10.7	7.85	10.0	2.22	2.51	2.31	3.07	3.83	3.39	7.04	5.01	6.43
Unclassified	23.7	9.58	20.4	1.43	0.56	1.16	4.69	1.01	3.14	14.3	4.14	11.3
Komokiacean-like	2.21	2.30	2.23	2.35	0.84	1.87	3.51	2.62	3.14	2.52	2.03	2.38
Komokiaceans												
Baculellidae	14.4	7.09	12.7	8.87	4.47	7.47	32.8	11.9	24.0	17.0	8.14	14.3
Komokiidae	9.65	10.9	9.94	29.7	6.42	22.3	6.88	6.05	6.53	13.9	7.99	12.1
Total monothalamids identified	**91.4**	**83.9**	**89.7**	**96.9**	**73.7**	**89.5**	**84.9**	**72.2**	**79.6**	**91.3**	**77.0**	**87.0**
Total monothalamids indet.	**7.78**	**8.62**	**7.97**	**2.74**	**15.9**	**6.93**	**12.7**	**12.7**	**12.7**	**7.63**	**12.0**	**8.94**
Total monothalamids	**99.1**	**92.5**	**97.6**	**99.6**	**89.7**	**96.4**	**97.7**	**84.9**	**92.3**	**98.9**	**89.0**	**96.0**
Grand Total identified	**92.1**	**88.9**	**91.4**	**744**	**78.2**	**91.0**	**87.1**	**81.2**	**84.6**	**92.2**	**83.3**	**89.5**
Grand Total indeterminate	**7.94**	**11.1**	**8.67**	**23**	**21.8**	**8.98**	**12.9**	**18.7**	**15.3**	**7.81**	**16.6**	**10.5**
Grand Total Numbers	**1762**	**522**	**2284**	**767**	**358**	**1125**	**683**	**496**	**1179**	**3212**	**1376**	**4588**

S1. TAXONOMIC APPENDIX: TOP 30 SPECIES IN ALL CATEGORIES

Description of the top-ranked species among complete specimens and fragments, live and dead combined. The names of formal taxa follow the higher-level classification of Pawlowski et al. (2013) and Kaminski (2014). The names of informal morphology-based groupings are given with inverted commas.

Multichambered taxa

Tubothalamea

Ammodiscidae

Glomospira gordialis (Jones & Parker 1860)

Trochammina squamata var. *gordialis* Jones & Parker, 1860, p. 304-305
Glomospira gordialis (Jones & Parker) Gooday and Goineau 2019; Supplementary Fig. S8F.

Gooday and Goineau (2019) provide the following information. ‘Our specimens of this widely distributed species typically measure around 200 µm (185-215 µm) in diameter. The test varies from being relatively flat to more three-dimensional and somewhat contorted, as in the illustrated specimen from Station M on the abyssal Californian margin assigned to this species by Enge et al. (2012, Pl. 1, fig. 11).’

Globothalamea

Rotaliida

Nuttallides umbonifera (Cushman 1933)

Pulvinulinella umbonifera Cushman, 1933, p. 90, Pl. 9, fig. 9
Nuttallides umbonifera (Cushman) Goineau and Gooday 2017, Supplementary Figure S2a.

A common species widely distributed in different oceans at abyssal depths and typically associated with carbonate-undersaturated bottom watermasses below the lysocline (Mackensen et al., 1995).

Hormosinidae

Hormosinella distans (Brady, 1881)

Reophax distans Brady, 1881, p.50
Reophax distans (Brady). Brady, 1884, p. 296, Pl. 31, figs 18–22.

See Jones (1994, Pl. 31, figs 18,19) and Schröder et al. (1988, Plate 5, Fig. 7; as *Reophax distans*). This distinctive species has a test comprising a small number of relatively large, more or less equally-sized oval chambers joined by stolons.

Hormosinella guttifera (Brady 1881)

Reophax guttifera Brady, 1881, p. 49
Reophax guttifera (Brady). Brady, 1884, p. 295, Pl. 31, figs 10–15.

See Jones (1994 Pl. 31, Figs.10–15). Another distinctive species comprising a long, more or less straight series of droplet-shaped chambers, often decorated with large agglutinated particles.

Hormosinella sp. 3
Supplementary Figure S9A

A small, delicate species comprising a spherical proloculus (~55-65 µm diameter) followed by a series of chambers of increasing length (90-200 µm) and relatively uniform width (65-70 µm).The wall is thin, finely-agglutinated and translucent, but often decorated with larger particles, mainly radiolarian fragments.

Hormosinella sp. 4
Supplementary Figure S9D

Small, 2-chambered species in which the second chamber is larger than the first and is produced into a fairly long neck. One specimen measures 690 µm in length, with individual chambers 240 and 440 µm long. Another measures 960 µm with chambers 310 and 625 µm long.

Hormosinella sp. 5
Supplementary Figure S9C

Small, delicate test comprising a more or less linear series of oval chambers (78-100 µm long) joined by relatively long stolons, 50-90 µm long. The largest specimen, which is probably complete, has an overall length of 570 µm.

Reophax aff. *helenae* Rhumbler, 1931

Goineau and Gooday 2017; Supplementary Figure S2b,c.

Goineau and Gooday (2017) note that this species resembles *R. helenae* (Rhumbler, 1931) of Enge et al. (2012) from Station M in the NE Pacific and Schröder (1986) from the NW Atlantic but differs from the original description of Rhumbler (in Wiesner, 1931), based on material from >4,000 m in the Caribbean, which has a test composed of large planktonic foraminiferal shell fragments rather than mineral grains.

Reophax scorpiurus de Montfort, 1808

Reophax scorpiurus de Montfort, 1808, p. 551-552, Pl.83.
Reophax scorpiurus de Montfort, 1808. Brönnimann and Whittaker 1980, p. 261,Figs 1-7, 12, 17.
Reophax scorpiurus de Montfort, 1808. Goineau and Gooday 2017, Supplementary Figure S2d,e
Reophax scorpiurus de Montfort, 1808. Goineau and Gooday 2019, Fig. 2I

Goineau and Gooday (2017) provide the following comments. 'Our specimens have the typical asymmetrical shape of this well-known and widely-distributed 'species', which was first described from beach sands in the Adriatic (Brönnimann and Whittaker, 1980). They resemble the specimen illustrated by Resig (1981; Pl. 9, Fig. 14). This 'species' is best considered a morphotype or species complex (Gooday and Jorissen, 2012).'

Reophax sp. 112/113

Reophax sp. 112/113. Gooday et al. 2010, Fig. 14A
Reophax sp. 9. Stefanoudis et al. 2016, Pl. 1, Figs. 11–12 (as *Reophax* sp. 9)
Reophax sp. 112/113. Gooday and Goineau 2019, Supplementary Fig. S3A,B.

A small delicate species, typically comprising 2-3 asymmetrical chambers of increasing size. In stained specimens the cytoplasm is confined to the final chamber. This species is well-known from the Porcupine Abyssal Plain (NW Atlantic).

Reophax sp. 1

Reophax sp. 1. Goineau and Gooday 2017, Supplementary Figure S2f–i.
Reophax sp. 1. Gooday and Goineau 2019, Fig. 2J.

Goineau and Gooday (2017) provide the following description of this species, which is the most common hormosinid in our samples.
'Test composed of 3–5 rounded to ovate, clearly-defined chambers, arranged along a straight or curved axis. Test coarse-grained and consisting of mineral grains. Aperture at end of short neck. Length 550–1350 μm.'

Reophax sp. 2

Goineau and Gooday 2017; Supplementary Figure S2j–l.

Goineau and Gooday (2017) provide the following description. 'Test composed of 2 to 3 rounded to slightly ovate chambers arranged along a more or less linear axis. Wall thin with a relatively smooth outer surface and often incorporating coloured mineral particles. Some specimens with a dusting of fine-grained particles that obscure parts of the test. The most characteristic feature is the development of a fairly long apertural neck, flared at the distal end. Length 300–800 μm.'

Reophax sp. 5
Figure 2A

Test somewhat fusiform in shape, comprising 3-5 chambers of increasing size along a straight to curved axis. Nine specimens from MC07 range from 420 to 910 µm in length. Wall coarse grained with uneven surface, composed of various mineral grains including characteristic red particles in addition to whitish or transparent particles and occasional micronodules.

Trochamminoidea

Adercotryma sp.

Adercotryma sp.. Gooday and Goineau 2019; Fig. 1G, H.

Gooday and Goineau (2019) provide the following information.
'Brönnimann and Whittaker (1987) distinguished *Adercotryma glomeratum*, for which they established a lectotype from a 146-m-deep site in the Canadian Arctic, from a new species, *A. wrighti*. Among the criteria used to distinguish the two species was the presence of four chambers in the final whorl in *A. glomeratum* compared with only three in *A. wrighti*. Some of our small specimens of *Adercotryma* have three whereas larger species tend to have four such chambers. Given this variation, and the fact that our samples originate from abyssal depths, we prefer to leave our Pacific species unidentified. Nevertheless, it is probably the same as *Adercotryma glomeratum* (Brady, 1878), Kuhnt et al. (2000) and Gooday et al. (2010) from the deep Atlantic, Resig (1981 Pl. 10, fig. 11) from the SE Pacific, and Enge et al. (2012) from Station M in the NE Pacific. These authors recognised more elongate and less elongate forms, both of which are present in the CCZ material.'

?*Paratrochammina challengeri* Brönniman & Whittaker, 1988
Supplementary Figure S9F-H

?*Paratrochammina challengeri* Brönniman & Whittaker 1988, p. 43-44, Figs. 16H–K

This species is close to *P. challengeri,* as illustrated by Brönnimann and Whittaker (1988). Two specimens from samples MC02 and MC07 measure 417 and 506 µm, respectively, and have 4 chambers in the final whorl.

Deuterammina aff. *grahami* Brönniman & Whittaker, 1988
Figure 2B

Our specimens resemble *Deuterammina grahami*, as illustrated by Brönniman & Whittaker (1988, p. 104-107, Figs. 38A–J, 39A–C), in having 6 chambers, each with a rounded periphery, in the final test whorl. However, the agglutinated particles do not include barite ('barytes') grains, which are present in varying proportions in the holotype and paratypes. It is probably not the same species as *D. grahami* as illustrated by Enge et al. (Pl. 2, figs15-16), which has a smoother test outline and surface, in addition to being composed of barite particles. Five specimens from samples MC04 and

MC07 measure between 190 and 230 µm in maximum diameter and have 6 chambers in the outer whorl.

Other Textulariids

Cribrostomoides subglobosa (Cushman, 1910)

Haplophragmium latidorsatum Bornemann. Brady 1884, p. 307-308, Pl. 34, Figs. 8–10
Haplophragmoides subglobosum Cushman1910, p. 105-106, Figs 162-164
Cribrostomoides subglobosum (M. Sars 1868). Thies, 1991, p. 23-24, Pl. 7, fig. 4a-c; Pl. 9, fig. 1-12; Pl. 10, fig1-13.
Cribrostomoides subglobosus forma *subglobosus* (Cushman 1910). Jones et al., 1993,Fig. 1.1-3, 1.5; Pl. 1; Pl.2 figs 6a-8b; Pl. 3
Cribrostomoides subglobosus forma *bradyi* (Cushman 1910). Jones et al., 1993,
Cribrostomoides subglobosa (Cushman). Enge et al. (2012, Pl. 2, fig. 1)
Cribrostomoides subglobosa (Cushman). Holbourn et al. (2013, p. 220).

This well-known deep-sea species has been widely reported from different oceans, for example, by Thies (1991), Enge et al. (2012) and Holbourn et al. (2013). We have not attempted to distinguish between the two varieties of the species (forma *bradyi* and forma *subglobosus*) of the species recognised by Jones et al. (1993) in their detailed taxonomic revision of the genus.

Cyclammina trullissata (Brady, 1879)

Trochammina trullissata Brady 1879, p. 37-38, Pl. 5, figs 10a,b,11
Trochammina trullissata Brady 1879. Brady 1884, p. 342-343, Pl. 40, figs 13-16.
CycIammina trullissata (Brady). Resig 1981, Pl.10, fig. 8
CycIammina trullissata (Brady). Schröder 1986, p. 49-50, Pl. 18, fig. 9

Our specimens are smaller than those on Brady's type slide (see Jones 1994, Plate 40, Fig. 6), which originated from much a shallower site (390 fm = 714 m) in the Caribbean. They are more similar to the abyssal specimen from the SE Pacific illustrated by Resig (1981). This abyssal form may represent a distinct species.

?*Verneuilinulla propinqua* (Brady, 1884)

Verneuilina propinqua Brady 1884, p. 387, Pl. 47, figs 8-12
?*Verneuilinulla propinqua* (Brady). Goineau and Gooday 2017, Supplementary Figure S2m–o.

A large species that is common in ABYSSLINE epibenthic sledge samples. See Brady's original figure in Jones (1994, Plate. 47, Figs. 8–12).

'Monothalamids'

Monothalamids encompass a heterogeneous assortment of basically single-chambered foraminifera, which we divide into categories based mainly on morphological criteria. We include here species of the Komokiacea, a group of uncertain taxonomic affinity.

Nodellum-like forms

Nodellum sp. 1

Nodellum sp. 1. Goineau and Gooday, 2017, Supplementary Figure S3g.

Goineau and Gooday (2017) provide the following brief description. 'Test elongate, rigid, organic, yellowish. Slender, spindle-shaped proloculus with closed pointed proximal end. Main part of test tubular (~40–50 μ m maximum width), straight or gently arcuate. One or two internal partitions may be present. Aperture terminal, round, constricted, sometimes with delicate, tubular extension. Length ~1,100–1,800 μm.'

This species is much smaller than *Nodellum aculeata* of Gooday et al. (2008) from the Challenger Deep (10,896 m).

Saccamminidae

Lagenammina difflugiformis (Brady, 1879)

Reophax difflugiformis Brady, 1879, p. 32-33, Pl. IV, figs 3a,b
Lagenammina difflugiformis (Brady) Goineau and Gooday, 2017; Supplementary Figure S6b,c.
Lagenammina difflugiformis (Brady) Gooday and Goineau, 2019; Supplementary Fig. S1C,D

Goineau and Gooday (2017) provide the following description. 'Droplet-shaped chamber tapering to short apertural neck. Test wall often distinctly rusty-brown in colour, composed of fairly coarse-grained mineral particles. Length ~300–400 μm.'. They comments that the ABYSSLINE specimens 'are similar to some of those assigned by Brady (1884; Pl.30, Figs. 1–4) to this species. This is probably the same species as the 'morphotype resembling *L. difflugiformis* ' from the abyssal NE Atlantic, illustrated by Gooday et al. (2010; Fig. 13C) and *Lagenammina sp.* of Gooday and Jorissen (2012; Fig.2e,f). It is one of the most common species in the ABYSSLINE material.'

Lagenammina tubulata (Rhumbler, 1931)
Supplementary Figure S9B

Saccammina tubulatum Rhumbler, 1931, in Wiesner 1931, p. 82, Pl. 23, fig. 1.
Lagenammina tubulata (Rhumbler). Kuhnt et al., 2000, p. 279; Pl. 1, fig. 14; Pl. 10, fig. 2
Lagenammina tubulata (Rhumbler) Enge et al., 2012, Pl. 1, Fig. 8
Lagenammina tubulata (Rhumbler, 1931). Gooday and Goineau, 2019; Supplementary Fig. S1F

Gooday and Goineau (2019) comment as follows. 'This distinctive species has a globular chamber followed by a long, straight neck. There is some confusion about the name. We refer to it here as *L. tubulata* (rather than *L. tabulata*), since this is the name more commonly used, including by Kuhnt et al. (2000) and Enge et al. (2012), who illustrate specimens from the Atlantic and Pacific, respectively, that resemble those found in our material.'

‘Flasks’

We include here several flask-like species that differ from *Lagenammina* that contain stercomata and have test walls that are composed, at least partly, of organic material.

Flask sp. 2
Supplementary Figure S9F-H

This curious form comprises a cluster of organic-walled flask-like chambers, each 220-310 μm long, with long necks. The flasks appear to lack any direct connection with each other but are pressed tightly together in an arc with the necks directed inwards. The wall typically gives rise to spiky processes around the bulbous proximal part. The interior often contains dark material, presumably the remains of stercomata.
Remarks. These clusters of flasks seem to be part of larger formations. Some specimens display komokiacean-like features, including long tubular filaments arising from tubercles.

Flask sp. 3

Goineau and Gooday 2017; Supplementary Figure S3d–f

Goineau and Gooday (2017) provide the following brief description.
‘Asymmetrical flask-shaped agglutinated chamber, ~150 μm in maximum width and 250 μ m in length, including the long (~100–150 μ m) tapered apertural neck. The interior is occupied by stercomata and stained material. The wall is composed of an organic layer overlain by a sparse agglutinated veneer comprising a mixture of mineral particles of different sizes, and in most cases with one or more radiolarian tests projecting from the outer surface.’

Flask sp. 4

Goineau and Gooday 2017; Figure 4: d–f.

Goineau and Gooday (2017) provide the following brief description.
‘Fairly coarsely-grained agglutinated chamber (~100–150 μm width), more or less spherical to somewhat angular. Two more or less straight open-ended tubes, often of different lengths (~50–100 μm and ~200–250 μm), extend from opposite sides of the chamber. Most specimens have dead radiolarian tests attached to the outer test surface. The cytoplasm appears dark brown in colour due to the presence of stercomata.’ Goineau and Gooday note that this species is distinguished from the genera *Astrammina* and *Armorella* by its much smaller size, the presence of stercomata, and the lack of an ‘allogromiid-like’ cell body of the type found in *Astrammina.*

‘Spheres’

Psammosphaerid sp. 19

Goineau and Gooday 2017, Figure 4j,k.

Goineau and Gooday (2017) provide the following brief description.
‘Spherical agglutinated test without visible aperture, and ranging from ~100 to ~300 µm. Wall finely granular and relatively thick, with variable numbers of radiolarian tests and mineral particles attached to the outer surface. Test interior with stained cytoplasm and stercomata.’

Psammosphaerid sp. 20

Goineau and Gooday, 2017; Supplementary Figure S3a

Goineau and Gooday (2017) provide the following brief description.
‘Tiny (<100 µm) agglutinated sphere without visible aperture. Wall fairly thick and finely granular with a rough surface. Interior with stercomata. Often attached to bigger mineral (micronodule) or biogenic (diatom frustule, radiolarian test) particle.’

Psammosphaerid with tubes sp. 5
Supplementary Figure S7E

The test is usually more or less oval and 180- 250 µm in maximum dimension. The wall is soft and translucent with a finely agglutinated surface and gives rise to 2-3 long delicate flexible tubes, up to 850 µm long. The interior is filled with stercomata.

Hyperamminidae

Hyperammina cylindrica Parr, 1950
Supplementary Figure S9K

Hyperammina cylindrica Parr, 1950
Hyperammina cylindrica Parr, 1950. Jones, 1994; Plate 23, Figs 4,7.
Hyperammina cylindrica Parr, 1950. Szerak, 2007, Pl. 1, Fig. 2.

Remarks. This species has a straight to slightly curved test. Two typical specimens from sample MC02 measure 2.3 and 2.5 mm long.

Hyperammina sp. 2
Supplementary Figure S10A,B

This distinctive species comprises a thin-walled organic tube originating from a clearly-developed proloculus and surrounded by a jumble of relatively large radiolarian shells, through which the organic tube is clearly visible. In ‘live’ specimens, the inner tube is filled with red-stained cytoplasm. A typical specimen measures ~1 mm long and 259-300 µm wide, including the radiolarians. The organic tube is 50-60 µm wide and the proloculus 250 µm long and 120 µm wide.

‘Tubes’

Bathysiphon sp. 2

Bathysiphon sp.2. Goineau and Gooday, 2017; Supplementary Figure S3h,i

Goineau and Gooday (2017) provide the following brief description.
‘Gently tapered tubular test, up to 2.3 mm long and ~30–40 μm wide, open at both ends and following a curved or sinuous course. Surface smooth, finely agglutinated, white with a reflective sheen.’

Rhizammina aff. *algaeformis*.Brady, 1879
Figure 2F

Rhizammina algaeformis Brady 1879. Kamenskaya et al., 2012, Fig. 5a

Test fragments are fairly stiff and relatively straight with occasional branches. The wall is finely but noticeably agglutinated from small transparent particles and fairly densely encrusted with whitish radiolarians shells, giving it a knobbly appearance. The width (without the radiolarians) typically ranges from about 200 to 270 μm. Grey masses of stercomata are clearly visible through the wall. In stained specimens a strand of cytoplasm runs alongside the stercomata mass, a typical feature of the genus.
Remarks This *Rhizammina* species is fairly similar to *R. algaeformis* of Brady (1884), although Brady’s type material in the Natural History Museum, London, is not densely encrusted with radiolarians. This species is probably the same as *Rhizammina algaeformis* of Kamenskaya et al. (2012) from the Interoceanmetal Joint Organization claim area of the eastern CCZ.

Rhizammina sp. 1
Supplementary Figure S10C,D

Goineau and Gooday 2017; Supplementary Figure S4g–i

The tubular test is to 1 mm or more in length and ~150–240 μm wide, straight or slightly bent, occasionally branching. The wall is thick (~50 μm) but delicate, comprising a mixture of fine, mostly transparent mineral grains, outwardly-directed sponge spicules and subordinate numbers of radiolarian tests forming an irregular bristling outer surface. Test interior with cytoplasm forming a narrow string (~20 μm width) extending along the entire length of the tube. A somewhat wider (~40 μ m width) strand of stercomata enclosed within a very delicate organic membrane runs along the tube parallel to the cytoplasm. This internal organisation confirms the placement in *Rhizammina*.

Rhizammina sp. 5
Figure 2G; Supplementary Figure S10E,F

Tube fragments are narrow, generally 62 – 83 μm diameter, and follow a somewhat curved, sinuous or uneven course. Dichotomous branches are fairly common (although not all fragments branch) and branches occasionally end blindly. The tube interior contains a mass of stercomata and a thread of stained cytoplasm is occasionally seen running parallel to it, supporting the identification as a *Rhizammina* species.

Tube sp. 2
Supplementary Figure S10G-I

The test is an organic-walled tube with closed ends in complete specimens and a more or less circular cross section. The longest specimen (from sample MC02) is 1.1 mm long and 70-85 µm wide, with two short triangular side processes. Four specimens from the same sample are 260, 590, 725 and 895 µm long and relatively much wider (100-125 µm) than the longest specimen, while a fifth has a triradiate test with 3 short arms. These wider tests give rise to several conical processes that extend into long thin tubular filaments. All specimens contain dark stercomata mixed with red-stained material.
Remarks. It is possible that the slender (Fig. S10G,H) and wider forms (Fig. S10I) are distinct species.

Tube sp. 2E
Figure 2I

The test is fairly irregular, forming either a single tubular structure or a number of broad branches, typically more or less crooked and sometimes rather flattened. The wall is soft, finely agglutinated with somewhat fluffy surface. The test interior is densely dotted with small stercomata.

Tube sp. 9

Goineau and Gooday, 2017; Supplementary Figure S6a–c

The following description is amended from that of Goineau and Gooday (2017).
Basically tubular test, up to at least 3 mm long and of variable width (~100–150 µm), with short side branches and lateral swellings. There is no visible aperture. Wall thin, basically organic with a dusting of fine particles on the outer surface; conical tubercles giving rise to fine organic filaments and tubes are often developed. Test interior filled with a dense mixture of cytoplasm and stercomata.'

Tube sp. 10
Supplementary Figure S10K,L

Goineau and Gooday, 2017; Supplementary Figure S5a–c

Goineau and Gooday (2017) provide the following brief description.
'Narrow (~50 µm width), curved to slightly sinuous a gglutinated tube, up to 1 mm long. Most specimens are fragments but a closed end is present in some cases. Wall fairly thin, composed of coarse, angular grains, giving a rough 'sparkly' surface under the stereomicroscope. Cytoplasm with stercomata is visible through wall in transmitted light.'
Remarks. During the analysis of samples we referred to these informally as 'sparkly tubes'.

Tube sp. 19

Goineau and Gooday, 2017; Supplementary Figure S5l,m

Goineau and Gooday (2017) provide the following brief description.

‘Transparent, organic-walled tube, 0.6–1.0 mm long and ~50– 80 μm wide; the wall is yellow, fairly thick, sometimes with a dusting of fine-grained particles. One end of the tube may be closed. Cytoplasm filled with dense stercomata. ‘

Tube sp. 23

Goineau and Gooday, 2017; Supplementary Figure S6: d–f

Goineau and Gooday (2017) provide the following brief description.
‘Delicate, branching, basically tubular test, ~50–80 μm wide and a few 100 μm in length. Wall composed of an organic layer covered by a thin dusting of fine-grained particles, and often incorporating radiolarian tests and large mineral grains. The organic layer gives rise to numerous short filaments extending from the organic part of the wall, giving a very fuzzy, ragged aspect. Cytoplasm contains large but relatively sparse stercomata.’

Tube sp. 25

Goineau and Gooday, 2017; Supplementary Figure S5f–i

Goineau and Gooday (2017) provide the following brief description.
‘Relatively short, more or less straight, slightly tapered tubular test, ~400–1,000 μm long and ~100 μm wide. One end is typically closed and the other end open. Wall noticeably granular under stereomicroscope, composed of small, angular particles and incorporating variable numbers of much larger radiolarian tests. Interior with stercomata embedded in red-stained material. ‘

Tube sp. 27

Goineau and Gooday, 2017; Supplementary Figure S5 j, k

Goineau and Gooday (2017) provide the following brief description.
Small, slender, spindle-shaped to tubular test, <500 μm long and ~40 μm maximum width. Wall with yellowish tinge and a variably developed, finely-agglutinated veneer overlying an organic base; a few scattered larger particles are sometimes present. Test contents finely granular, containing numerous tiny stercomata-like bodies.

Tube sp. 32

Goineau and Gooday, 2017; Supplementary Figure S3j–l

Goineau and Gooday (2017) provide the following brief description.
‘Basically tubular test, from a few 100 μm up to 2.6 mm long and ~150–250 μm wide, usually more or less straight or slightly crooked, sometimes with slight constrictions or swollen sections. One or both ends are closed in specimens that appear complete. Wall fairly thin but semi-opaque, finely agglutinated and typically with tiny scattered dark particles. A few larger biogenic particles and micronodules may be attached on the wall.’

Goineau and Gooday remark that smaller specimens of this species have an equidimensional shape that make it difficult to classify morphologically. It is rather similar to the xenophyophore

genus *Aschemonella* but lacks the internal features (stercomare and granellare) typical of xenophyophores.

Tube sp. 33/36

Goineau and Gooday, 2017; Supplementary Figure S6g–h

Goineau and Gooday (2017) provide the following brief description.
‘Delicate, fragmentary, tubular test, unbranched and either straight or gently curved; fragment are <500 μ m long and ~100 μ m wide. Wall with a distinct basal organic layer overlain by a very heterogeneous and coarse-grained mixture of angular quartz grains and biogenic particles, mainly radiolarian tests, that project to create a very un even outer surface. Cytoplasm filled with stercomata.’

Tube sp. 39
Supplementary Figure S10J

The test forms a basically tubular structure that follows a more or less irregular course and is constricted at regular intervals to form rather weakly-defined ‘pseudochambers’. The longest specimen is 3.75 mm in length (measured along the tube) and the ‘pseudochambers’ decrease in width from 290 μm near the aperture to 125 μm at the proximal end. A second specimen is smaller, measuring 1.43 mm along the length and tapering from 160 to 42 μm. The wall is finely but noticeably agglutinated from mineral grains of different sizes. Fine hair-like filaments arise from the distal part of the structure. The largest specimen contains stained cytoplasm in the distal third end and stercomata in the proximal two thirds.

Tube sp. 40

Goineau and Gooday, 2017; Supplementary Figure S5d, e

Goineau and Gooday (2017) provide the following brief description.
‘Unbranched, tubular test, typically fragmented, 500 μm or more long and of somewhat variable width (generally ~150–200 μm), agglutinated with coarse, angular particles, with one closed end and an aperture at the opposite end. The tube follows a more or less straight or somewhat crooked course. Wall is noticeably granular under the stereomicroscope and composed of small quartz grains. It may give rise to fine, flexible filaments, although these are not always developed. Cytoplasm contains sparse stercomata.’

Tube sp. 41

Goineau and Gooday, 2017; Supplementary Figure S6i, j

Goineau and Gooday (2017) provide the following brief description.
‘Test forms a curved, sometimes slightly twisted, tapered tube, ranging in length from ~0.5 to 2.3 mm (measured along the length) and with a maximum width of ~150 μ m. Transverse constrictions are more or less well developed and the narrower (proximal) end is closed, forming a rounded proloculus (40–80 μ m diameter). The test interior is interrupted by occasional transverse septae. The entire tube is reddish in colour when stained. The wall is translucent and comprises a relatively

thick organic base overlain by a fine-grained agglutinated layer of variable thickness. Cytoplasm contains stercomata.’

Tube sp. 43

Goineau and Gooday, 2017; Figure 5n–p

Goineau and Gooday (2017) provide the following brief description.
‘Delicate, brownish tubular test that is occasionally branched. The longest pieces are 500–900 μm in length and ~80–100 μm wide. Specimens are often open-ended and appear to be fragments, but one closed end is sometimes observed. The tubes have a neat, finely agglutinated wall, ~20 μ m thick, and at least one closed end. The test interior contains dark stercomata that appear, either singly or in clumps, as a series of dots along the length of the tube. ‘

Tube sp. 44

Goineau and Gooday, 2017; Supplementary Figure S7i, j

Goineau and Gooday (2017) provide the following brief description.
‘Delicate, narrow, branching tube, typically ~0.5 up to 1.5 mm long and <50 μ m wide. The wall is thin and composed of fine particles. There is no obvious aperture, although the ends of the tubes are often broken. Cytoplasm contains numerous stercomata.’ Goineau and Gooday (2017) comments that this form ‘resembles Tube sp. 43 but is considerably narrower and more often branched.’

Tube sp. 45

Goineau and Gooday, 2017; Supplementary Figure S7a–f

Goineau and Gooday (2017) provide the following brief description.
‘Tubular test, ~0.6–1.4mm long (complete specimens) and~100–150 μ m wide, either branched or unbranched, sometimes with short side lobes; ends are sometimes closed. Test wall soft and fine-grained and of relatively even thickness (~20 μ m). Test interior with dense stercomata.’. They remark that Tube sp. 45 resembles Tube sp. 43 but is ‘distinctly wider’.

Tube sp. 46

Goineau and Gooday, 2017; Supplementary Figure S7g, h

Goineau and Gooday (2017) provide the following brief description.
‘Tubular test follows a more or less straight or somewhat crooked course; it is usually unbranched but sometimes has a short side lobe. Intact ends are closed, but all available specimens appear to be fragments with one or both ends broken. Most are <1mm but the longest reaches ~3 mm in length; the width varies from 230 to 350 μ m. The wall is thick, finely agglutinated with a slightly fuzzy surface; the thickness is generally between 25 and 35 μm but a thinner-walled variant also occurs. The test interior is densely packed with a mass of stercomata and red-stained material, the outline of which is visible through the wall when the tube is immersed in glycerol.’

Tube sp. 48

Goineau and Gooday, 2017; Figure 4a–c

Goineau and Gooday (2017) provide the following description.
‘Typical specimens are elongate and best described as approximately spindle-shaped, tapering towards both ends and sometimes with short triangular processes or tapering side branches. These typical spindles grade into more tubular tests. Most specimens are probably complete and measure from ~0.3 to 0.8 mm long and 60 to 220 μ m wide. Occasionally, two spindles are joined end to end. The wall is translucent with a very fine granularity visible when viewed under the stereomicroscope. Under high magnification in a compound microscope, the wall appears basically organic with a variably developed veneer of fine particles, normally 5–15 μ m thick but sometimes more. In some samples, a few radiolarians or other biogenic particles project from the test wall. Large, dark stercomata, sometimes densely packed, are a prominent feature of the test interior. Several variants are included within this form. In one type, the test has a smoother outline, is devoid of radiolarians, triangular processes and short side branches but sometimes bifurcates. Another variant has a rather irregular shape and a ‘fluffy’surface with short filaments. All types contain dense stercomata.
Remarks. These spindle-shaped tubes are among the most common monothalamids in our samples. They exhibit considerable variability, however, and may possibly encompass more than one species. We regard individual spindles as individuals, although the occasional presence of two joined end to end suggests that at least some may be fragments of longer chain-like formations.

Tube sp. 54

Goineau and Gooday, 2017; Figure 4g–i

Goineau and Gooday (2017) provide the following description.
‘Test basically tubular to spindle-shaped, 0.2–0.8 mm long and relatively wide (~50–150 μm); some specimens bifurcate while others comprise two spindle-shaped elements, one of which buds off the side of the other. Wall fairly delicate and seems basically organic with variably developed surface layer of flat-lying, mainly siliceous particles resulting in a relatively smooth outer surface. Test contents very heterogeneous, including stercomata but also a variety of crumpled organic sheets and organic-walled cyst-like structures. A variant form includes tubular to spindle-shaped tests of similar size to typical specimens. Some intact tests have one end that is rounded and closed and the XII other end narrower and drawn out into a delicate organic filament. Compared to typical specimens, this form has a thicker wall that is more distinctly granular when observed in a compound microscope. The test interior is also dominated to a much greater extent by dark stercomata.’

Tube sp. 56

Goineau and Gooday, 2017; Supplementary Figure S4a–c

The tubular test occurs only as fragments, ranging in width from 90 to 155 μm (typically 110-140 μm). A few fragments have closed ends. The wall is finely agglutinated and largely devoid of larger particles. The interior contains dark stercomata mixed with stained particles.
Remarks These tubes superficially resemble *Rhizammina* but lack the typical internal organisation of this genus, i.e., a strand of cytoplasm running alongside a mass of stercomata. A few fragments also have closed ends, another feature that is not typical of *Rhizammina*.

Tube sp. 57

Goineau and Gooday, 2017; Supplementary Figure S4d–f

Goineau and Gooday (2017) provide the following brief description and remarks.
‘Unbranched or occasionally branched tubular test, up to 1 cm or more in length and 75–100 μm wide, open at both ends and following a curved, often somewhat crooked course. Wall finely granular with relatively smooth outer surface. Interior with dense stercomata and red-stained material.’
‘Remarks. Tube sp. 57 differs from Tube sp. 56 in being somewhat narrower and always open-ended rather than sometimes having a closed end. Although the agglutinated wall is fine-grained, the grains are noticeably larger than those that constitute the wall of Tube sp. 56 when observed under a compound microscope. Like Tube sp. 56, this species lacks internal features typical of Rhizammina a genus to which it was originally assigned. ‘

Tube sp. 73
Figure 2E

The tubes are relatively large, the longest fragment (from sample MC13) measuring 2.8 mm in length. The overall width ranges from 140 to 210 μm in 5 fragments from MC13. They follow a curved, somewhat sinuous or crooked course; one specimen branches and two others give rise to short, triangular projections, probably incipient side branches. The wall is fine-grained but dotted with a few larger particles, mainly radiolarian shells. It is fairly thick and almost opaque in reflected light. The test interior contains masses of stercomata in a red-stained matrix.

Tube sp. 92
Figure S9J

The largest tube fragment is 1.15 mm long. The tubes are relatively thick (160-215 μm) in relation to their overall size. They branch, in some cases several times, and where not broken, the branches are short and have rounded terminations. The wall is soft, very thick and uniformly fine-grained. The lumen contains stercomata, which form a dark core that is visible through the wall and occupies about a third of the width of the tube.

Tube sp. 122
Supplementary Figure S10M

The tubular test fragments are straight and usually unbranched; all have broken ends with no sign of closure. They range in width from 280 to 410 μm. The wall is thin, transluscent, and noticeably granular under a stereo microscope. It is composed mainly of small transparent grains but also dotted with tiny dark particles.

‘Chains’

Although superficially appearing multichambered, we consider chains-like morphotypes to comprise a series of ‘pseudo-chambers’ or ‘segments’ rather than true chambers, and therefore include them with the monothalamids.

Chain sp. 13

Goineau and Gooday, 2017; Figure 5d–g

Goineau and Gooday (2017) provide the following brief description.
‘The elongate test is 0.5–1.5 mm long in specimens that are apparently complete (although most appear to be fragments) and ranges from <100 μ m to ~260 μm in width, according to the thickness of the agglutinated layer. It occasionally branches but most specimens are unbranched. The wall is basically organic so that the entire test stains red. The organic layer is overlain by a layer of finely agglutinated material that varies in thickness from 90–100 μm (in which case the test interior is largely obscured) to ~15 μ m, or in some cases is almost non-existent. Beneath this layer, the basically tubular organic part of the test is partitioned into a series of globular pseudo-chambers, each containing a clump of dark stercomata.’

‘Unclassified monothalamids’

Monothalamid sp. 19

Goineau and Gooday, 2017; Supplementary Figure S9d–f

Goineau and Gooday (2017) provide the following brief description.
‘Test rounded, generally ovate, sometimes more irregular in shape; small lobes may be developed, usually at one end of the test. Length ~0.20–0.45 m. Wall translucent to almost transparent, composed of an organic inner layer covered by a very thin layer of fine-grained agglutinated material. There is no obvious aperture. Test content very heterogeneous, including stercomata together with sheet-like and cyst-like structures of probable biogenic origin.’ They remark that the heterogeneous test contents of this species closely resemble those of Tube sp. 54, although the test morphology is different.

Monothalamid sp. 27

Goineau and Gooday, 2017; Figure 5h–j

Goineau and Gooday (2017) provide the following brief description.
‘Agglutinated test typically resembling a triangle or an arrow head with three or four pointed ends. Wall neat, fine-grained, ~20–30 μm thick, and sometimes slightly produced at the pointed ends where it becomes much thinner. One wider variant (Fig. 5i) divides into two short broad branches with lobate extremities tapering on the opposite side to a single aperture. Length ~200–450 μm. Width of ‘pointed’ variant ~200–300 μm, and width of ‘branched variant ~420–600 μm.’

Monothalamid sp. 85
Figure 2C,D

This form inhabits a spherical radiolarian test. It accumulates a veneer of fine-grained sediment on the exterior of the host test to create a sphere between 160 and 258 μm (generally 175-220 μm) in diameter. This gives rise to a delicate transluscent tube, up to 275 μm (generally 160-210 μm) long and 35-45 μm in diameter, with a fine-grained agglutinated surface. The interior of the radiolarian host contains relatively large stercomata that are visible through the wall as a dark mass.
Remarks. This is the second most abundant species overall, despite being largely restricted to sample MC25.

Monothalamid sp. 98
Supplementary Figure S11D

Clusters of short, branched arms, often expanding in width where branching occurs close to the extremities. The largest specimen measures 725 µm maximum dimension, but most are half of that size. The wall is very soft, fine-grained, and the dark, stercomata-rich core is vlearly visible through it.

'Komokiacean-like'

We reserve this grouping for forms with some komokiacean-like features, for example, the division of the test of Komokiacean-like sp. 20 into compartments that resemble those subdividing *Normanina* chambers, but that lack typical komokiacean characters, notable tubules.

Komokiacean-like sp. 20

Goineau and Gooday, 2017; Figure 4l,m

Goineau and Gooday (2017) provide the following brief description.
'Variably shaped test, often subtriangular, spindle-shaped or more rounded and often with tubular extensions (~40–100 µm long). Komokiacean-like wall structure with a fine-grained agglutinated veneer overlying an organic layer. Test interior compartmentalised to resemble a honeycomb and filled with masses of stercomata. Maximum dimension ~150–180 µm (without tubular extensions).'

Komokiacean-like sp. 26
Supplementary Figure S11A-C

The test forms a complex segmented structure, sometimes branched, comprising more or less bulbous sections, which themselves may give rise to lateral swellings, and are separated by more or less distinct constrictions. The segments are subdivided internally into compartments by partitions. The wall is fairly thick, brownish and appears to be largely organic. The surface gives rise to fine fibres, in places in dense concentrations. The illustrated specimen measures ~90 µm in maximum dimension (not inclusing the fibres).
Remarks. The appearance of the test is reminiscent of *Baculella,* a relationship that is strengthened by the development of fine fibres.

Komokiacea: Baculellidae

Baculella globofera Tendal & Hessler, 1977

Baculella globofera Tendal and Hessler, 1977; Pl. 15, Figs. A,B

Remarks. Our specimens resemble those illustrated by Tendal and Hessler (1977)

Baculellidae sp. 8
Supplementary Figure S11E

The test comprises clusters of tiny brown bead-like chambers and more elongate protuberances that arise from a basal tubule. A few specimens comprise two such clusters joined by a short stalk. thick branches with an overall dimension of 275-350 µm.

Baculella aff. *hirsuta*
Figure 2H

An elongate formation in which the test is largely obscured by fine-grained muddy sediment, the main visible structures being short outwardly-projecting tubules. The longest specimen is ~1.9 mm long and ~420 µm wide. Some pieces have more or less distinct 'segments' joined by a narrow neck. This may be a species of *Baculella.* The accumulation of fine-grained sediment around the test is reminiscent of, *B. hirsuta.*

'Edgertonia' floccula Shires, Gooday & Jones, 1994

Shires et al., 1994; Plate 1, Figs. 1–7.

Remarks. Mudballs with a flocculent surface in which small chambers 'float' in a tangle of very fine fibres, first described in the abyssal NE Atlantic, are widely distributed in the lower bathyal and abyssal deep sea.

Edgertonia sp. 4

Goineau and Gooday, 2017; Supplementary Figure S10a,b

Goineau and Gooday (2017) provide the following brief description.
'Clusters of short, finger-like branching tubules, typically ~50 µm wide, usually ending in slightly bulbous swellings or clusters of swellings. Tubes and swellings contain discrete clumps of stercomata, often separated by more or less distinct septae that subdivide the interior into compartments. Wall organic with finely granular outer surface.'

Edgertonia sp. 5

Goineau and Gooday, 2017; Supplementary Figure S10c,d

Goineau and Gooday (2017) provide the following brief description.
'Branching tubules (~50 µm wide) ending in 1–2 bulbous swellings, ~100 and ~200 µm maximum dimension. Wall composed of organic layer overlain by variably developed agglutinated veneer. Test interior with sparse stercomata and stained material.' They remark that it 'differs from *Edgertonia* sp. 4 in having larger and more pronounced terminal swellings, no septae, and a flimsier wall.'

Edgertonia sp. 7

Goineau and Gooday, 2017; Figure 5k-m

Goineau and Gooday (2017) provide the following brief description.
'Irregularly-shaped cluster of globular chambers (each ~50 μm wide), loosely to fairly tightly packed within a variably-developed fine-grained matrix and sometimes surrounded by fine organic fibres. Individual clusters measure up to 750 μm (usually 250–500 μm) in maximum dimension.

Edgertonia sp. 8
Supplementary Figure S11F

Delicate spheres (110-140 μm diameter), somewhat droplet-shaped, connected together in a bunch by delicate, flexible extensions. The wall is relatively thin and fine-grained. These formations are probably the same as the 'probable komokiacean chambers' of Nozawa et al. (2006, Fig. 3H)

Edgertonia sp. 8A
Supplementary Figure S11G,H

Droplet-shaped spheres connected together by delicate threads and resembling *Edgertonia* sp. 8. The main differences are that the spheres are smaller (typically 50-55 μm, maximum 70 μm, in length) and the walls are coarser-grained with a distinctly granular appearance compared to *Edgertonia* sp. 8.

Komokiacea: Komokiidae

Ipoa fragila Tendal and Hessler, 1977
Supplementary Figure S12A,B

A single complete specimen (Fig. S12A) of this distinctive komokiacean was found in sample MC13 (0-0.5cm, >300, #3); other examples are fragments. They are easily identifiable by the wider basal tubule that divides into narrower branches (Fig. S10B)

Reticulum sp. 1

Goineau and Gooday, 2017; Supplementary Figure S11a,b

Goineau and Gooday (2017) provide the following brief description.
'Test consists of branching and anastomosing tubules. Tubules non-septate, more or less parallel sided and following a somewhat irregular course between the branches. Distinct organic layer of wall overlain by variably developed fine-grained coating. The width of the inner organic tubule = 14–19 μm; width of the outer agglutinated layer = 5–6 μm; total tubule width = 22–30 μm.'

Reticulum sp. 4

Goineau and Gooday, 2017; Supplementary Figure S11c,d

Goineau and Gooday (2017) provide the following brief description.

‘Loose clump of narrow, branching, reticulated tubules (~10–15 µm width). Tubules non-septate, parallel-sided. Organic wall covered by a very thin fine-grained coating. Clumps, assumed to be fragments, are up to 1 mm or more in size. We place this species in the genus *Reticulum* because the tubules are fairly tightly meshed, more so than in the closely related genus *Lana.’*

Komokiidae sp. 10
Supplementary Figure S12C,D

Mudball structure packed with poorly-defined compartments (~90-100 µm across), each containing a single, or a cluster, of small stercomata. The specimens are probably either fragments or are damaged; the largest measures 1.34 mm maximum dimension.

Komokiidae sp. 13
Supplementary Figure S12E,F

The specimens, which are probably fragmentary, comprise a very fine tubule system, the details of which are very difficult to discern, embedded in a muddy matrix. The general appearance is that of a mudball densely speckled with tiny dark dots, corresponding to individual stercomata.

References

Brady, H.B. 1881. Notes on some of the reticularian Rhizopoda of the Challenger Expedition. Part III. 1. Classification. 2. Further notes on new species. 3. Note on *Biloculina* mud. Q. J. Microsc. Sci., new series 21, 31–71.

Brady, H.B., 1884. Report on the foraminifer dredged by H.M.S. Challenger during the years 1873–1876. Report of the scientific results of the voyage of H.M.S. Challenger, 1873–1876. Zoology 9, London, England.

Brönnimann, P., Whittaker, J.E., 1980. A revision of *Reophax* and its type-species, with remarks on several other Recent hormosinid species (Protozoa: Foraminiferida) in the collections of the British Museum (Natural History). Bull. Br. Mus. Nat. Hist. (Zool.) 39, 259-272.

Brönnimann, P., Whittaker, J.E., 1988. The Trochamminacea of the Discovery Reports. British Museum (Natural History). 152 pp.

Cushman, J.A., 1933. Some new recent Foraminifera from the tropicalPacific. Contributions from the Cushman Laboratory for Foraminiferal Research 9, 77–95.

Enge, A.J., Kucera, M., Heinz, P., 2012. Diversity and microhabitats of living benthic foraminifera in the abyssal Northeast Pacific. Mar. Micropaleontol 96, 84–104.

Goineau, A., Gooday, A.J., 2017. Novel benthic foraminifera are abundant and diverse in an area of the abyssal equatorial Pacific licensed for polymetallic nodule exploration. Scientific Reports **7,** 45288. doi:10.1038/srep45288

Gooday, A.J., Goineau, A., 2019. The contribution of fine sieve fractions (63-150 µm) to foraminiferal abundance and diversity in an area of the eastern Pacific Ocean licensed for polymetallic nodule exploration. Front. Mar. Sci. http://doi:10.3389/fmars.2019.00114.

Gooday, A.J., Malzone, M.G., Bett, B.J., Lamont, P.A., 2010. Decadal-scale changes in shallow infaunal foraminiferal assemblages at the Porcupine Abyssal Plain, NE Atlantic. Deep-Sea Res II 57, 1362–1382, doi:10.1016/j.dsr2.2010.01.012.

Gooday, A.J., Todo, Y., Uematsu, K., Kitazato, H., 2008. New organic-walled Foraminifera (Protista) from the ocean’s deepest point, the Challenger Deep (western Pacific Ocean). Zool. J. Linn. Soc. 153, 399–423, doi:10.1111/j.1096-3642.2008.00393.x.

Holbourn, A., Henderson, A.S., MacLeod, N., 2013. Atlas of benthic foraminifera. John Wiley & Sons.

Jones, R.W. , Bender , H. , Charnock, M.A. , and Kaminski, M.A. , 1993. Emendation of the foraminiferal genus *Cribrostomoides* Cushman, 1910, and its taxonomic implications . J. Micropalaeontol. 12, 181 – 193.

Jones, R.W., 1994. The Challenger foraminifera. Oxford University Press and The Natural History Museum, London.

Jones, T.R.; Parker, W.K. (1860). On the rhizopodal fauna of the Mediterranean compared with that of the Italian and some other Tertiary deposits. *Q. J. Geol. Soc. London.* 16, 292-307

Kamenskaya, O.E., Gooday, A.J., Radziejewska, T., Wawrzyniak-Wydrowska, B., 2012. Large, enigmatic foraminiferan-like protists in the eastern part of the Clarion-Clipperton. Marine Biodiversity fracture zone (abyssal eastern equatorial Pacific): biodiversity and vertical distribution in the sediment. Mar Biodiv 42, 311-327. DOI: 10.1007/s12526-012-0114-7.

Kaminski, M., 2014. The year 2010 classification of the agglutinated foraminifera. Micropaleontology 60, 89-108.

Kuhnt, W., Collins, E., Scott, D., 2000. Deep water agglutinated foraminiferal assemblages across the Gulf Stream: distribution patterns and taphonomy. In: Hart, M., Kaminski, M., Smart, C. (Eds.), Proceedings of the Fifth International Workshop on Agglutinated Foraminifera. Grzybowski Foundation Special Publication, 7, 261–298, pls 1-12.

Mackensen, A., Schmiedl, G., Harloff, J. and Giese, M., 1995. Deep-sea foraminifera in the South Atlantic Ocean: Ecology and assemblage generation. Micropaleonotology 41, 342-358.

Nozawa, F., Kitazato, H. Tsuchiya, M. and Gooday, A.J., 2006, 'Live' benthic foraminifera at an abyssal site in the equatorial Pacific nodule province: abundance, diversity and taxonomic composition. Deep-Sea Res 51, 1406-1422.

Pawlowski, J., Holzmann, M., Tyszka, J., 2013. New supraordinal classification of Foraminifera: Molecules meet morphology. Mar. Micropaleontol. 100, 1–10.

Resig, J.M., 1981. Biogeography of benthic foraminifera of the northern Nazca plate and adjacent continental margin. Geol. Soc. Am. Mem. 154, 619–666, doi:10.1130/MEM154-p. 619.

Schröder, C.J., Scott, D.B., Medioli, F.S., Bernstein, B.B., Hessler, R.R., 1988. Larger agglutinated foraminifera: comparison of assemblages from central Pacific and western North Atlantic (Nares Abyssal Plain). J. Foramin Res 18, 25-41.

Shires, R., Gooday, A.J. , Jones, A.R., 1994. The morphology and ecology of an abundant new komokiacean mudball (komokiacea, Foraminiferida) from the bathyal and abysal N E Atlantic. J. Foramin. Res 24, 214-225.

Stefanoudis, P.V., Schiebel, R., Mallet, R., Durden, J.M., Bett, B.J., Gooday, A.J., 2016. Agglutination of benthic foraminifera in relation to mesoscale bathymetric features in the abyssal NE Atlantic (Porcupine Abyssal Plain). Mar Micropaleontol 123, 15–28.

Szarek, R., Nomaki,H., Kitazato, H. (2007). Living deep-sea benthic foraminifera from the warm and oxygen-depleted environment of the Sulu Sea. Deep-Sea Res I 54, 145-176.

Schröder, C.J., 1986. Deep-water arenaceous foraminifera in the northwest Atlantic Ocean. Can.Tech. Rep. Hydrogr. Ocean Sci. 71, 1-191

Thies, A. 1991. Die Benthos-Foraminiferen im Europäischen Nordmeer. Ber. Sondersforschungsbereich 313, Univ. Kiel 31, 1-97.

Tendal, O.S., Hessler, R.R., 1977. An introduction to the biology and systematics of Komokiacea: Galathea Rep 14, 165-194, pls 9-26.

Wiesner, H., 1931. Die Foraminiferen der Deutschen Südpolar-Expedition. In: von Drygalski, E. (Ed.), Deutsche Südpolar-Expedition, 1901-1903, 20:49-169

S2. Supplementary Figure captions

Figure S1. Location of sampling sites in the three Strata; from north to south UK-1A, UK-1B, and OMS.

Figure S2. 'Live' complete data (ignoring singletons). A) Species ranked by abundance. B) Species recorded from 1-2 samples, ranked by abundance. C) Species recorded from 9-11 samples, ranked by abundance; red = 11 samples; blue = 10 samples; yellow = 9 samples.

Figure S3. Dead complete data (ignoring singletons). A) Species ranked by abundance. B) Species recorded from 1-2 samples, ranked by abundance. C) Species recorded from 9-11 samples, ranked by abundance; red = 11 samples; blue = 10 samples; yellow = 9 samples.

Figure S4. 'Live' + dead complete data (ignoring singletons). A) Species ranked by abundance. B) Species recorded from 1-2 samples, ranked by abundance. C) Species recorded from 9-11 samples, ranked by abundance; red = 11 samples; blue = 10 samples;

Figure S5. Total number of species recognised in individual samples (MC02, MC04 etc), individual strata (UK1-A, UK1-B, OMS) and all strata combined.

Figure S6. Rarefaction curves based on complete live (A) and complete live and dead (B) specimens. Solid lines are based on actual data; dashed lines are extrapolated curves up to 1,500 specimens for each sample.

Figure S7. Sample-based rarefaction curves based on number of complete (stained + dead) specimens from individual strata and the 11 samples (solid lines) and extrapolated up to 15 or 30 samples (dotted lines), respectively (A). Corresponding number of new species added for each additional sample, based on the extrapolated sample-based rarefaction curves (B). For each sample, vertical bars indicate the 95% confidence interval.

Figure S8. Number of species (ignoring singletons) represented by live + dead specimens, arranged by the number of samples in which they occur (from 1 to11). Data are given separately for 'live' (stained), dead, and 'live' + dead assemblages. For some data points the 'live' and/or dead occurrences exceed the 'live + dead occurrences. This is because species occurring in a particular number of samples in the 'live' assemblage will drop out of that datapoint if represented by dead specimens in other samples. A) Number of species. B) Percentage of species.

Figure S9. **A)** *Hormosinella* sp. 3; MC02, 0-0.5 cm, 150-300 µm. **B)** *Lagenammina tubulata;* MC02, 0-0.5 cm, 150-300 µm. **C)** *Hormosinella* sp. 5; MC02, 0-0.5 cm, 150-300 µm. **D)** *Hormosinella* sp. 4; MC09, 0-0.5 cm, >300 µm. **E)** Psammosphaerid with tubes sp. 5; MC04, 0.5-1.0 cm, 150-300 µm. **F-H)** *Paratrochammina challengeri?* **I)** Flask sp. 2; MC07, 0.5-1.0 cm, >300 µm (possibly a komokiacean). **J)** Tube sp. 92; MC25, 0.5-1.0 cm, >300 um. **K)** *Hyperammina cylindrica;* MC02, 0.5-1.0 cm, >300 um.

Figure S10. **A,B)** *Hyperammina* sp. 2; MC09, 0.5-1.0 cm, >300 µm. **C,D)** *Rhizammina* sp. 1; MC11, 0-0.5 cm, >300 µm (note the strand of stained cytoplasm alongside the stercomata). **E,F)** *Rhizammina* sp. 5; MC22, 0-0.5 cm, >300 µm. **G,H)** Tube sp. 2; MC02, 0-0.5 cm, 150-300 µm. **I)** Tube sp. 2; MC02, 0.5-1.0 cm, 150-300 µm. **J)** Tube sp. 39 (segmented); MC07, 0.5-1.0 cm, >300 µm. **K,L)** Tube sp. 10; MC02, 0-0.5-1.0 cm, 150-300 µm. **M)** Tube sp. 122; MC25, 0.5-1.0 cm, 150-300 µm.

Figure S11. **A-C)** Komokiacean-like sp. 26; MC13, 0.5-1.0 cm, >300 µm. **D)** Monothalamid sp. 98; MC22, 0-0.5 cm, 150-300 µm. **E)** Baculellidae sp. 8; MC04, 0.5-1.0 cm, 150-300 µm. **F)** *Edgertonia* sp. 8; MC05, 0.5-1.0 cm, 150-300 µm. **G,H)** *Edgertonia* sp. 8A; MC22, 0-0.5 cm, >300 µm.

Figure S12. **A)** *Ipoa fragila*; MC13, 0-0.5 cm, >300 µm. **B)** Possible fragment of *Ipoa*; MC22, 0.5-1.0 cm, >300 µm. **C)** Komokiidae sp. 10; MC09, 0.5-1.0 cm, 150-300 µm. **D)** Komokiidae sp. 10; MC13, 0-0.5 cm. **E,F)** Komokiidae sp. 13; MC04, 0.5-1.0 cm, >300 µm.

Supplementary Fig. S1

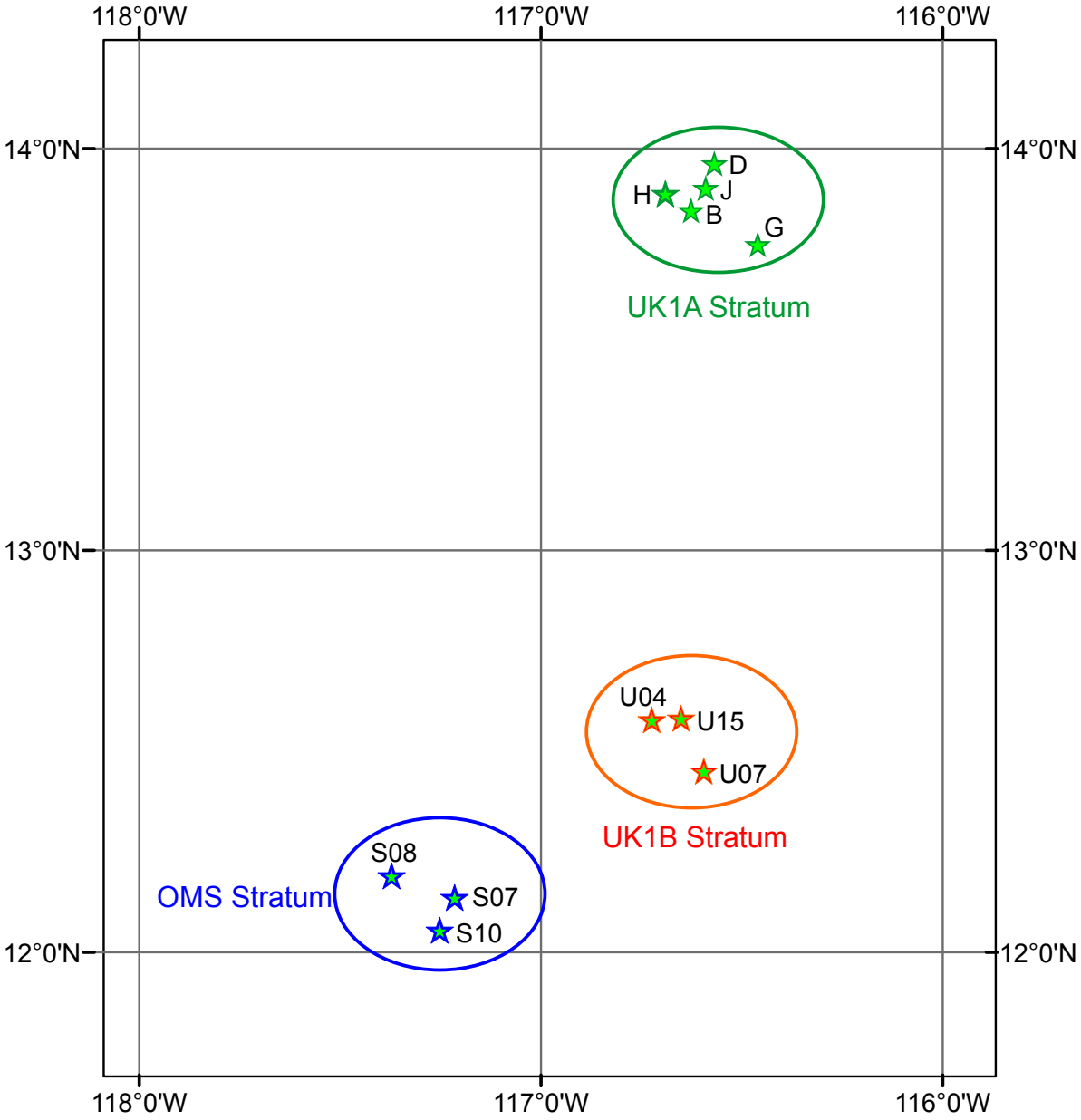

Figure S2

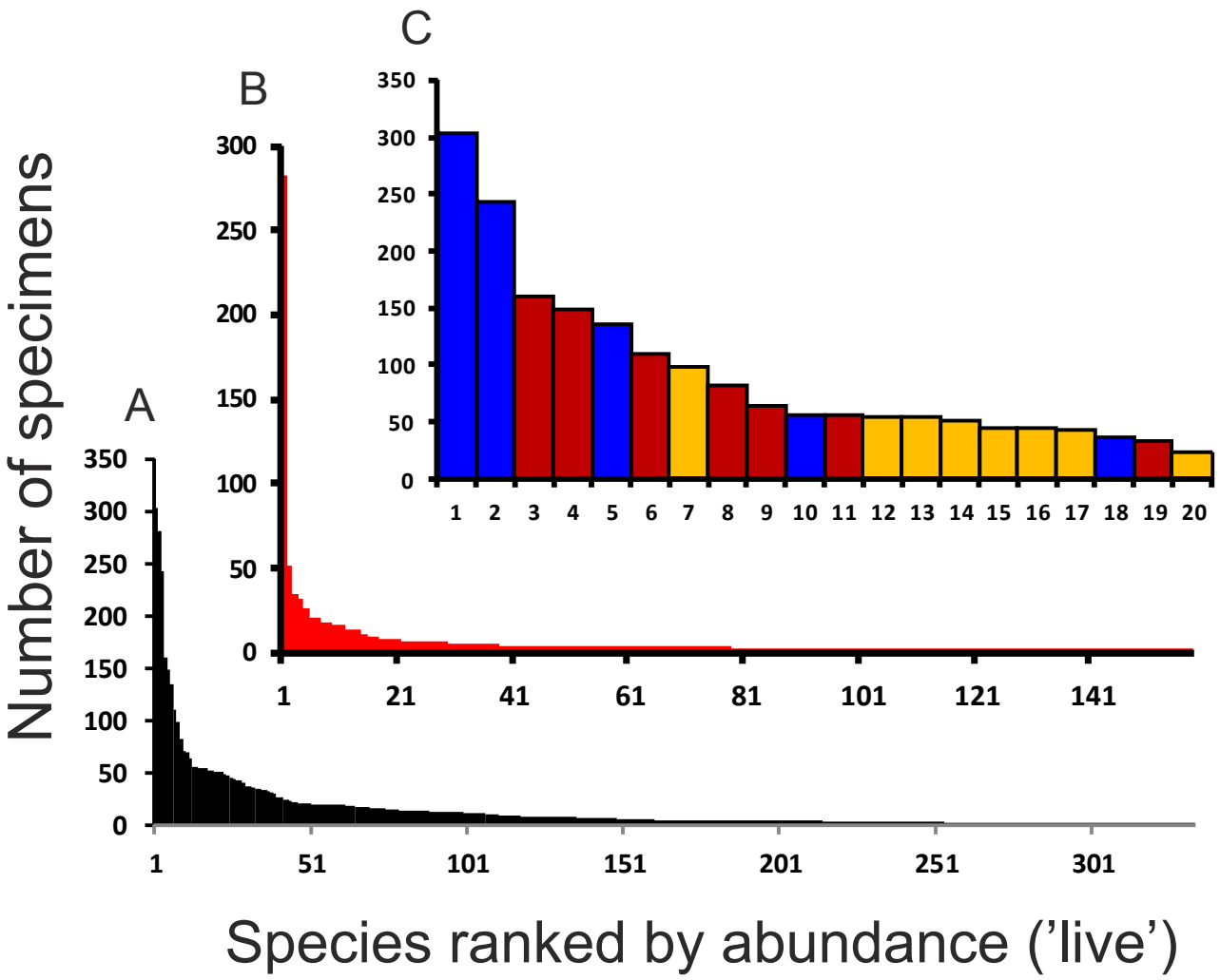
C
B
A
Number of specimens
350
300
250
200
150
100
50
0
1 2 3 4 5 6 7 8 9 10 11 12 13 14 15 16 17 18 19 20
300
250
200
150
100
50
0
1 21 41 61 81 101 121 141
350
300
250
200
150
100
50
0
1 51 101 151 201 251 301
Species ranked by abundance (’live’)

Figure S3

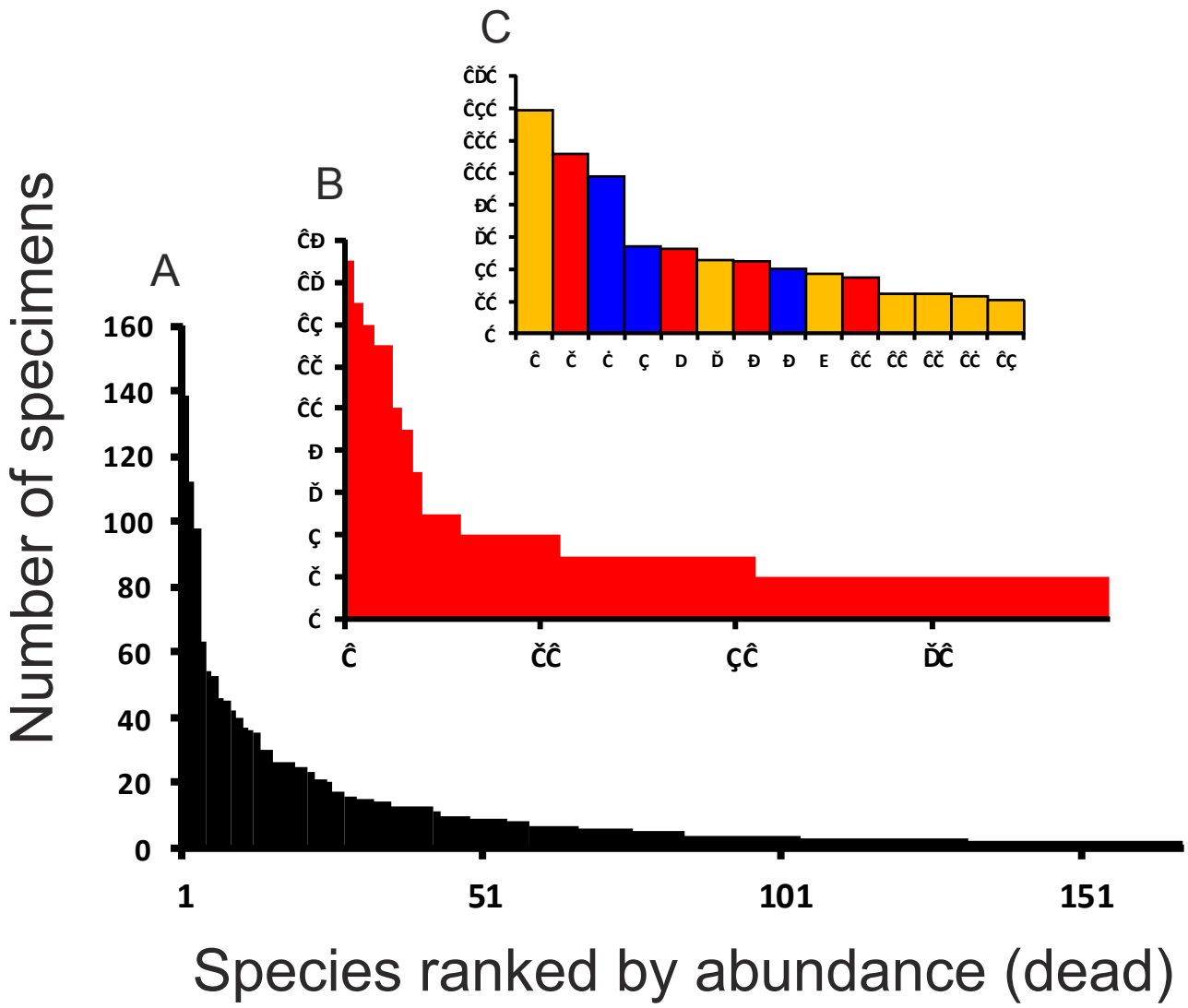
A
B
C
Number of specimens
160
140
120
100
80
60
40
20
0
1
51
101
151
Species ranked by abundance (dead)

Figure S4

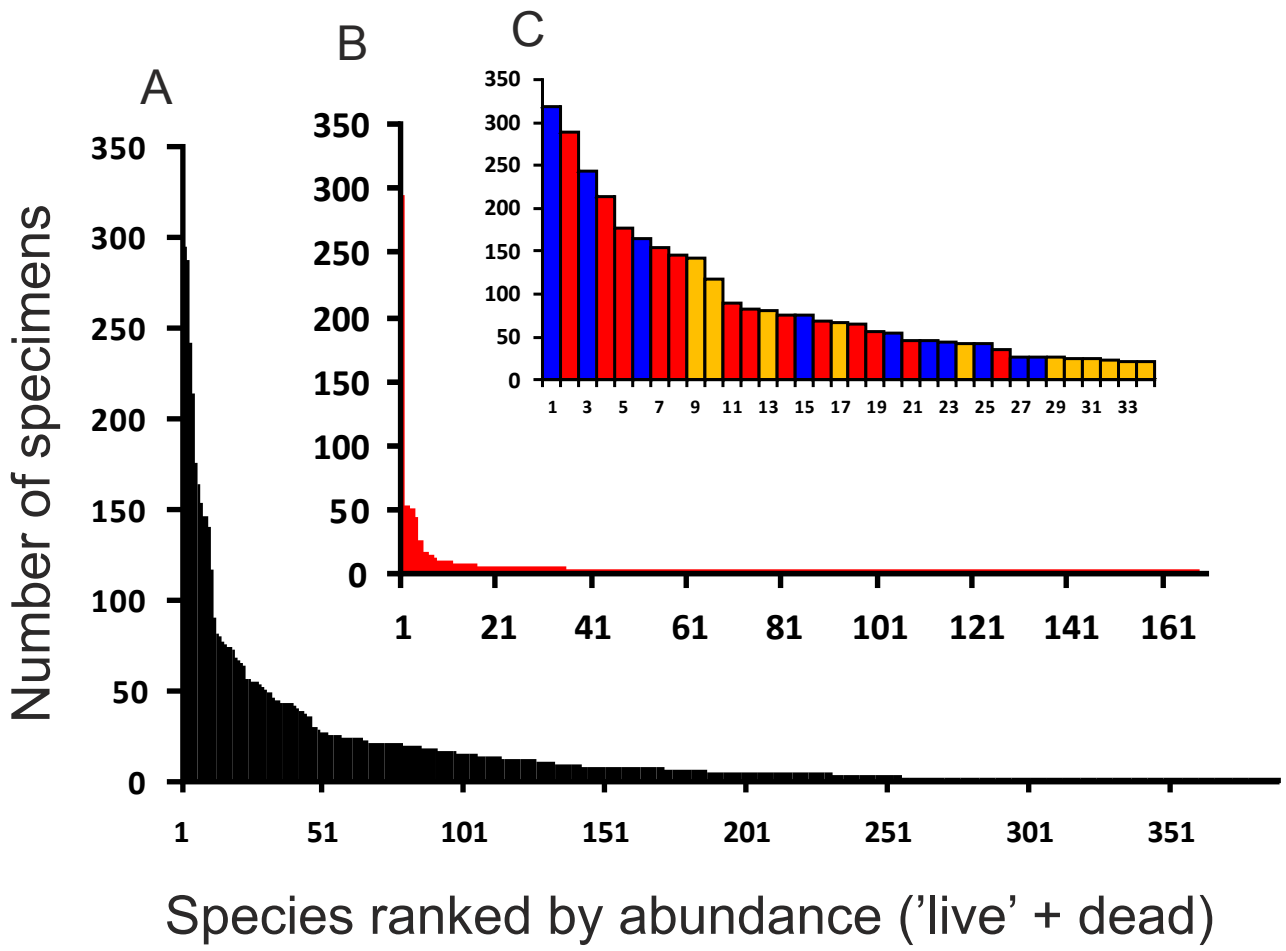
A
B
C
Number of specimens
350
300
250
200
150
100
50
0
1
51
101
151
201
251
301
351
21
41
61
81
101
121
141
161
3
5
7
9
11
13
15
17
19
21
23
25
27
29
31
33
Species ranked by abundance (’live’ + dead)

Supplementary Fig. S5: Total number of species recognised in individual samples (MC02, MC04 etc), individual strata (UK1-A, UK1-B, OMS) and all strata combined.

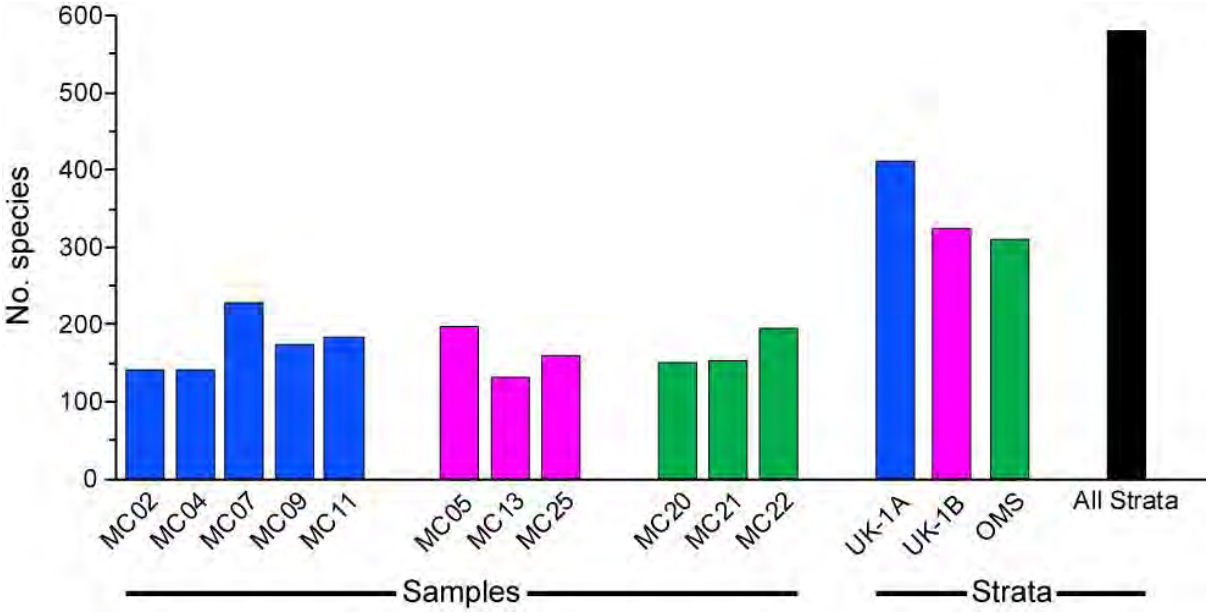

Supplementary Fig. S6: Rarefaction curves based on complete live (A) and complete live and dead (B) specimens. Solid lines are based on actual data; dashed lines are extrapolated curves up to 1,500 specimens for each sample.

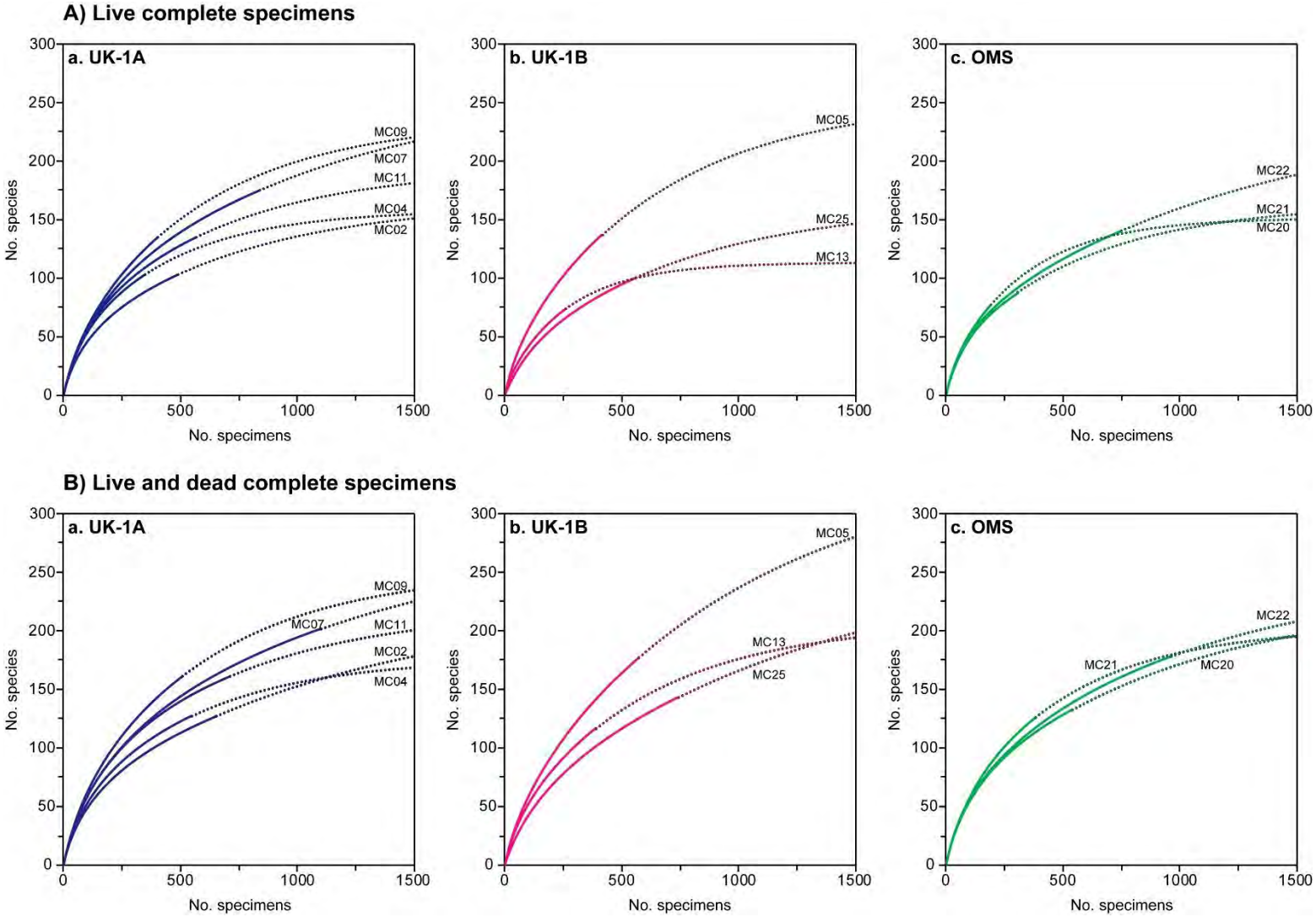

Supplementary Fig. S7: Sample-based rarefaction curves based on the number of complete (live and dead combined) specimens from the 11 analysed samples, and extrapolated up to 15 or 30 samples (A). Corresponding number of new species added per additional sample based on the sample-based extrapolated rarefaction curves (B). Estimates are shown for single strata, and for all strata combined. For each sample, vertical bars indicate the 95% interval confidence.

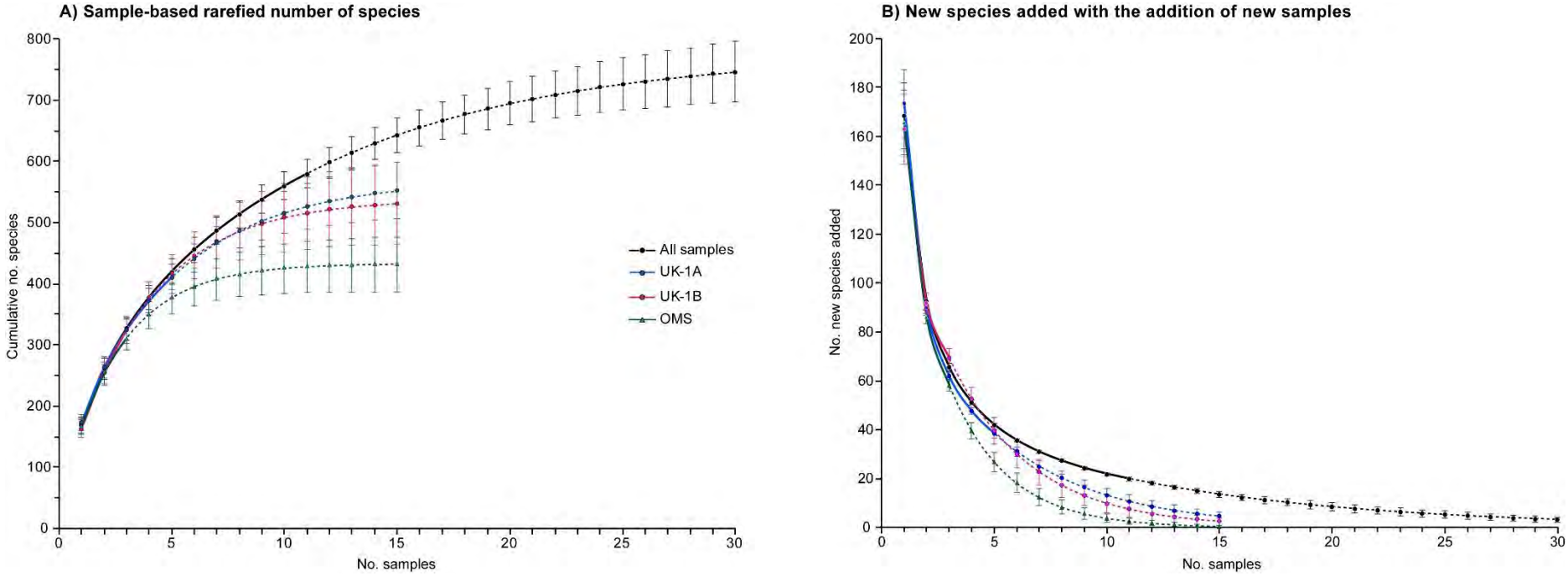

Supplementary Figure S8

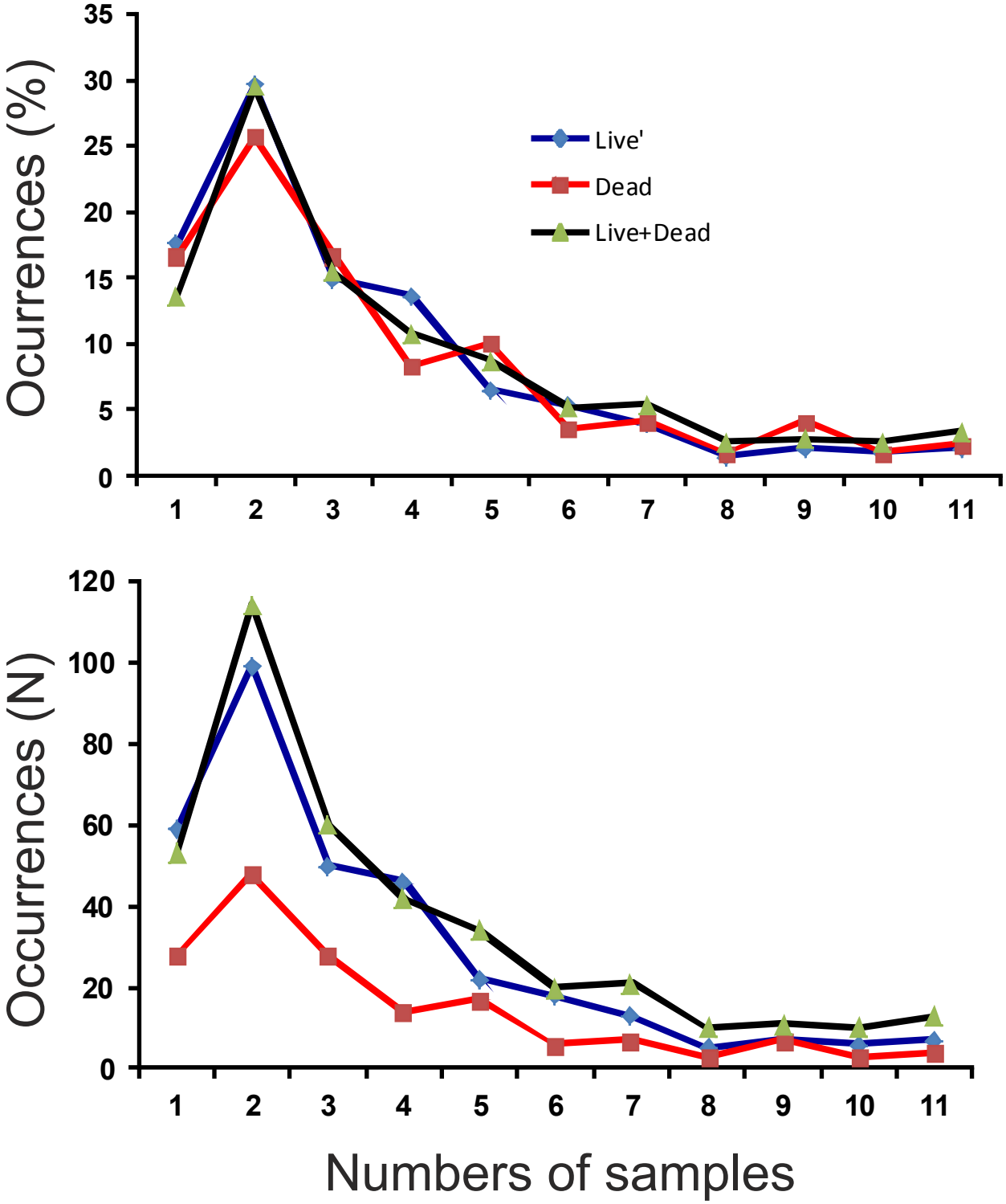

Supplementary Figure S9

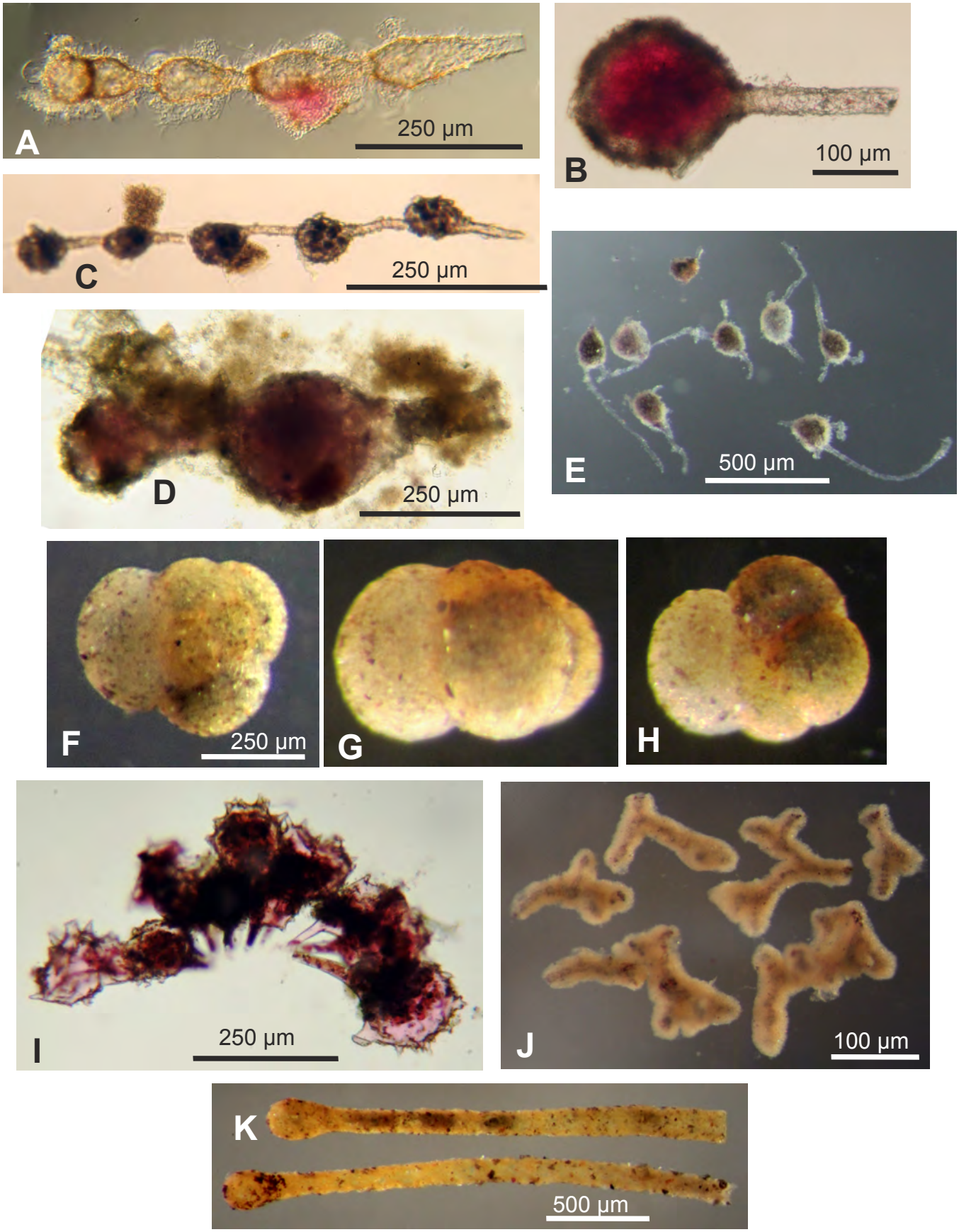

Supplementary Fig. S10

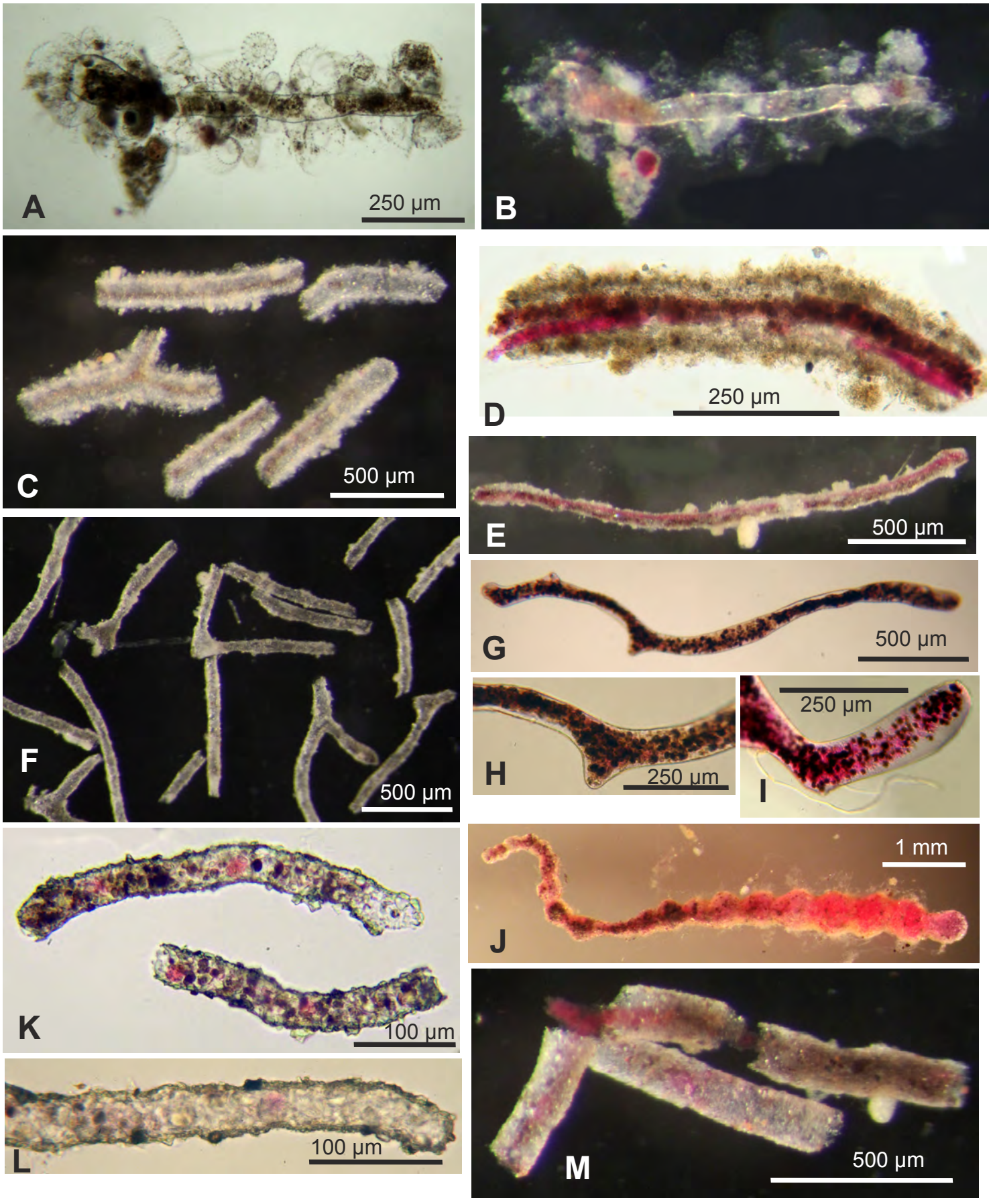

Supplementary Figure S11

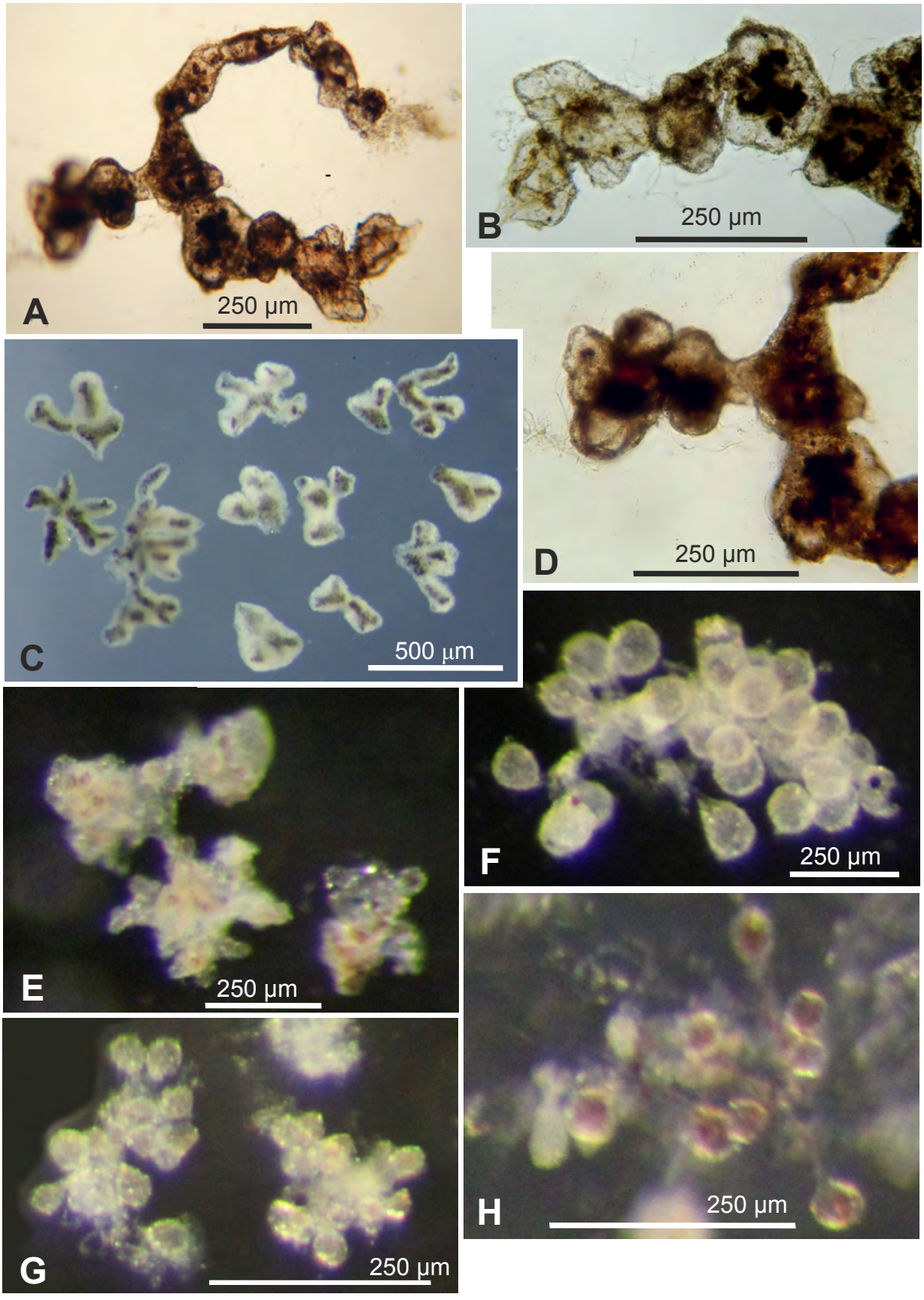

Supplementary Figure S12